440
2-19-80

DR. 829

DOE/JPL/954833-2

WIND LOADS ON FLAT PLATE PHOTOVOLTAIC ARRAY FIELDS

Phase II Final Report

By
Ronald Miller
Donald Zimmerman

September 1979

Work Performed Under Contract No. NAS-7-100-954833

Boeing Engineering and Construction Company
Seattle, Washington

MASTER

U.S. Department of Energy

DISTRIBUTION OF THIS DOCUMENT IS UNLIMITED

Solar Energy

DISCLAIMER

This report was prepared as an account of work sponsored by an agency of the United States Government. Neither the United States Government nor any agency Thereof, nor any of their employees, makes any warranty, express or implied, or assumes any legal liability or responsibility for the accuracy, completeness, or usefulness of any information, apparatus, product, or process disclosed, or represents that its use would not infringe privately owned rights. Reference herein to any specific commercial product, process, or service by trade name, trademark, manufacturer, or otherwise does not necessarily constitute or imply its endorsement, recommendation, or favoring by the United States Government or any agency thereof. The views and opinions of authors expressed herein do not necessarily state or reflect those of the United States Government or any agency thereof.

DISCLAIMER

Portions of this document may be illegible in electronic image products. Images are produced from the best available original document.

NOTICE

This report was prepared as an account of work sponsored by the United States Government. Neither the United States nor the United States Department of Energy, nor any of their employees, nor any of their contractors, subcontractors, or their employees, makes any warranty, express or implied, or assumes any legal liability or responsibility for the accuracy, completeness or usefulness of any information, apparatus, product or process disclosed, or represents that its use would not infringe privately owned rights.

This report has been reproduced directly from the best available copy.

Available from the National Technical Information Service, U. S. Department of Commerce, Springfield, Virginia 22161.

Price: Paper Copy $~~6.50~~ 9.50
Microfiche $3.~~00~~ 50

DOE/JPL/954833-2
Distribution Category UC-63b

WIND LOADS
ON FLAT PLATE PHOTOVOLTAIC ARRAY FIELDS

JPL Contract No. 954833

Low Cost Solar Array Project
Engineering Area

Phase II Final Report

DISCLAIMER

This book was prepared as an account of work sponsored by an agency of the United States Government. Neither the United States Government nor any agency thereof, nor any of their employees, makes any warranty, express or implied, or assumes any legal liability or responsibility for the accuracy, completeness, or usefulness of any information, apparatus, product, or process disclosed, or represents that its use would not infringe privately owned rights. Reference herein to any specific commercial product, process, or service by trade name, trademark, manufacturer, or otherwise, does not necessarily constitute or imply its endorsement, recommendation, or favoring by the United States Government or any agency thereof. The views and opinions of authors expressed herein do not necessarily state or reflect those of the United States Government or any agency thereof.

September 1979

Ronald Miller
Donald Zimmerman

"The JPL Low Cost Solar Array Project is sponsored by the U.S. Department of Energy and forms part of the Solar Photovoltaic Conversion Program to initiate a major effort toward the development of low-cost solar arrays. This work was performed for the Jet Propulsion Laboratory, California Institute of Technology by agreement between NASA and DOE."

Prepared for

MASTER

Jet Propulsion Laboratory
4800 Oak Grove Drive
Pasadena, California 91103

By the

Boeing Engineering and Construction Company
(A Division of The Boeing Company)
Seattle, Washington

DISTRIBUTION OF THIS DOCUMENT IS UNLIMITED

ABSTRACT

This report describes a theoretical study of the aerodynamic forces resulting from winds acting on flat plate photovoltaic arrays. Local pressure distributions and total aerodynamic forces on the arrays are shown. Design loads are presented to cover the conditions of array angles relative to the ground from 20° to 60°, variable array spacings, a ground clearance gap up to 1.2 m (4 ft) and array slant heights of 2.4 m (8 ft) and 4.8 m (16 ft).

Several means of alleviating the wind loads on the arrays are detailed. The expected reduction of the steady state wind velocity with the use of fences as a load alleviation device are indicated to be in excess of a factor of three for some conditions. This yields steady state wind load reductions as much as a factor of ten compared to the load incurred if no fence is used to protect the arrays. This steady state wind load reduction is offset by the increase in turbulence due to the fence but still an overall load reduction of 2.5 can be realized. Other load alleviation devices suggested are the installation of air gaps in the arrays, blocking the flow under the arrays and rounding the edges of the array.

Included is an outline of a wind tunnel test plan to supplement the theoretical study and to evaluate the load alleviation devices.

TABLE OF CONTENTS

		PAGE
1.0	SUMMARY	1
2.0	INTRODUCTION	5
2.1	Study Objectives	5
2.2	Study Ground Rules	6
2.3	Study Requirements	6
2.4	Report Organization	10
3.0	BASIC AERODYNAMIC EQUATIONS AND DEFINITIONS	11
3.1	Analysis Definitions and Nomenclature	11
3.2	Solar Energy - Aerodynamic Synonyms	13
3.3	Aerodynamic Sign Convention and Basic Equations	13
4.0	HISTORICAL DEVELOPMENTS - AIR FLOW ABOUT BLUFF BODIES	15
4.1	Theoretical Developments Synopsis	15
4.2	Experimental Studies Synopsis	15
4.3	Wind Velocity Profiles in Ground Proximity	23
5.0	AERODYNAMICS LOADS - FLAT PLATE ARRAYS	27
5.1	Theoretical Analysis - Constant Velocity Profile	29
6.0	AERODYNAMIC DESIGN LOADS AND LOAD REDUCING PROCEDURES	37
6.1	Appraisal of Theoretical Analysis for 1/7 Power Law Velocity Profile	37
6.2	Proposed Wind Design Forces for High Aspect Ratio Arrays	41
6.3	Array Key Load Parameters and Sensitivities	45
6.4	Protective Wind Barriers and Resulting Array Loads	47
6.5	Miscellaneous Potential Load Alleviation Techniques	56
6.6	Unsteady Winds and Structural Dynamics Relationship	58
7.0	PROPOSED WIND DESIGN PRESSURE DISTRIBUTIONS FOR HIGH ASPECT RATIO ARRAYS	59

			PAGE
8.0	WIND TUNNEL TEST PLAN		65
9.0	CONCLUSIONS AND RECOMMENDATIONS		67
10.0	NEW TECHNOLOGY		69
11.0	REFERENCES		71
	APPENDIX A	Theoretical Aerodynamic Analysis of Flat Plate Arrays in the Separated and Potential Flow Regime	75
	APPENDIX B	Photovoltaic Array Wind Tunnel Test Plan	107

1.0 SUMMARY

This report describes a theoretical study of the aerodynamic forces resulting from winds acting on flat plate photovoltaic arrays. Local pressure distributions and the total aerodynamic forces on the arrays are shown. Recommended aerodynamic design loads are presented for use in designing the photovoltaic array local structure as well as the overall support structure. Design wind loads were calculated to cover the conditions of the array tilt angles of from 20° to 60°, a ground clearance gap up to 1.2 m (4 ft), various array spacings, array slant height of 2.4 m (8 ft) and 4.8 m (16 ft), and with and without the benefit of protective wind barriers. Two wind environments were considered; a uniform velocity and a 1/7 power law profile referenced to 40 meters/sec (90 mph) at 10 m (32.8 ft).

For flat plates positioned at tilt angles greater than 15°, the air flow detaches from the plate and separated flow analysis theories must be used to analyze the aerodynamic forces on the flat plates. Using a prototype separated flow analysis program developed by the Boeing Commercial Airplane Company, the aerodynamic forces were calculated for arrays positioned at several tilt angles between 20° and 90° with the wind direction from both the front and rear. From the results, it was determined that the aerodynamic loads on the arrays increase with increasing tilt angle and decreasing ground clearance. It was also estimated that a reduction of wind forces of as much as 60% can be attained by spacing the arrays such that the downstream arrays are in the wake of upstream arrays. Figure 1-1 summarizes the aerodynamic load sensitivity of arrays for key array parameters.

Because the angle between the sun and the horizon varies, depending on time of year and geographic location, the tilt angle of fixed arrays will vary depending on their location. Expected wind aerodynamic forces on the arrays in close ground proximity were calculated using the normal force coefficients determined by the separated flow analysis program and the design wind dynamic pressure on the arrays.(The geometric position of the arrays with respect to the ground were considered when calculating the wind dynamic pressure). These forces, shown in Figure 1-2, are recommended for use in designing the arrays for steady state wind loads without the benefit of protective fences.

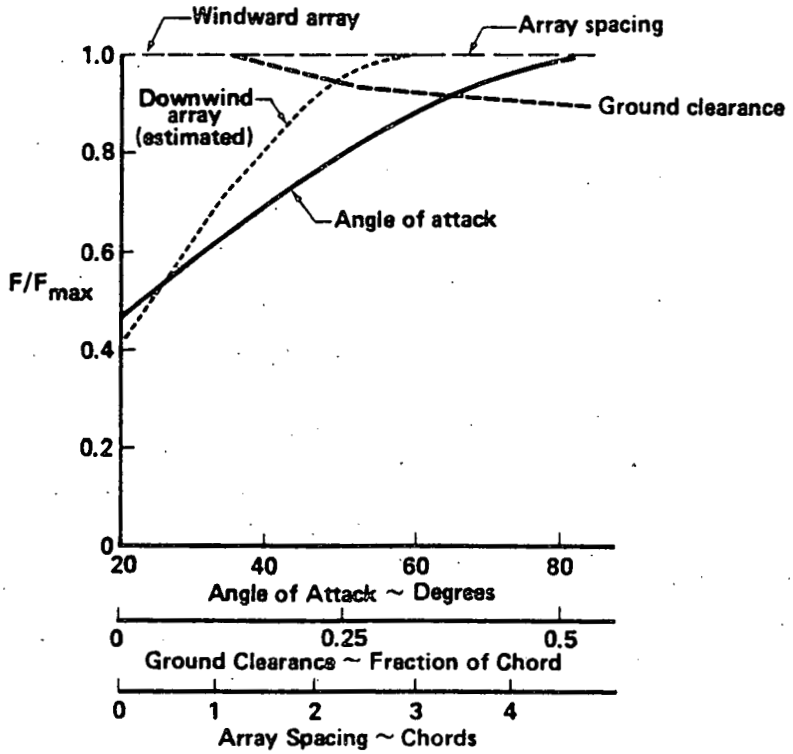

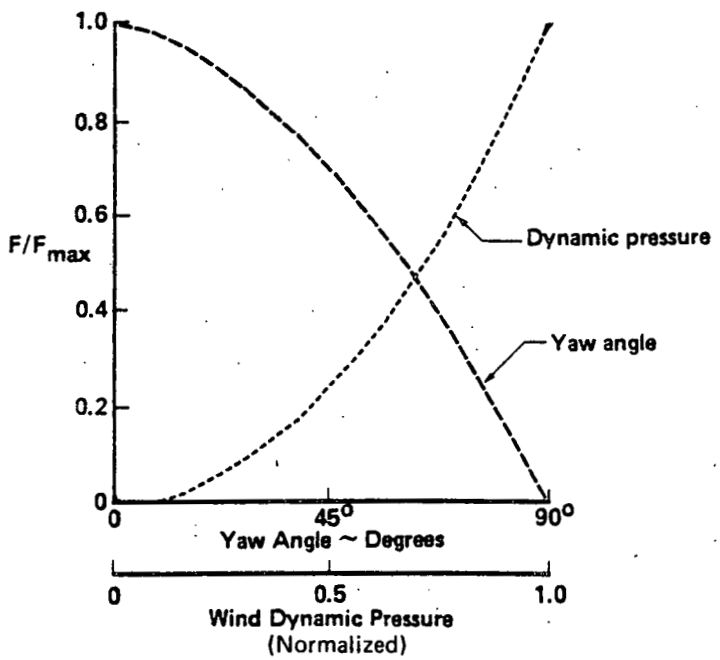

Figure 1-1. Key Wind Loads Parameters and Their Sensitivity in Separated Flow Analyses

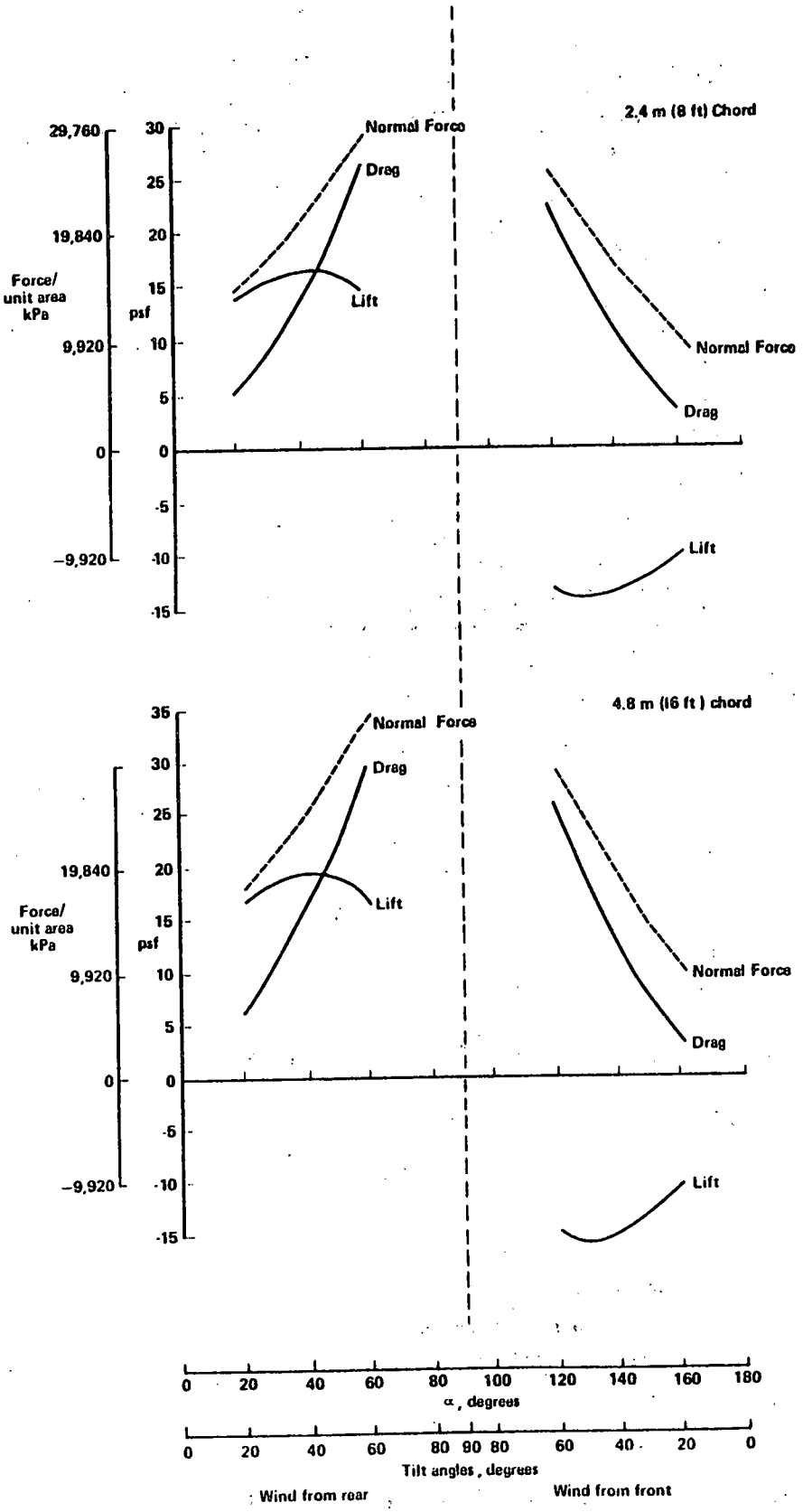

Figure 1-2. Envelope of Wind Forces per Unit Area on Arrays (1/7 Power Law Wind Profile, No Protective Barriers, Single Array)

Protective fences can effect a considerable decrease in the wind velocity behind the fence compared to the wind velocity windward of the fence. The amount of reduction is dependent upon several parameters, particularly the fence porosity and the distance behind the fence. In general, the largest decrease in wind velocity is located close behind the fence. The wind velocity tends to increase with increasing distance to the freestream velocity at a distance behind the fence of from 13 to 17 times the fence height. Isotachs (lines of constant velocity) behind four different porosity fences are presented. These isotachs can be used to estimate the aerodynamic forces that photovoltaic arrays may incur when positioned at various locations behind a fence.

Several other techniques were suggested as possible means to reduce the wind loads. Incorporating porosity into the arrays at the perimeters of the solar panels may reduce the wind forces on the arrays and may also tend to clean the arrays by introducing swirling motions to the wind. Other techniques that may reduce wind loads are blocking the flow of air under the arrays and rounding the edges of the arrays.

These wind load reduction techniques will be appraised in a recommended wind tunnel test. In addition, the recommended wind tunnel test will also determine whether the estimated 60% reduction in wind loads on the arrays can be attained when arrays are spaced such that arrays are in the wind wake of other arrays.

2.0 INTRODUCTION

This report describes a theoretical analysis of the aerodynamic loading on long flat plate photovoltaic arrays resulting from exposure to the wind environment. The study was performed under contract number 954833 to the Jet Propulsion Laboratory as part of the Engineering Area analyses for the Low-Cost Solar Array (LSA) Project. This project is being managed by JPL for the Department of Energy, Division of Solar Technology.

2.1 Study Objectives

The Department of Energy (DOE) photovoltaic program[1] has the overall objective to ensure that photovoltaic conversion systems will contribute significantly (50 GWe) to the nation's energy supply by the year 2000. The DOE has established specific price goals which are deemed necessary to achieve the desired industry growth and market penetration. These goals, i.e., producing energy at 50-80 mills/KW·h by 1986 (expressed in constant 1975 dollars), are recognized as very challenging, since to meet them industry must reduce all aspects of costs related to the construction and maintenance of the arrays.

One such area where some reduction of costs may be attained is in the structural costs of the photovoltaic panels, panel and array support structure and foundations of a photovoltaic power station. Any reduction in the wind design loads will result in some reduction in structural costs. Previous studies have shown that the design wind loads on the photovoltaic arrays can significantly affect structure costs. A design study of flat plate array support structure[3] showed that the arrays (structural framework and foundation) costs were of the same order of magnitude as the photovoltaic module costs. Furthermore, the array costs were strongly dependent on the assumed wind loading, for loads in the range of 35 to 75 psf. Another conceptual design study[2] evaluated a photovoltaic array design using transparent inflated enclosures to protect the modules from wind loads. The loading on the enclosures for this study were based on limited data available in the literature, wind tunnel test results, and/or analysis. Predicted wind loadings on the enclosures were near the low end of the range compared to those used in Reference 3, and showed significant cost savings compared to conventional arrays with similar wind loading criteria.

This report evaluates the aerodynamic loading on very high aspect ratio (span/chord length is very large) flat plate photovoltaic arrays located on or in close proximity to the ground, in close proximity to each other, and exposed to the wind environment. The objective of the study was to determine wind loading criteria for flat plate photovoltaic arrays with various configurations in relation to chord lengths, array spacings, height of the arrays from the ground, wind directions, and array angles of attack. A further objective was to determine means of reducing the aerodynamic loads on the arrays by using protective fences, building porosity into the arrays, or any other techniques considered feasible as a load reducing method.

2.2 Study Ground Rules

The basic approach to this study was to use existing state of the art theoretical aerodynamic techniques to predict the aerodynamic loads and to investigate means of reducing the loads on flat plate arrays. Existing published experimental results would be used (when possible) to validate the results and to predict aerodynamic flow patterns and loads for conditions that cannot be satisfactorily solved by existing theories.

2.3 Study Requirements

The requirements of this study involves analysis and test planning within five specific areas. They are:

i) Wind Profiles
ii) Wind Loads on Flat Plates
iii) Key Wind Loads Parameters and Parameter Sensitivity
iv) Load Reduction Techniques
v) Test Program Planning

Non-dimensional wind profiles were to be developed in the vicinity of flat-plate array fields with and without protective wind barriers, utilizing existing theoretical techniques and data published in the literature. The aerodynamic pressure loading and resulting structural support forces are strongly dependent on these wind profiles. The aerodynamic pressures and forces resulting from the wind environment was to be determined for specific

free stream wind profiles, wind angles, array heights, spacings, and tilt angles and protective barriers. Figures 2.1 and 2.2 summarize these array configurations and working environment. Key parameter and the parameter sensitivities affecting the aerodynamic loads and means of reducing the aerodynamic loads were to be determined from the analysis. A test program was then to be planned that would verify and augment the analytical results. The following is a detailed summary of the statement of work.

- Analytically develop non-dimensional wind profiles in the vicinity of, and within flat-plate array fields utilizing existing data found in the literature. The wind profiles developed in this study were to be normalized to the reference profile, a 1/7th power wind velocity profile associated with open terrain having a 40 meter/second wind velocity at an elevation of 10 meters with sea level standard atmospheric conditions. The following represent areas for evaluation:
  - i) Identify possible natural terrain features that would produce a more severe profile than the reference, and depict their associated velocity profiles.
  - ii) Determine the effects on the reference profile of artificial barriers. Determine and depict the profile downstream from the barrier and at specified horizontal distances in terms of barrier heights and at the point of optimum expected reduction in the velocity profile for fences 2.5 and 5.0 meters high for:
    - a) solid fences with incident wind angles of 0° (head-on) and 45°.
    - b) 50% geometrically porous fences with incident wind angles of 0° (head-on) and 45°.
  - iii) Identify any variations of the barriers or other types of barriers that would further reduce the velocity profiles and depict their associated profiles.
  - iv) Determine the effects on the reference profile of array field parameters at a horizontal distance of two meters upstream of a single row array for:
    - a) Incident wind angles of 0° (head-on), 45°, 90°, 135°, and 180°.

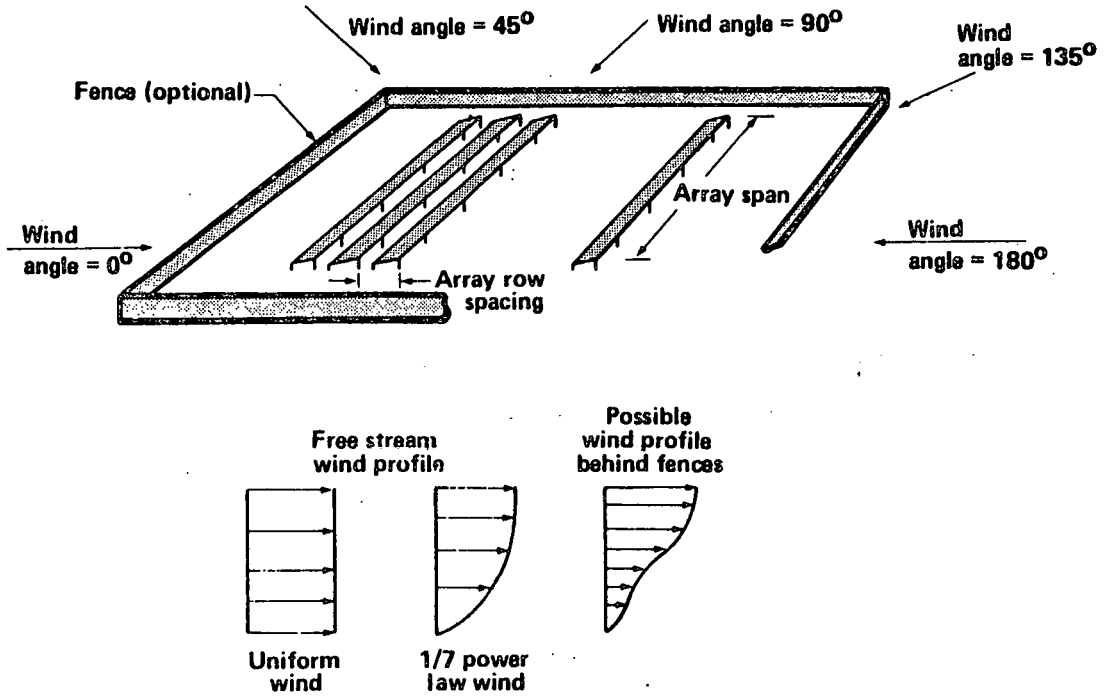

Figure 2-1. Wind Environment on Study Arrays

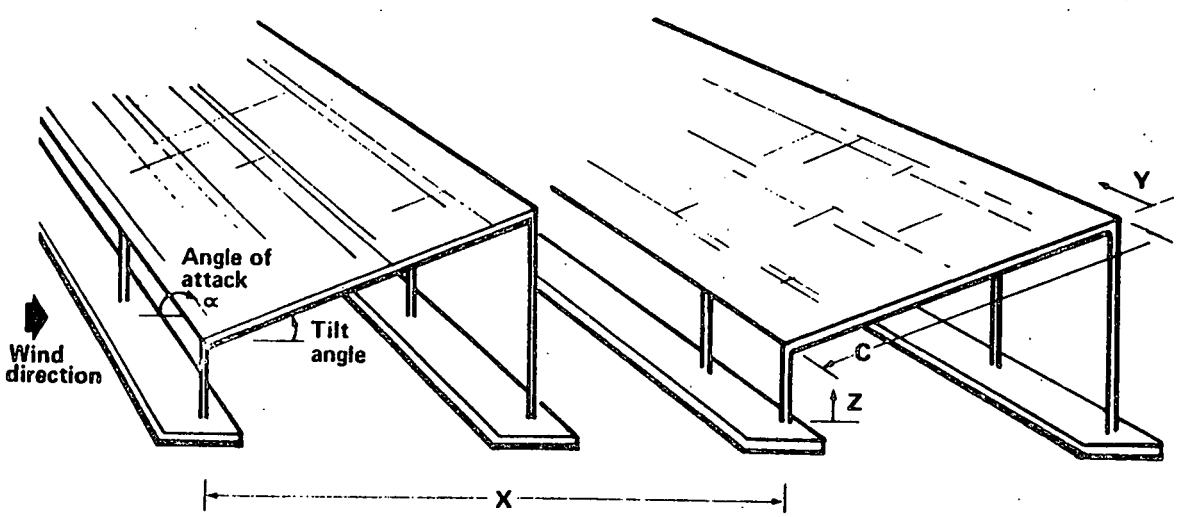

Ground clearance (Z) = 0 → 1.2 m (0 → 4 ft)
Slant height (C) = 2.4 m and 4.8m (8 and 16 ft)
Array spacing (X) = 1C → 5C
Angle of attack (α) = 0° → 180°
Tilt angle = 0° → 90°
Span (Y) = ∞

Figure 2-2. Array Variables Used to Study Aerodynamic Loads

b) No barrier, the optimum barrier, and an intermediate barrier.

c) Array field parameters including:

1) specified array slant heights.

2) specified array leading edge ground clearance heights.

3) specified array tilt angles.

v) Determine the effects on the reference profile of rows of arrays. Determine and depict the profile at specified horizontal distances upstream of an array field and at horizontal distances halfway in between specified rows of an array field for:

a) A combination of array field parameters determined from iv).

b) Specified incident wind angles.

c) No barrier, and the optimum barrier wind profile.

d) Specified array row spacings.

- Determine the resultant wind loads on the modules and panels that would be transmitted to the array support structure and foundations for each of the following:

  i) The most severe wind profile found previously at an incident wind angle of 0° (head-on), 45°, 90°, 135°, and 180°.

  ii) The optimum barrier wind profile at an incident wind angle of 0° (head-on), 45°, 90°, 135°, and 180°.

- Interpret the resultant wind loads on the modules, panels, and support structure to identify key parameters, and load sensitivities to those parameters.

- Identify possible design configurations that would further reduce wind loading on the arrays.

- Outline and describe a test program that would verify the analytical results including an assessment of the level of confidence of the test program results.

2.4 Report Organization

The remainder of this report presents the detailed study results with proposed design aerodynamic loads and conclusions. Section 3.0 presents basic aerodynamic equations, definitions, and nomenclature used in the analysis. Section 4.0 gives a brief synopsis of the existing literature that is related to this study. A brief summary of the theoretical results for both potential and separated flow analysis on flat plat arrays is presented and discussed in Section 5.0. Section 6.0 presents proposed design loads for flat plate arrays and potential wind load reducing devices for the arrays. Proposed wind design pressure distributions along the chord of the arrays are presented in Section 7.0. In Section 8.0, the purposes of a proposed wind tunnel test plan and gains to be realized from a test are given. Conclusions and recommendations are in Section 9.0.

Appendix I presents the detailed results for the theoretical aerodynamic analysis of the flat plat arrays in both the separated and potential flow regimes. Appendix II details a comprehensive wind tunnel test plan.

3.0 BASIC AERODYNAMIC EQUATIONS AND DEFINITIONS

The analyses used in this report required the use of aerodynamic theoretical methods and calculated results in aerodynamic terms. Since most people employed in the design of photovoltaic arrays are not aerodynamicists, this section explains the basic aerodynamic terms and nomenclature and defines basic aerodynamic equations such that any engineer may understand the results. In addition, synonyms between aerodynamic and solar energy terms are given where applicable.

3.1 Analysis Definitions and Nomenclature

Aerodynamic coefficients:	non-dimensional coefficients.
pressure coefficient (C_p):	relates lifting surface pressure to freestream dynamic pressure, $C_p = p/q$.
C_{p_α}	slope of the pressure coefficient curve; relates pressure coefficient to angle of attack, $C_p = C_{p_\alpha} \cdot \alpha$.
normal force coefficient (C_n, C_N):	relates lifting surface force normal to surface to freestream dynamic pressure, $C_N = F_n/qA$.
C_{N_α}	slope of the normal force coefficient curve, relates normal force coefficient to angle of attack, $C_N = C_{N_\alpha} \cdot \alpha$.
lift coefficient (C_L):	relates lifting surface force normal to freestream velocity to freestream dynamic pressure, $C_L = L/qA$.
drag coefficient (C_D):	relates lifting surface force in freestream velocity direction to freestream dynamic pressure, $C_D = D/qA$.
center of pressure ($\bar{X}$):	location of total force on lifting surface measured from the leading edge.
Angle of attack (α):	angle measured from the wind vector to the plane of the lifting surface.

Array:	a mechanically integrated assembly of panels together with support structure (including foundations).
Array field:	the aggregate of all arrays.
Array spacing:	horizontal distance measured from one array to the identical location on the next array.
Aspect ratio ($\mathcal{AR}$):	aerodynamic geometric parameter (span/chord for a rectangular array).
Base pressure face:	downwind side of lifting surface.
Bluff body:	a nonstreamline body that causes airflow about itself to become separated and turbulent.
Chord (C):	distance of array between leading and trailing edges and perpendicular to the edges, i.e.: slant height of array.
Doublet:	source and sink located at the same location, an analytical device used in potential flow theory.
Dynamic pressure (q):	pressure due to freestream velocity ($q = .5\rho V^2$).
Ground clearance (Z):	distance between the ground and the lowest point on the panels forming the array.
Inviscid:	frictionless flow.
Leading edge:	windward edge of the array.
Module:	the smallest complete environmentally protected assembly of solar cells.
Normal wash, downwash:	flow of air perpendicular to the lifting surface plane.
Panel:	a collection of one or more modules fastened together forming a field installable unit.
Plate:	thin rectangular shaped structure that acts as a lifting surface.
Pressure (p):	force per unit area
Reynolds Number:	indicates inertia effects of fluid, $RE = \frac{\rho V \ell}{\mu}$
Span (b):	distance of an array between the two side edges i.e.: length of array.

Solar Cell:	the basic photovoltaic device which generates electricity when exposed to sunlight.
Tilt angle:	angle measured from the horizontal to the plane of the array panels.
Trailing edge:	downwind edge of the array.
Viscous:	flow that has friction.
Windward face:	windward side of lifting surface.
Yaw angle:	angle measured from wind direction to the normal of the array leading edge.
A:	array surface area.
ℓ:	length.
V:	wind velocity.
ρ:	air density.
μ:	coefficient of viscosity.
ν:	kinematic viscosity.
η:	fraction of span.
S:	area of lifting surface.

3.2 Solar Energy - Aerodynamic Synonyms

Solar Energy	Aerodynamics	Comments
Tilt angle and wind direction	Angle of attack	Restricted to horizontal winds
Slant height	Chord	
Wind angle	Yaw angle	Symbol is α.

3.3 Aerodynamic Sign Convention and Basic Equations

Sign Convention:

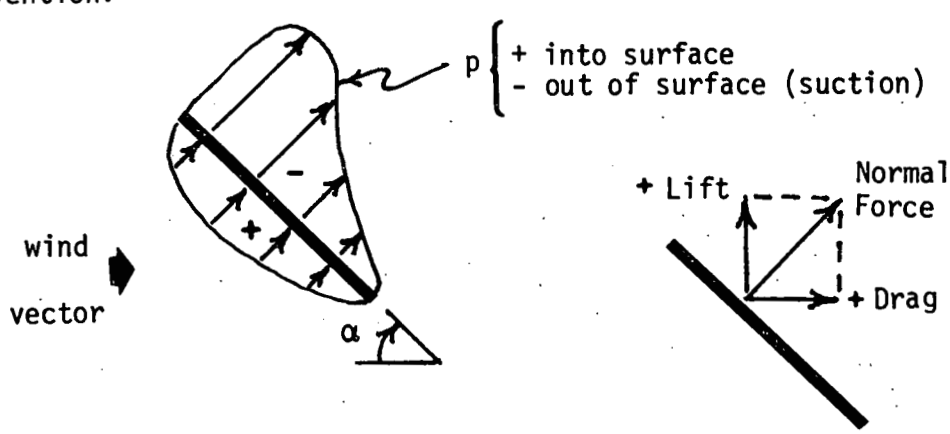

Aerodynamic Equations:

1. Pressures and pressure coefficients are related by:

$$p = q\,C_p$$

2. Normal forces and normal force coefficients are related by:

$$F_N = q\,SC_n$$

3. When the pressure coefficients and normal force coefficients are linear with respect to angle of attack, the above expressions can be changed to:

$$p = q\,C_{p_\alpha} \cdot \alpha$$

$$F_n = q\,SC_{n_\alpha} \cdot \alpha$$

4. Normal force coefficient for chordwise strips can be obtained from the pressure coefficients by integrating the pressure coefficient along the chord and is expressed by:

$$C_n = \frac{1}{C} \oint_c C_p$$

or for a surface as:

$$C_n = \frac{1}{S} \oint_s C_p$$

5. Lift and drag coefficients are related to the normal force coefficient by the angle of attack as:

$$C_L = C_n \cos\alpha$$

$$C_D = C_n \sin\alpha$$

6. Lift and drag forces are given by:

$$L = q\,SC_L$$

$$D = q\,SC_D$$

4.0 HISTORICAL DEVELOPMENTS - AIR FLOW ABOUT BLUFF BODIES

Until recently, most research on the prediction of the aerodynamic forces on and air flow about bluff bodies has been concentrated mainly on the flow over and around fences and buildings. The number of investigators and papers written on this subject is immense as illustrated by the review of the publications referenced by Van Eimern[4], Frost[5], and Cermak[6]. Since this study is concerned with the wind flow about and aerodynamic forces on photovoltaic flat plate arrays, only publications that are applicable in some respects to this problem are briefly reviewed.

4.1 Theoretical Developments Synopsis

The main features of air flow over bluff bodies in contact with the ground is shown in Figure 4-1 and consists of the five zones[7] shown in the figure.

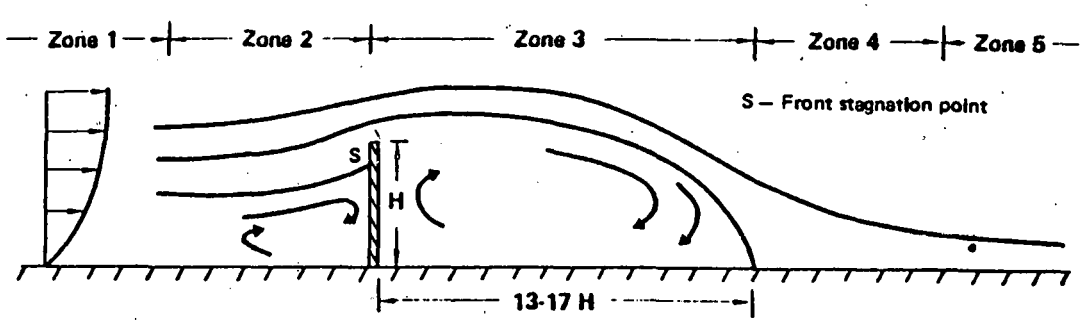

Zone 1: Zone of unobstructed flow
Zone 2: Zone of pressure rise
Zone 3: Standing eddy zone
Zone 4: Zone of redevelopment
Zone 5: Zone of redeveloped flow

Figure 4-1. Air Flow Concept About Bluff Bodies Immersed in the Wind Boundary Layer

In Zone 2, a standing vortex is located on the windward side of the barrier in the corner between the ground and the windward face; the vortex diameter is approximately equal to the distance between the ground and front stagnation point on the windward wall. At the barrier top edge the flow is accelerated and separates and then reattaches to the ground at the Zone 3 - Zone 4 boundary downstream of the barrier at a distance of approximately 13-17H, where H is the height of the barrier[8,9]. The flow between the barrier and the reattached flow and below the separated flow boundary consists of a standing eddy zone of reduced steady state velocity and increased turbulence indicated as Zone 3.

The exact theoretical representation of the boundary layer equations of motion for incompressible flow are the Navier Stokes equations given as:

$$\frac{Du}{Dt} = -\frac{1}{\rho}\frac{\partial p}{\partial x} + \nu \nabla^2 u$$

$$\frac{Dv}{Dt} = -\frac{1}{\rho}\frac{\partial p}{\partial y} + \nu \nabla^2 v$$

$$\frac{Dw}{Dt} = -\frac{1}{\rho}\frac{\partial p}{\partial z} + \nu \nabla^2 w$$

where

$$\frac{D}{Dt} = \frac{\partial}{\partial t} + u\frac{\partial}{\partial x} + v\frac{\partial}{\partial y} + w\frac{\partial}{\partial z}$$

and

$$\nabla^2 = \frac{\partial^2}{\partial x^2} + \frac{\partial^2}{\partial y^2} + \frac{\partial^2}{\partial z^2}$$

and ρ = fluid density

ν = kinematic viscosity

u, v, w = fluid velocity in the x, y, z directions, respectively

Because of the complex boundary layer flow, these equations are difficult to solve without simplifications even for flow over simple bluff-bodies.

Several authors have performed theoretical analyses of the flow over bluff-bodies with limited success. Bitte[10] employed several different theories to predict the flow over a two dimensional solid fence perpendicular to the free stream flow. One method employed by Bitte and also Kiya[11,12] was the use of inviscid flow to develop the equations of motion. This method produced results that matched wind tunnel results fairly well as used by Sakamoto[13] for the flow on the windward side of a fence, the flow outside of the standing eddy zone, and for the windward face pressure distribution on a fence. The flow in the standing eddy zone was not predicted using this method. Predicting the flow in all of the zones does require empirical data usually obtained from wind tunnel results. The required empirical data is the windward face stagnation point location and pressure, the separation point location and pressure and the downstream reattachment point location. Sakamoto[14] applied this method to include two-dimensional plates perpendicular to the free stream flow. He showed good comparison of the theoretically predicted pressures on the windward surface to those obtained from a wind tunnel study. Bitte also applied the concepts of turbulent boundary layer theory with the inviscid flow equations to predict the flow in the wake. He related the eddy viscosity to the mean flow through the Prandtl mixing length hypothesis and described the viscous turbulent atmospheric motion upstream of the fence by a logarithmic velocity distribution.

Taulbee[15] used a rotational flow analysis, dubbed "frozen vorticity theory" to predict the flow and pressure distribution in front of and on the windward surface of a forward facing step. Seginer[16] proposed a method based on the momentum equation and knowledge of the flow field to calculate drag and moment on a two dimensional porous fence of porosity greater than approximately 40 percent. Seginer did not show any comparison of his method

with experimental results. This method uses a logarithmic velocity profile and requires knowledge of the pressure and shear stress along the surface. Parkinson[17] used two-dimensional compressible potential flow theory and conformal mapping to predict the flow and wake geometry of a symmetrical bluff-body (flat plate) which is not in the turbulent boundary layer or attached to the floor. Counihan[18] employed a simple eddy viscosity theory to describe the wake geometry behind two-dimensional surface obstacles in turbulent boundary layers. This theory describes the mean velocity reasonably well. It also suggests that the velocity deficit is affected by the roughness of the terrain.

Most of these theoretical analyses require prior knowledge of the flow and are only applicable to two-dimensional flows. The flow predictions from these analyses on the windward side of a fence match results from wind tunnel tests fairly well. In most cases, the velocity profile in the standing eddy zone behind the bluff-body is not predicted.

4.2 Experimental Studies Synopsis

There have been numerous experimental wind tunnel studies and a few natural wind studies on the air flow about fences. In contrast, studies of flat plates inclined to the free stream velocity are relatively few in number. One of the more referenced studies on airflow about fences was performed by Good and Joubert[8] who performed a tunnel test of the flow over a fence with the wind boundary layer profile simulated as a 1/7 power law. Good and Joubert measured the velocity field windward and behind a two-dimensional solid fence as well as the pressure distribution on the fence. Of considerable importance in their findings is that the relative extent of upstream influence of the bluff plate on the boundary layer is found to increase rapidly as h/δ decreases where h is the height of the bluff plate and δ is the boundary layer thickness. Of significance in their study is that they did not correct their results due to tunnel blockage effects. Tunnel blockage effects were studied for the flow field and drag of a two-dimensional solid fence by Castro[19] and was shown to significantly affect the flow field and pressures.

Woodruff[20] performed both wind tunnel tests and natural full size tests of from one to three fences positioned 15 times their height behind each other. From the tests, it appears as if the flow behind one or all three fences are not very different. Woodruff also performed full size tests of three dimensional fences at an oblique angle of approximately 45° to the air flow. The turbulent flow behind these fences also does not appear to be much different whether the flow is perpendicular or at an oblique angle, providing the flow is compared along the direction of airflow. This is also shown to be true by Van Eimern[4] provided the flow angles to the fence are less than 50°.

The effect of fence porosity on the turbulent flow and fence drag is reported by Jensen[21], Baltaxe[22], and Raine[23]. Raine showed that a solid or low permeable fence (0%-20% permeable) gives slightly better wind protection than a 34% or 50% permeable fence (Figure 4-2). Raine also showed that local turbulence increases with decreasing permeability (Figure 4-3). This turbulence spectrum close to the fence is dominated by the high frequency turbulence shed by the fence elements (Figure 4-4). Farther aft of the fence, this high frequency turbulence decays and the turbulence spectrum is dominated by the approach flow turbulent spectrum. Most authors have assumed that Reynold's numbers do not affect the flow above a given Reynold's number; Raine stated that this is true only if the ratio of fence height to surface roughness remains constant. Raine's findings indicate that criteria related to the wind loading on panels behind a fence must consider the free stream turbulence, fence induced turbulence, and the reduction of the free stream velocity by the fence.

Wind tunnel studies of the air flow over flat plates inclined to the free stream velocity were performed by Sakamoto[14], Raju[24], and Modi[25]. Sakamoto mounted the plate in the boundary layer profile with one edge on the ground plane and varied the inclination (angle of attack) of the plate from 30° to 150° to the free stream velocity. Windward and base pressure distributions were presented for the various inclination angles. Modi mounted a plate in the free stream air flow and varied the angle of attack from 0° to 90° to

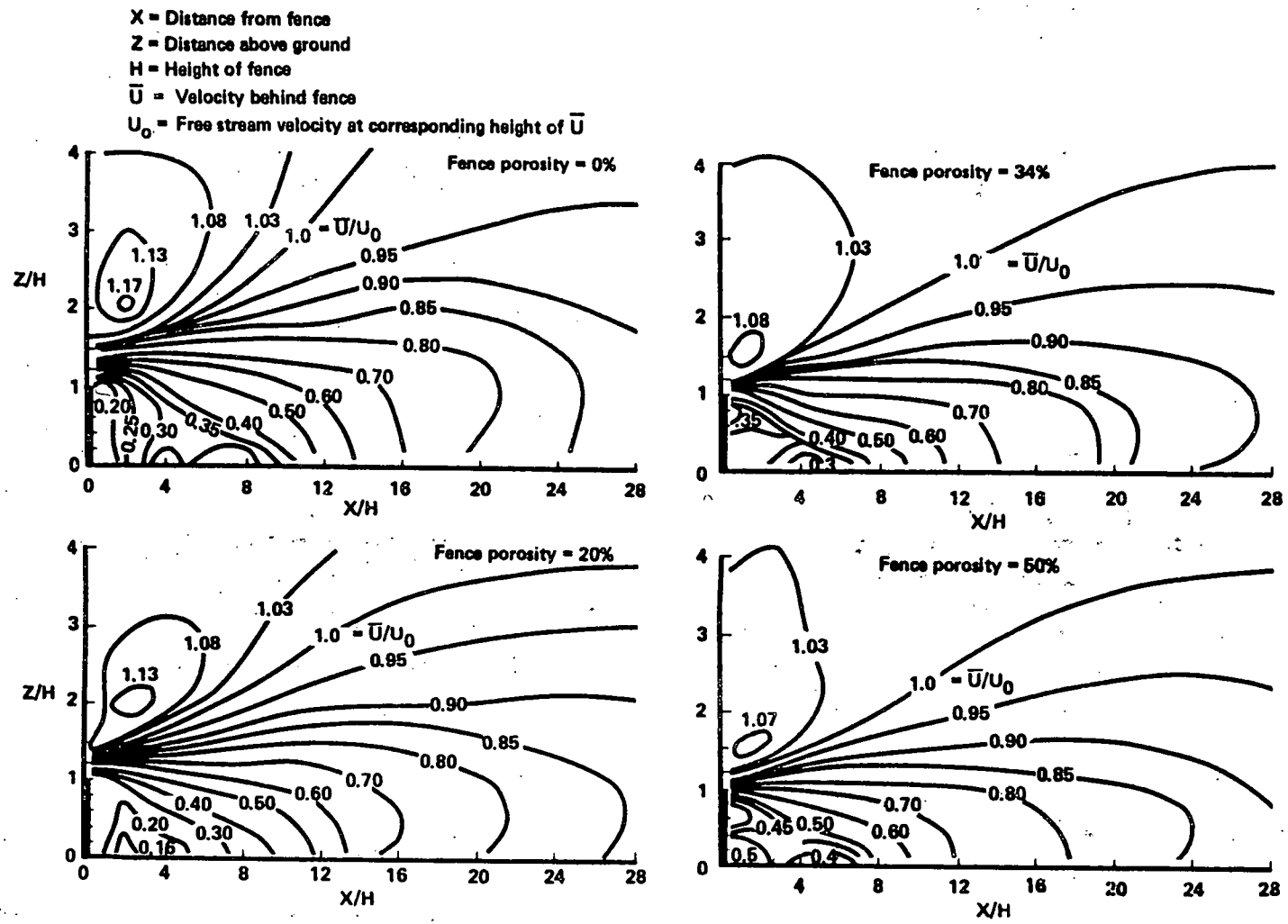

Figure 4-2. Effect of Fence Porosity on Wind Steady State Velocity

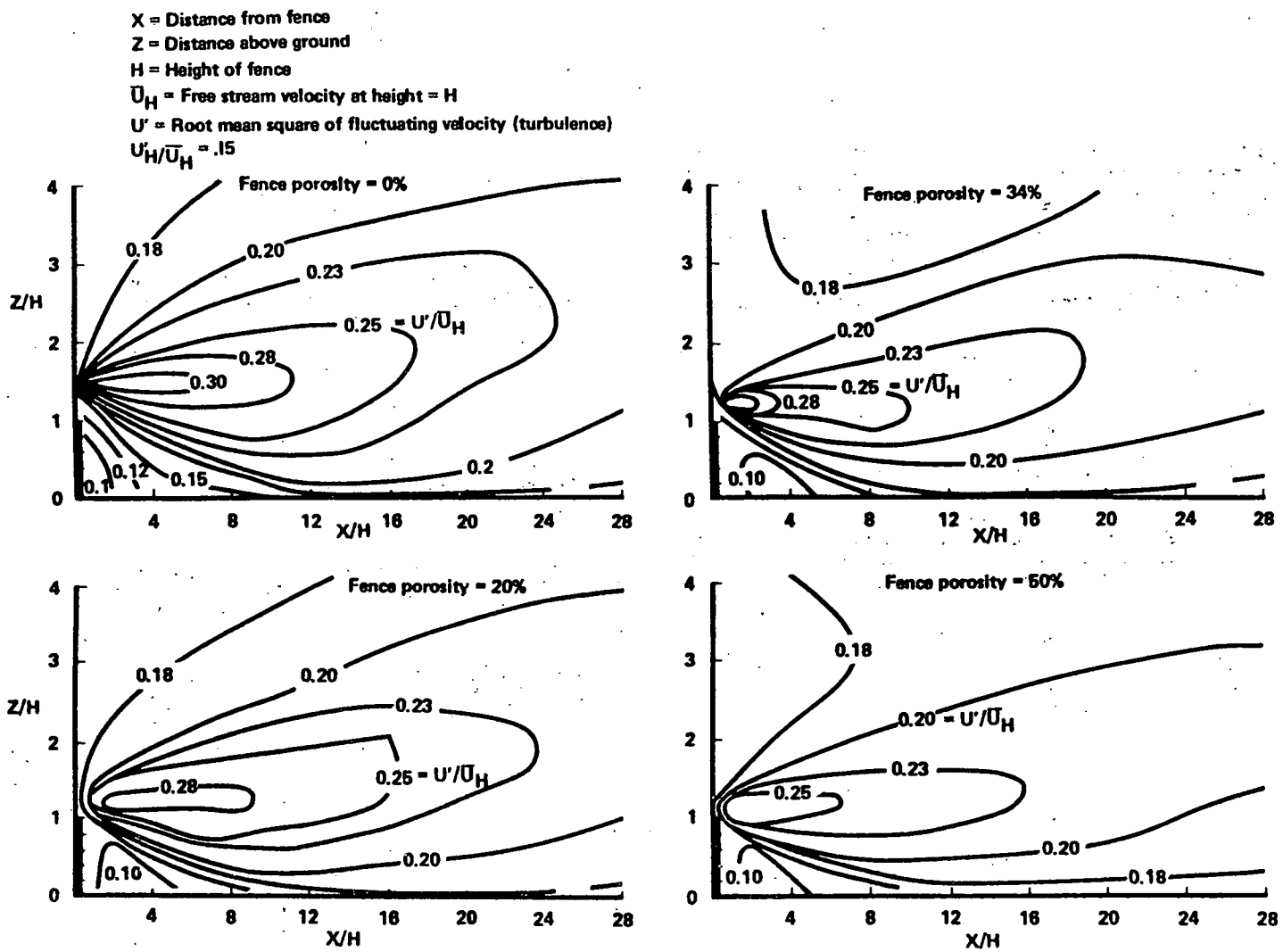

Figure 4-3. Effect of Fence Porosity on Wind RMS Turbulence

$\overline{U}$ = Mean steady state velocity
n = Frequency (Hz)
$\overline{u}$ = Mean of fluctuating velocity
H = Height of fence
X = Distance from fence
Z = Distance above ground

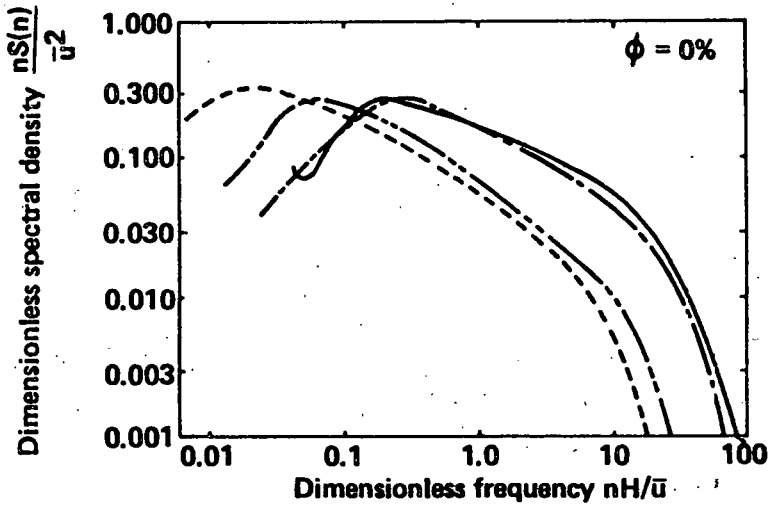

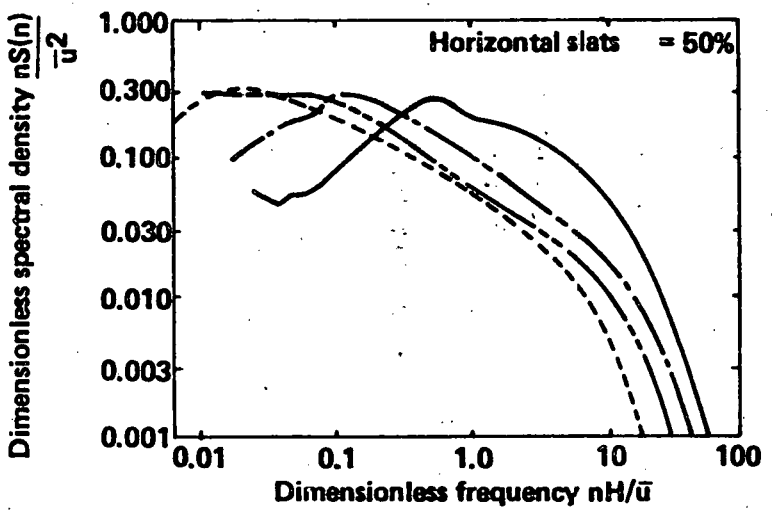

------- Approach flow spectrum at z = 50mm

Symbol	x/H	z/H	$\overline{U}$ (local)
———	2	0.6	2.35 m/sec
—·—·—	6	0.6	3.8
—··—	15	1.0	8.0

$\overline{U}_H$ = 11.34 m/sec

------- Approach flow spectrum at z = 50mm

Symbol	x/H	z/H	$\overline{U}$(local)
———	2	0.6	4.3 m/sec
—·—·—	6	0.6	6.1
—··—	15	1.0	9.15

Figure 4-4. Effect of Fence Porosity on Turbulence Behind Fence

obtain lift and drag force coefficients. The results from Modi's study were used in this contract to validate the theoretical results calculated using a Boeing developed computer program for separated flow analysis.

4.3 Wind Velocity Profiles in Ground Proximity

Investigators have assumed a variety of shapes for the velocity profile used in theoretical and experimental studies to match the natural boundary layer velocity profile found in nature. There are essentially two analytical representations used consisting of either a logarithmic or power law.

The logarithmic representation was developed using Prandtl's mixing length hypothesis. Prandtl [26] assumed that ℓ (length) is proportional to y (boundary layer thickness), i.e.,

$$\ell = ky$$

Then the change in velocity (V) in the boundary layer is

$$\frac{\partial V}{\partial y} = \frac{1}{ky}\sqrt{\bar{\tau}/y}$$

which on integration yields

$$V = \frac{1}{k}\sqrt{\bar{\tau}/\rho}\ \ln y + \text{constant}$$

where $\bar{\tau}$ = shear stress including Reynolds stress

ρ = fluid density

Von Karman's [27] hypothesis and Squire [28] dimensional theory yield results which differ from Prandtl's only in the value of the constant k. In general, the logarithmic profile is found to be valid only in regions close to the surface where viscous effects tend to dominate over turbulent mechanisms. Sakamoto [13,14] and Seginer [16] used logarithmic velocity profiles in their studies.

The power law for velocity distribution has its beginning in the older literature of aerodynamics. The power law does lend itself to matching experimental results. It has its origin in the early work (1913) of

Blasius. Prandtl proposed a velocity profile of the form

$$\frac{V}{V_0} = \left(\frac{y}{\delta}\right)^n$$

where V = velocity at height y

V_0 = reference velocity at δ

δ = boundary layer thickness

and found n to equal 1/7 using appropriate assumptions for τ_w (laminar shear stress) based on steady flow considerations. The actual value used for n varies considerably among investigators. Taulbee[15] used a power deficiency law with several different exponents. Counihan[18], Good[8], and Raine[23] used a power law mean velocity profile with exponents of 1/8, 1/7, and 1/6, respectively. Davenport[29] matched theoretical power law velocity profiles to measured profiles over a number of different terrains and reported the results in a table that shows the exponent to vary from 1/2 to 1/10.5. He recommended using 1/7 as the exponent for most open flatlands. Sturrock[30] also measured the wind profile over several types of flatland and growth. Figure 4-5 shows his results compared to a 1/7 power law.

From the overall data and results presented by the numerous investigators, it is concluded that a power law velocity profile with an exponent of 1/7 appears to match most of the velocity profiles found in nature and is a satisfactory velocity profile to use for design purposes for use in open country terrain.

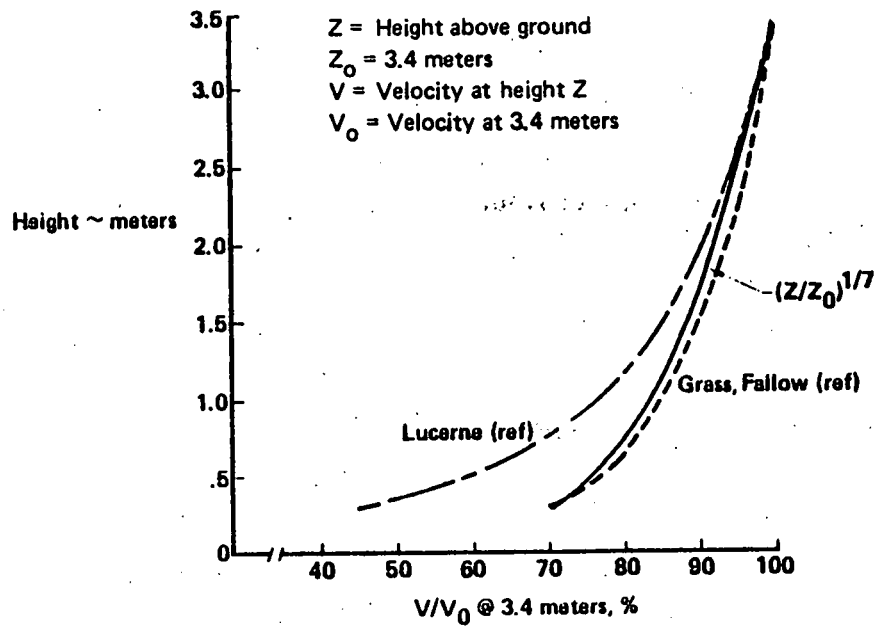

Figure 4-5. Comparison of 1/7 Power Wind Velocity Profile and Experimentally Determined Profiles

THIS PAGE

WAS INTENTIONALLY

LEFT BLANK

5.0 AERODYNAMIC LOADS - FLAT PLATE ARRAYS

Wind aerodynamic forces on bluff bodies is an everyday occurrence and no significance is placed onto its destructive potential until a strong wind storm occurs. After such a storm, the damaging effects of wind caused aerodynamic forces on bluff bodies are readily apparent by the number of roofs torn off of buildings, windows blown out, and trees and fences blown down. Of primary importance in the solar energy field is the wind aerodynamic forces that the solar arrays may be expected to be subjected to during the working life of the arrays. These solar arrays consist of in essence flat plates with aspect ratios that vary from unity to very large. The wind caused aerodynamic forces on these arrays are similar to the aerodynamic forces on fences for large aspect ratio arrays and on sign boards for small aspect ratio arrays. This study is directed at only the wind generated forces on large aspect ratio arrays.

The normal force coefficients determined in aerodynamic experiments on flat plates has a form depicted in Figure 5-1. When a plate is exposed to the wind at a small angle of attack* (angle measured from the wind vector to the plate), the pressure distribution is linear with the angle of attack. At small angles, the flow remains attached to the plate and potential flow aerodynamic theories are valid (Figure 5-2). As the angle of attack is increased, the flow begins to separate from the plate and the total pressure decreases (Figure 5-3). The boundary of the separated flow encompasses a region that is turbulent in nature and is commonly known as the wake. With further increase in the angle of attack, more of the flow separates from the plate, the total pressure decreases to a minimum value and then gradually increases as the width of the wake increases, creating a larger region of turbulent flow. Since the flow is non-linear and turbulent at these larger angles of attack, more sophisticated analysis techniques than potential flow theories must be used to analyze the flow.

*The array tilt angle and the angle of attack (when less than 90°) are identical in magnitude for horizontal winds. However, the definitions and implications of each is completely different and should be recognized. The tilt angle is defined as the angle from horizontal to the plane of the array, whereas the angle of attack is defined as the angle measured from the wind vector to the plane of the array. Consequently, the angle of attack varies as the direction of wind varies and can vary from zero to 180°, whereas the tilt angle varies from 0° to 90°. In addition, for angle of attack measurements the wind does not need to be horizontal.

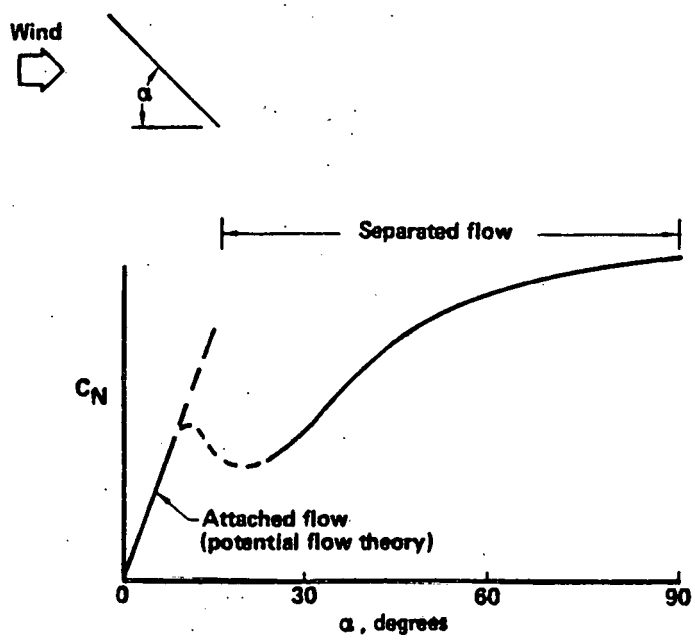

Figure 5-1. Typical Steady State Two-Dimensional Plate Normal Force Coefficient Distribution

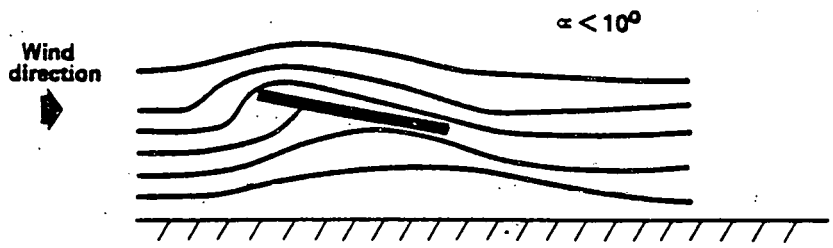

Figure 5-2. Flow Visualization for Flat Plates at Small Angles of Attack

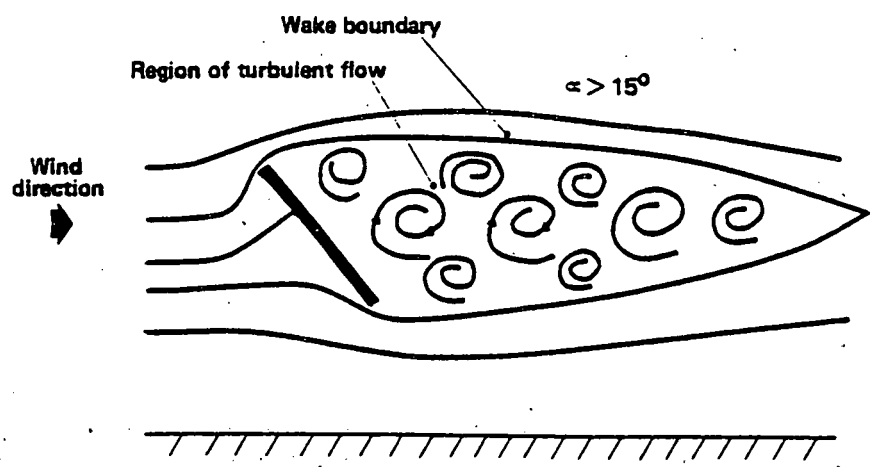

Figure 5-3. Flow Visualization for Flat Plates at Large Angles of Attack

Historically, aerodynamic theoretical methods and procedures have been developed for use in aircraft and aerospace related projects. Most of these methods and procedures were derived for operating in a constant dynamic pressure, constant velocity profile environment. The theoretical development and use of any aerodynamic method is much simpler if the wind environment is a constant velocity profile rather than a varying profile. Consequently, this section evaluates the aerodynamics on high aspect ratio flat plates exposed to a constant wind environment. The effects of velocity profiles on the aerodynamics, specifically a 1/7 power law velocity, is appraised in Section 6.0.

5.1 Theoretical Analysis - Constant Velocity Profile

For fixed photovoltaic arrays that have tilt angles between 20° and 90°, the wind angle of attack is sufficiently large that the air flow over the array is in the separated flow regime. A prototype computer program[32] was used to predict the wake behind the array and the pressure distribution on the array surfaces. Figure 5-4 shows typical results from the computer program (the wake definition and wind velocity on the wake boundaries relative to the freestream velocity for a flat plate array in close ground proximity). The corresponding pressure coefficient distribution on the array is shown in Figure 5-5. (The pressure coefficient distribution and wakes were calculated for a number of different angles of attack and several ground clearances including arrays in free air. The description of the analysis and the results are presented in detail in Appendix A.) It can be seen in Figure 5-4 that the width and length of the turbulent wake and the wake boundary velocity at the array edges increases as the angle of attack (tilt angle) increases. This causes the pressure coefficients to increase on the array surface as the angle of attack increases as shown in Figure 5-5.

Figures 5-4 and 5-5 are for a single array. The computer program cannot analyze the aerodynamic forces on arrays in the wake of other arrays. However, from the literature it is estimated that an aerodynamic force reduction of as much as 2.5 will be attained on the arrays immersed in the wake of other arrays. From the geometry of the arrays (assuming that one array should not be in the shadow of another array with the sun perpendicular to the array face) and that a minimum separation of arrays of 8 feet is required for maintenance access, the location of downwind arrays were determined and superimposed on Figure 5-4 and shown in Figure 5-6. This shows that the arrays will

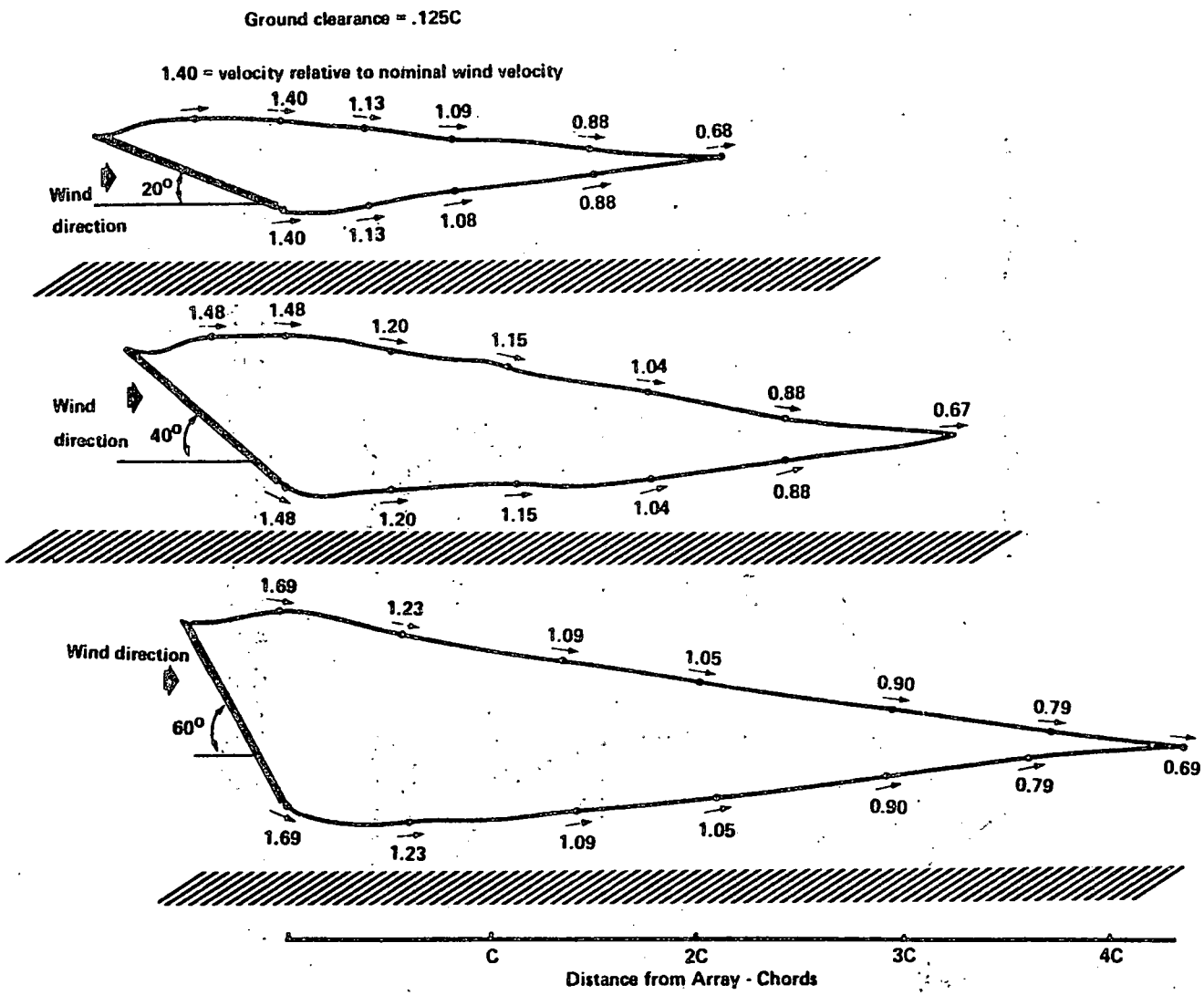

Figure 5-4. Wake Definition and Velocity on Wake Boundaries for Flat Plates in Close Ground Proximity and at Large Angles of Attack

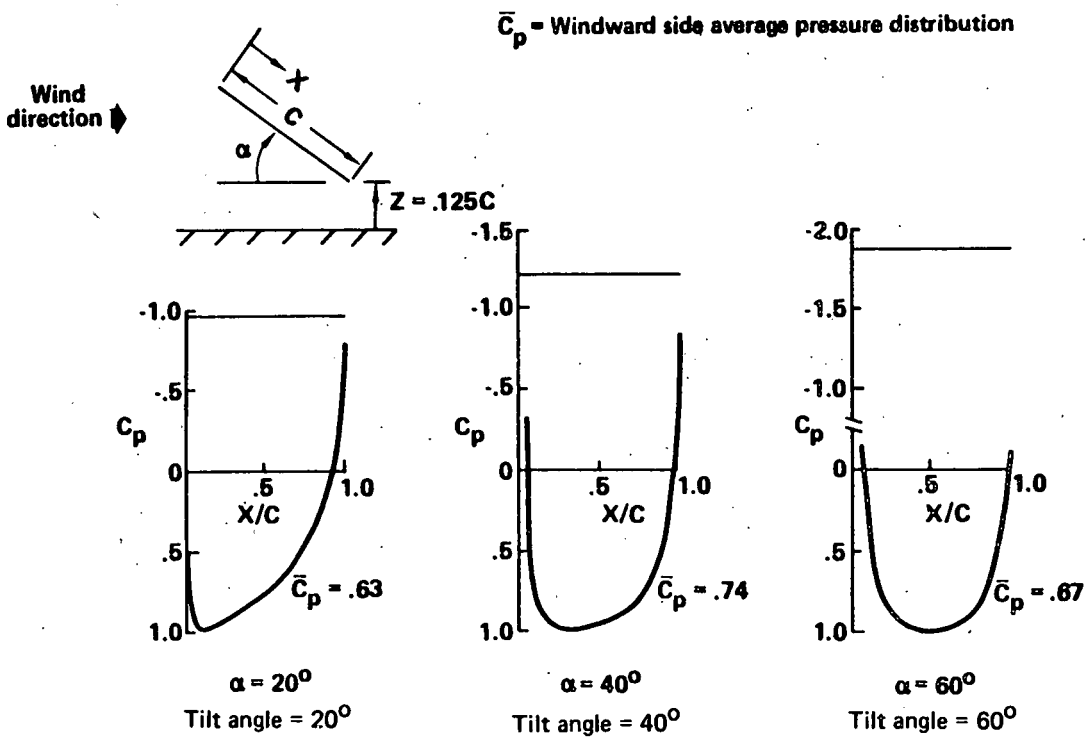

Figure 5-5. Effect of Angle of Attack on Two-Dimensional Theoretical Plate Pressure Distribution in Close Ground Proximity

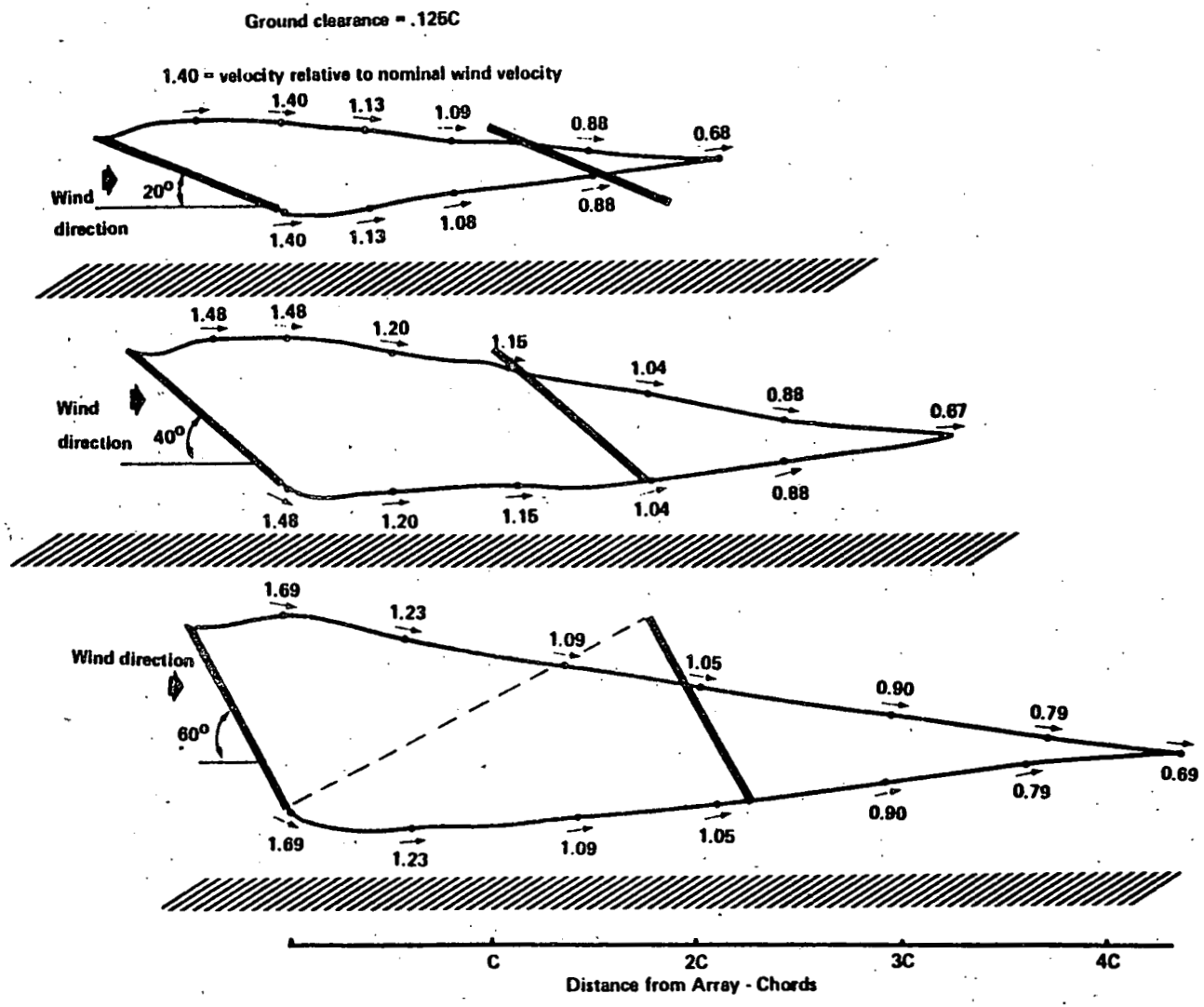

Figure 5-6. Conceptual Location of Downstream Arrays Relative to the Upstream Arrays

be in the wake of each other (at least at minimum array spacing) and a reduction in aerodynamic forces on the downwind arrays will be realized.

If the tilt angle of the fixed photovoltaic arrays are less than 20°, the aerodynamic forces on the arrays must be analyzed by potential flow theory. Since these angles will seldom occur in the continental United States, the results of the potential flow theoretical aerodynamic analysis is only highlighted in this section but is presented in detail in Appendix A together with the separated flow analysis.

Figure 5-7 shows typical pressure coefficient per unit angle of attack distributions along the chord when in close ground proximity. The large pressure coefficients on the leading edge and with a center of pressure located at the quarter chord location are typical for flat plates at small angles of attack. The normal force slope coefficients along the span shown in Figure 5-8 are also typical for potential flow analyses.

When the wind comes at an oblique angle, different than head-on to the array (effectively, the array is yawed to the wind), the aerodynamic pressures will decrease. Figure 5-9 presents the results for a single array with the array yawed at 45° to the wind. Figure 5-9 is a plot of the normal force slope coefficient along the span with the array yawed at 45° to the wind compared to the results for a head-on wind. The magnitude of the results for the yawed array are significantly lower. However, the shape of the force slope coefficient with the wind at 45 degrees is similar but slightly displaced compared to the head-on results.

The aerodynamic pressure coefficients are useful for determining the local pressures on the panels of the photovoltaic arrays. To obtain the total aerodynamic loads on the support structure, the pressures are integrated over the chord to produce normal force coefficients on the panels. Using these normal force coefficients, the area of the panels and the wind dynamic pressure, the total aerodynamic force normal to the array photovoltaic panels can be calculated by the equation:

$$F_N = q\ S\ C_N$$

Figure 5-10 presents the normal force coefficient (C_N) as a function of the array angles of attack for both the potential and separated flow regimes. This figure shows that arrays with tilt angles of around 20°-25° would experience the lowest aerodynamic loads.

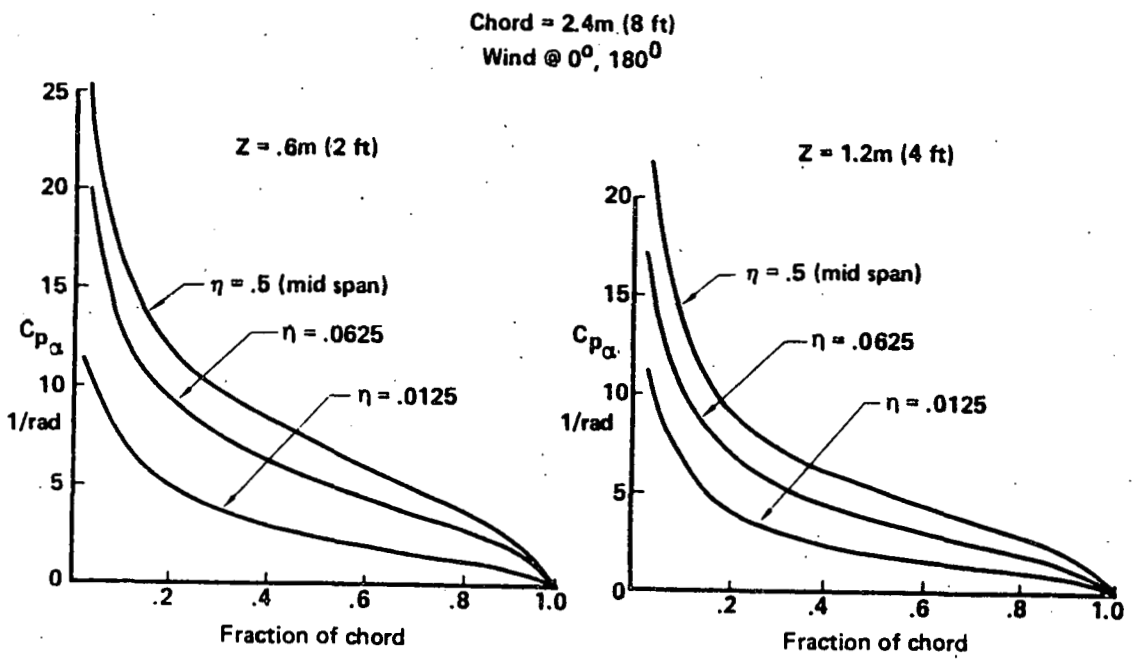

Figure 5-7. Chordwise Pressure Coefficient Distribution at Small Angles of Attack

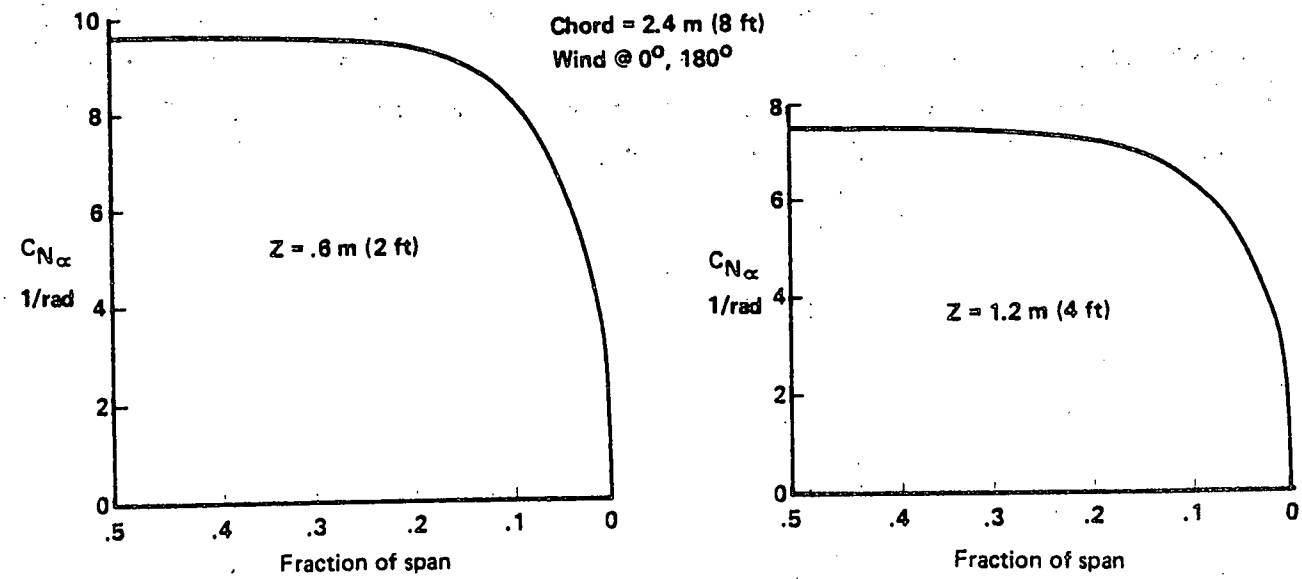

Figure 5-8. Spanwise Force Slope Coefficient Distribution for a Flat Plate at Small Angles of Attack

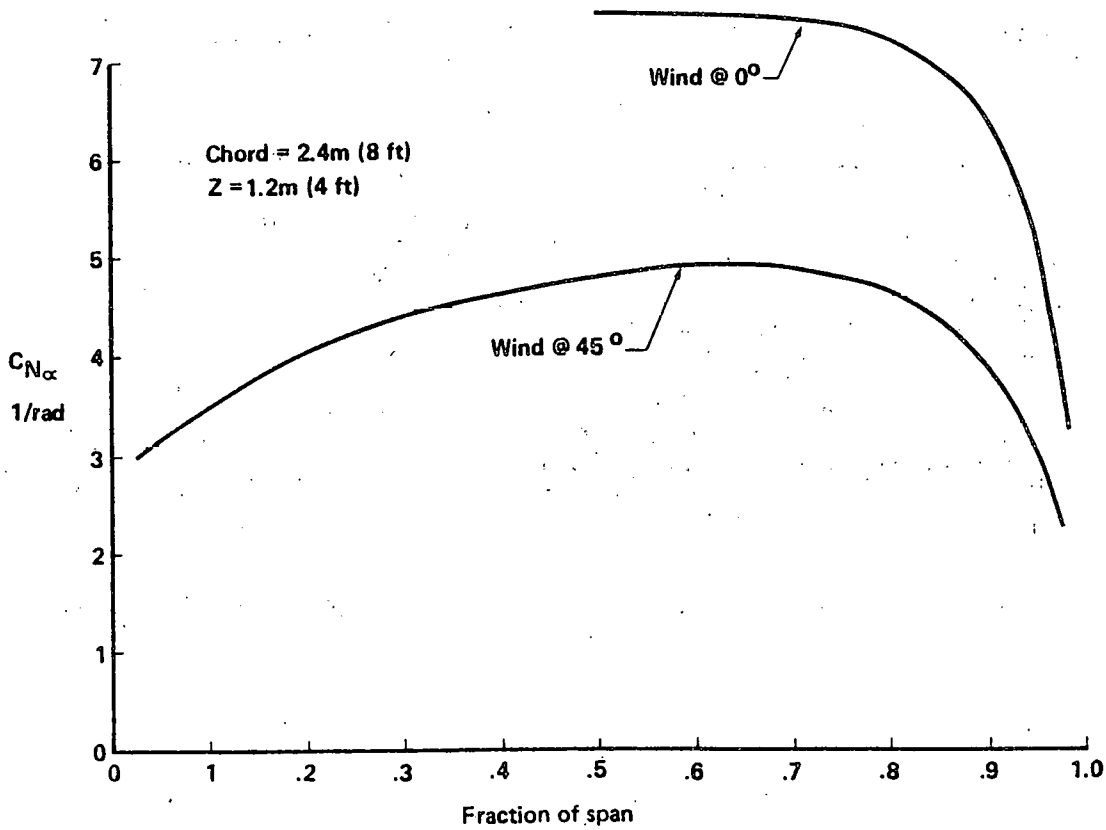

Figure 5-9. Effect of Yawed Wind on Spanwise Force Slope Coefficient Distribution for a Flat Plate

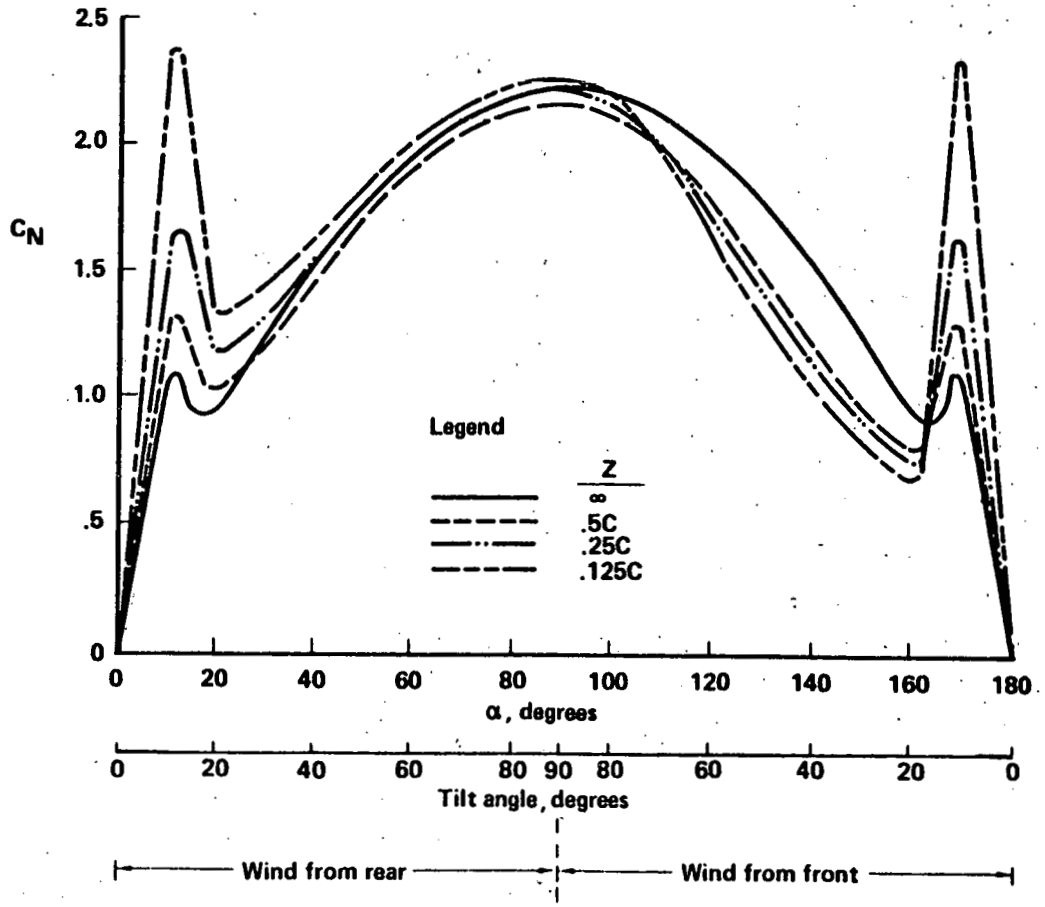

Figure 5-10. Two-Dimensional Plate Theoretical Normal Force Coefficient in Free Air and in Close Ground Proximity

6.0 AERODYNAMIC DESIGN LOADS AND LOAD REDUCING PROCEDURES

Wind aerodynamic loads on a structure will always occur in nature. However, the design of the structure can significantly affect the magnitude of the aerodynamic loads on the structure. This section will present proposed wind design forces for high aspect ratio arrays using the results from the analysis technique defined in Section 5.0 and also identify several means of reducing the wind aerodynamic loading on flat plate arrays. The load alleviation techniques are identified only as wind load reducing devices and are not evaluated for their initial cost requirements and thus whether an actual cost reduction of the total structure is realized.

6.1 Appraisal of Theoretical Analysis for 1/7 Power Law Velocity Profile

In order to develop wind design forces for high aspect ratio arrays, it is necessary to determine the effect of velocity profiles on the aerodynamics of the arrays. The results in Section 5.0 were derived for a constant profile wind. This section will appraise how the results would be affected by a wind profile that varies as a 1/7 power law.

The fact that the aspect ratio of the arrays studied is large, that is, the length to chord ratio is large, the flow around the side edges has no impact on the forces over much of the structure. The side edges only affect the pressures very close to the side. For separated flow on a high aspect ratio array, the base pressure is at least twice the windward-side pressures.[33] Also, the windward pressures are affected very little by the velocity profile and are only a function of the average dynamic pressure on the windward face. As a result, only the base pressures need to be evaluated for wind profile effects, and only the air flow over the top and bottom edges need to be considered for determining the base pressure distribution.

For conditions where an array is placed in close proximity to the ground but with a gap between the array and the ground, air will flow through this ground clearance gap. Because the array is blocking the air flow, the volume of blocked air must flow up over the top of the array or through the ground clearance. Because of the deflection of air caused by this blockage,

the air velocity must increase to allow the blocked volume of air to flow over and under the array. The tendency is for the air velocity to adjust itself to be equal at both the top and bottom edges of the array when the flow over the array is separated flow. If the velocities are not equal, there will be a pressure difference between the top and bottom on the base pressure side and a flow of air from the higher to lower pressure area. In practice, the pressures are found to be essentially constant across the rear side of a plate for large angles of attack.

The difference in array aerodynamic forces resulting from a 1/7 power law velocity profile compared to a constant velocity profile can be appraised by examining the difference in the volume of air blocked (deflected) by arrays using these two profiles. This volume of blocked air can be approximated by the equation:

$$\text{Vol/unit length} = \bar{V} \times \text{Zarray}$$

where

Zarray = height of the array

$\bar{V}$ = average wind velocity over the height of the array

Since the array height is equal for both velocity profiles, the volume of air blocked (deflected) is only affected by the average freestream velocity extending over the region of the array height (elevation from the bottom to the top of the array). By examining Figure 6-1 (the velocity profile of a 1/7 power law), the difference in average velocities between the two profiles can be estimated. This is best done with an example as shown on Figure 6-1.

Assume that a 2.4 m (8 ft) chord array with a ground clearance of .6 m (2 ft) and positioned at an angle of 90° to the ground is to be studied, the average velocity to use for the constant velocity profile would be that of the 1/7 power law velocity at the top of the array. This value is 33.7 meters/sec. Estimating the average velocity for the 1/7 power law velocity profile from Figure 6-1 as 31 meters/sec., using the constant velocity profile would be conservative by 8% for the average velocity which translates into approximated 16% for pressures and forces, since pressures vary as the velocity squared. In general, the wind velocity over the top

and bottom edges for a constant wind profile and a 1/7 power law profile are very nearly equal (8% difference using the example) with the velocity resulting from a constant wind profile being slightly larger. In calculating design aerodynamic loads, if the normal force and pressure coefficient data is obtained using a constant wind profile and the dynamic pressure of the 1/7 power law wind profile at the elevation of the top of the array is used to calculate aerodynamic forces and pressures, the results would be fairly accurate and conservative.

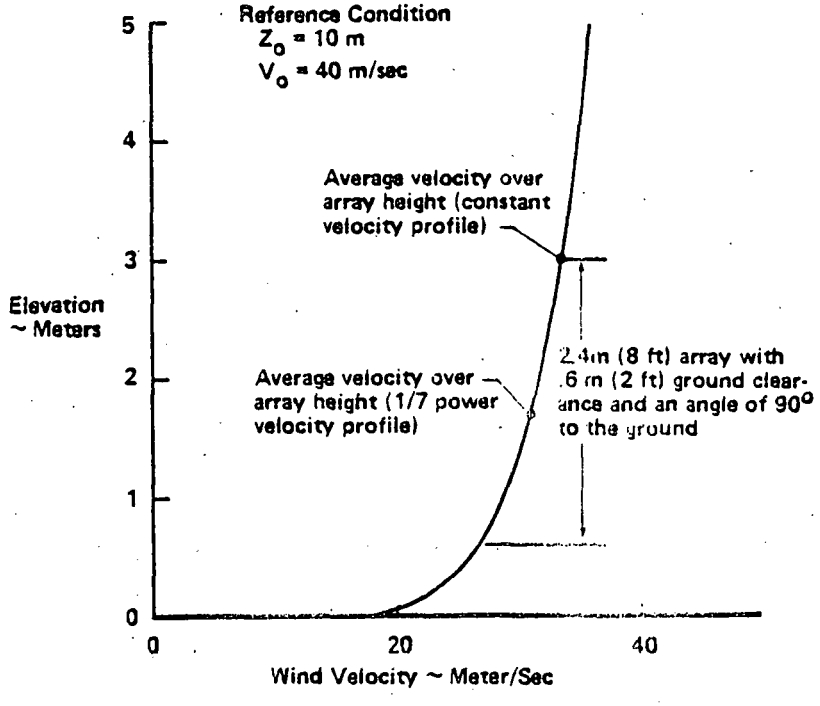

Figure 6-1. One-Seventh Power Law Velocity Profile

Figure 6-2 shows an application of this procedure to obtain the dynamic pressure for use in the calculations. The variation of dynamic pressure with respect to height for a 1/7 power law wind profile with a nominal wind speed of 40 m/sec (90 mph) at a 10 meter (32.8 ft) elevation was calculated and is shown in Figure 6-2. From the geometry of the array (the angle the array makes with the ground, ground clearance, and array chord length), the elevation at the top of the array can be calculated. Figure 6-2 shows the elevation of an array top edge superimposed on the 1/7 power law velocity plot for a 2.4 m (8 ft) chord array with a ground clearance of 1.2 m (4 ft) and for various angles that the array is positioned. The dynamic pressure

to be used in the force and pressure calculations can be easily determined from the specified wind velocity, V_0, and height Z_0, and plotted similar to Figure 6-2 for the array at its design configuration with respect to the ground by using the equations:

$$q = 1/2\,\rho\,V^2$$

where

q = dynamic pressure

ρ = air density

$$V = V_0\left(\frac{Z_H}{Z_0}\right)^{1/7}$$

Z_H = top edge elevation of arrays

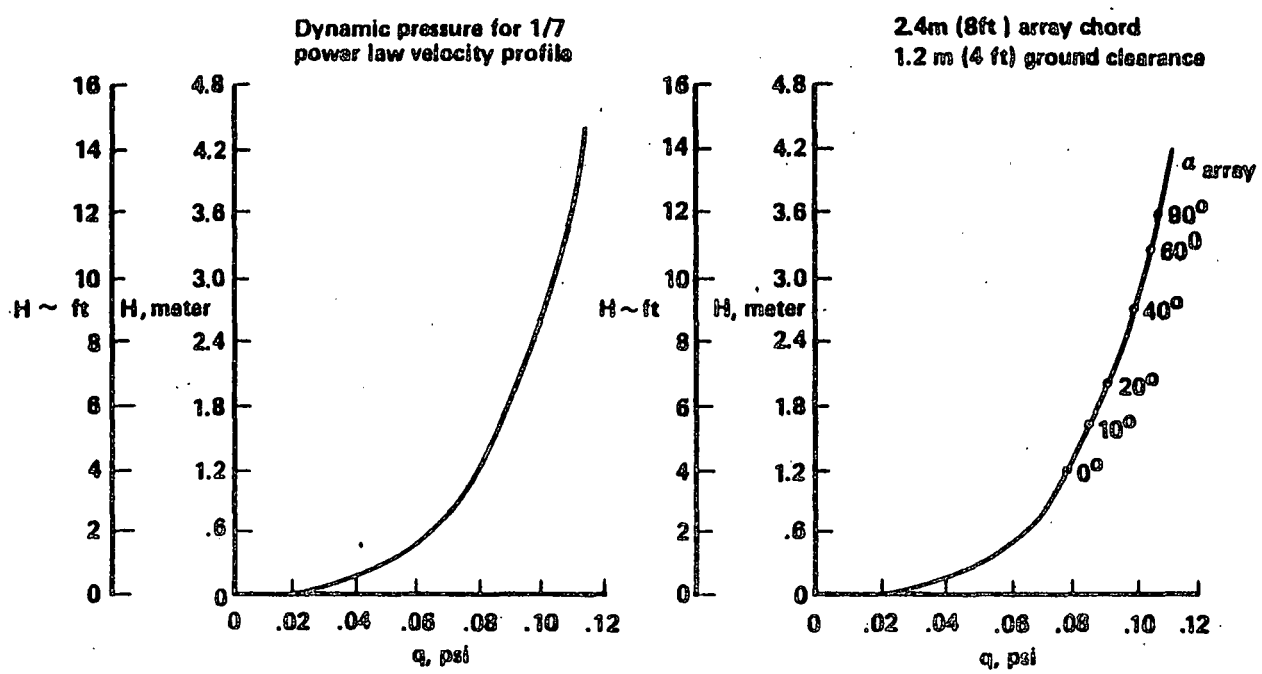

Figure 6-2. Effective Wind Dynamic Pressures for Different Array Angles of Attack

6.2 Proposed Wind Design Forces for High Aspect Ratio Arrays

From the results presented in Section 5.0 and Appendix A, and using the method in Section 6.1 to calculate the dynamic pressure, a set of recommended wind design forces were developed that should provide conservative design loads of array structural supports. Because of the angle of the sun over the continental U.S.A., the angles that the arrays will be relative to the ground are expected to vary from 20° to 60° depending on location. Using this range of angles and the results from Figure 5-10, normal forces, lift forces, and drag forces were calculated for angles of attack from 20° to 60° and 120° to 160° and for ground separation of distances up to 1.2 m (4 ft) but excluding the condition of no ground separation. The dynamic pressures used in the calculations were obtained using the velocity at the elevation of the top edge of the array from the 1/7 power law velocity profile. An interesting result is obtained from the force calculations: although the aerodynamic coefficients increase with decreasing ground clearance, the dynamic pressure decreases with decreasing ground clearance because of a slightly lower elevation at the array top edge. The net result is that the forces calculated at different ground clearances are nearly equal and within the uncertainty of the analysis. The values of the normal force, lift, and drag forces (average forces on the array) are tabulated as a function of ground clearance for various angles of attack and for the 2.4 m (8 ft) and 4.8 m (16 ft) chords and presented in Table 6.1. The envelope of these forces are shown in Figure 6-3 for both chord lengths.

To facilitate the use of this table, the following example is presented as a guide. For this example, assume an array positioned at a tilt angle of 40° with a ground clearance of .6 m (2 ft), a slant height of 2.4 m (8 ft) and subjected to a design wind of 40 m/sec at 10 meters that has a 1/7 power velocity profile. A schematic of this configuration and the aerodynamic forces are shown in Figure 6-4.

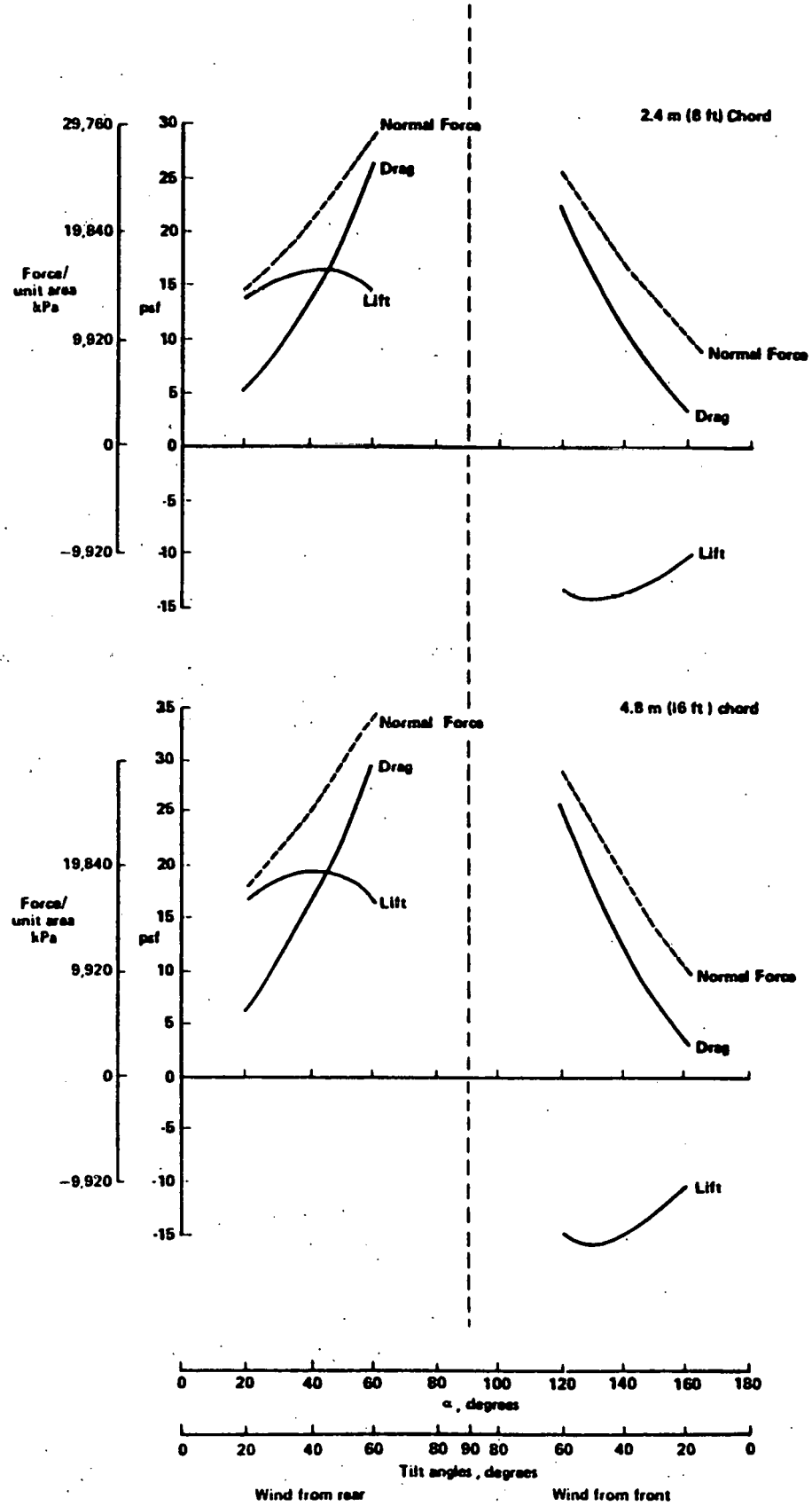

Figure 6-3. Envelope of Wind Forces per Unit Area on Arrays (1/7 Power Law Wind Profile, No Protective Barriers, Single Array)

Table 6-1. Recommended Wind Design Loads (1/7 Power Law Wind Profile, No Protective Barriers, Single Array)

ARRAY CHORD LENGTH=8 ft

Ground Clearance=2 ft

	TILT ANGLE DEGREES	ALPHA DEGREES	WIND VELOCITY FPS	DYNAMIC PRESSURE PSF	C_N	F_N PSF	F_D PSF	F_L PSF
Wind from rear	20	20.0	99.5	11.7	1.18	13.8	4.7	13.0
	25	25.0	101.3	12.2	1.25	15.2	6.4	13.8
	30	30.0	102.9	12.5	1.34	16.8	8.4	14.6
	35	35.0	104.3	12.9	1.44	18.6	10.6	15.2
	40	40.0	105.5	13.2	1.55	20.5	13.1	15.7
	45	45.0	106.5	13.5	1.68	22.6	16.0	16.0
	50	50.0	107.5	13.7	1.79	24.5	18.8	15.8
	55	55.0	108.2	13.9	1.89	26.3	21.5	15.1
	60	60.0	108.9	14.1	1.98	27.9	24.1	13.9
Wind from front	60	120.0	108.9	14.1	1.70	23.9	20.7	-11.9
	55	125.0	108.2	13.9	1.58	22.0	18.0	-12.6
	50	130.0	107.5	13.7	1.44	19.7	15.1	-12.7
	45	135.0	106.5	13.5	1.31	17.6	12.5	-12.5
	40	140.0	105.5	13.2	1.18	15.6	10.0	-11.9
	35	145.0	104.3	12.9	1.06	13.7	7.8	-11.2
	30	150.0	102.9	12.5	.95	11.9	5.9	-10.3
	25	155.0	101.3	12.2	.85	10.3	4.3	- 9.4
	20	160.0	99.5	11.7	.77	9.0	3.1	- 8.5

Ground Clearance=4 ft

ALPHA DEGREES	WIND VELOCITY FPS	DYNAMIC PRESSURE PSF	C_N	F_N PSF	F_D PSF	F_L PSF
20.0	104.6	13.0	1.04	13.5	4.6	12.7
25.0	106.0	13.3	1.15	15.3	6.4	13.9
30.0	107.2	13.6	1.26	17.2	8.6	14.9
35.0	108.3	13.9	1.37	19.1	10.9	15.6
40.0	109.3	14.2	1.48	21.0	13.5	16.1
45.0	110.1	14.4	1.61	23.2	16.4	16.4
50.0	110.9	14.6	1.72	25.1	19.2	16.1
55.0	111.5	14.8	1.83	27.0	22.1	15.5
60.0	112.1	14.9	1.93	28.8	24.9	14.4
120.0	112.1	14.9	1.74	26.0	22.5	-13.0
125.0	111.5	14.8	1.62	23.9	19.6	-13.7
130.0	110.9	14.6	1.49	21.7	16.6	-14.0
135.0	110.1	14.4	1.36	19.6	13.8	-13.8
140.0	109.3	14.2	1.22	17.3	11.1	-13.2
145.0	108.3	13.9	1.11	15.4	8.8	-12.6
150.0	107.2	13.6	1.00	13.6	6.8	-11.8
155.0	106.0	13.3	.91	12.1	5.1	-11.0
160.0	104.6	13.0	.82	10.6	3.6	-10.0

ARRAY CHORD LENGTH=16 ft

Ground Clearance=2 ft

	TILT ANGLE DEGREES	ALPHA DEGREES	WIND VELOCITY FPS	DYNAMIC PRESSURE PSF	C_N	F_N PSF	F_D PSF	F_L PSF
Wind from rear	20	20.0	106.2	13.4	1.34	17.9	6.1	16.8
	25	25.0	108.6	14.0	1.40	19.6	8.3	17.8
	30	30.0	110.7	14.5	1.46	21.2	10.6	18.4
	35	35.0	112.5	15.0	1.54	23.1	13.2	18.9
	40	40.0	114.0	15.4	1.63	25.1	16.1	19.3
	45	45.0	115.3	15.8	1.75	27.6	19.5	19.5
	50	50.0	116.4	16.1	1.86	30.0	22.9	19.2
	55	55.0	117.4	16.3	1.96	32.1	26.3	18.4
	60	60.0	118.2	16.6	2.04	33.9	29.3	16.9
Wind from front	60	120.0	118.2	16.6	1.58	26.2	22.7	-13.1
	55	125.0	117.4	16.3	1.46	23.9	19.6	-13.7
	50	130.0	116.4	16.1	1.33	21.4	16.4	-13.7
	45	135.0	115.3	15.8	1.21	19.1	13.5	-13.5
	40	140.0	114.0	15.4	1.09	16.8	10.8	-12.9
	35	145.0	112.5	15.0	.98	14.7	8.4	-12.0
	30	150.0	110.7	14.5	.88	12.8	6.4	-11.1
	25	155.0	108.6	14.0	.80	11.2	4.7	-10.1
	20	160.0	106.2	13.4	.72	9.6	3.3	- 9.0

Ground Clearance=4 ft

ALPHA DEGREES	WIND VELOCITY FPS	DYNAMIC PRESSURE PSF	C_N	F_N PSF	F_D PSF	F_L PSF
20.0	109.8	14.3	1.18	16.9	5.7	15.9
25.0	111.9	14.8	1.25	18.6	7.8	16.8
30.0	113.6	15.3	1.34	20.5	10.2	17.8
35.0	115.1	15.7	1.44	22.7	13.0	18.6
40.0	116.5	16.1	1.55	25.0	16.0	19.1
45.0	117.6	16.4	1.68	27.6	19.5	19.5
50.0	118.7	16.7	1.79	29.9	22.9	19.2
55.0	119.5	16.9	1.89	32.1	26.3	18.4
60.0	120.3	17.2	1.98	34.0	29.4	17.0
120.0	120.3	17.2	1.70	29.2	25.3	-14.6
125.0	119.5	16.9	1.58	26.8	21.9	-15.3
130.0	118.7	16.7	1.44	24.1	18.4	-15.5
135.0	117.6	16.4	1.31	21.5	15.2	-15.2
140.0	116.5	16.1	1.18	19.0	12.2	-14.5
145.0	115.1	15.7	1.06	16.7	9.5	-13.6
150.0	113.6	15.3	.95	14.5	7.2	-12.6
155.0	111.9	14.8	.85	12.6	5.3	-11.4
160.0	109.8	14.3	.77	11.0	3.7	-10.3

NOTE: THE FORCES, F_N, F_L, AND F_D ARE <u>NOT</u> ADDITIVE, SEE FIGURE 6-4 BELOW.

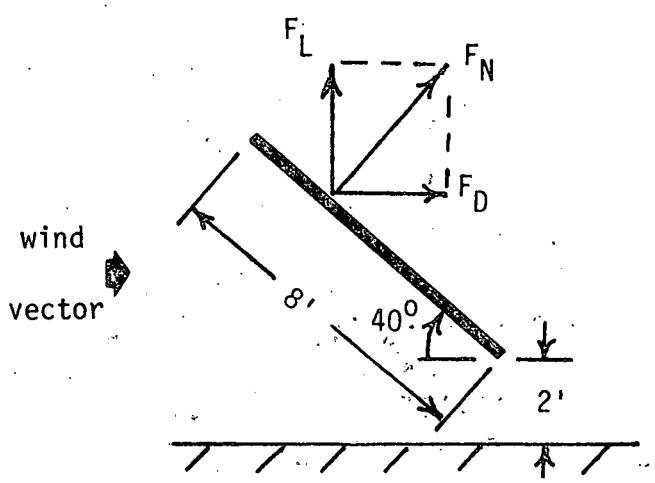

Figure 6-4. Array Configuration and Aerodynamic Force Schematic

The wind can approach the array from either the front or back so both conditions must be considered. Figure 6-4 shows the wind from the back which will produce an aerodynamic force normal to the array and in an upward direction. Conversely, a wind from the front will also produce an aerodynamic force normal to the array but in a downward direction. This normal force can be resolved into a horizontal and vertical force (drag and lift, respectively by the tilt angle geometric parameter and the direction of the wind. This is already performed in Table 6-1 as F_D and F_L. Using Table 6-1, the average normal force on the array is 20.5 psf and 15.6 psf for a wind angle of 180° and 0°, respectively, and for a tilt angle of 40°. For a slant height of 8', the normal force per foot of span is:

$$F_N = 8 \times 20.5 = 164 \text{ lbs/ft @ wind angle} = 180°$$

$$= 8 \times 15.6 = 122.4 \text{ lbs/ft @ wind angle } 0°$$

If the average normal force needs to be resolved into horizontal and vertical components, F_D and F_L respectively, they can be obtained directly from the table as:

$$F_D = 13.1 \text{ psf @ wind angle} = 180°$$
$$= 10.0 \text{ psf @ wind angle} = 0°$$
$$F_L = 15.7 \text{ psf @ wind angle} = 180°$$
$$= -11.9 \text{ psf @ wind angle} = 0°$$

From this, it is seen that the vertical force is up for a wind from the rear and down for a wind from the front. The drag force is always in the direction of the wind.

Although arrays positioned behind the windward front array would have reduced aerodynamic forces, the theoretically calculated reduction (limited to spacings with arrays not in wakes) is not sufficient to affect the results by more than 10%. To obtain forces on arrays in the wake of other arrays other than an estimated reduction of 60% requires use of test methods. Consequently, the forces shown in Figure 6-3 and Table 6-1 would be satisfactory design loads at this time for all of the arrays with the forces for the arrays behind the front array being considerably more conservative than the front array forces.

6.3 Array Key Load Parameters and Sensitivities

A designer can minimize the loads on the basic solar arrays by optimizing the position of the arrays with respect to the ground, themselves, and wind directions. This section identifies the key parameters on the basic array and their sensitivity to these parameters based on the results from Section 5.0 and Appendix A.

Key parameters affecting the aerodynamic loads on arrays when the arrays are positioned at tilt angles greater than 15° are:

- plate angle of attack
- ground clearance
- array spacing
- array yaw angle to the wind
- wind dynamic pressure (varies as the freestream wind velocity squared which is dependent on the reference velocity, velocity profile and elevation of the top of the array).

Figure 6-5 shows the sensitivity of these parameters for typical ranges that these parameters may encompass. The sensitivity is shown as a function of the aerodynamic force for each parameter normalized to the maximum expected value of the parameter.

Of these parameters the array yaw angle must be selected to give the maximum force which occurs at zero yaw angle for most locations since the wind direction usually can come from any direction. For other parameters the aerodynamic forces increase with increasing angle of attack, wind dynamic pressure, and decreasing ground clearance (until very close to the ground where the flow becomes significantly blocked from flowing through the ground clearance gap).

The sensitivity to array spacing is essentially constant when one array is outside of the wake of another. The wake distance depends on the angle of attack and was calculated to be from 2 to 5 array chords in length. When the downwind array is positioned in the wake of the upstream array, the sensitivity was estimated from the wake velocity profiles behind fences as determined from the literature. A wind tunnel test would be required to accurately determine the aerodynamic force sensitivity to this parameter.

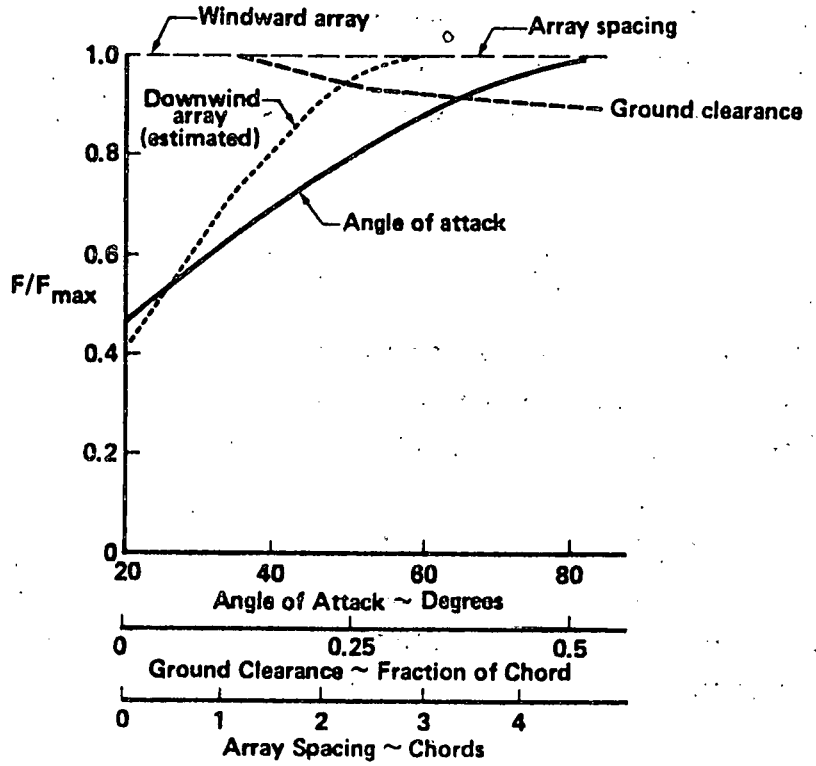

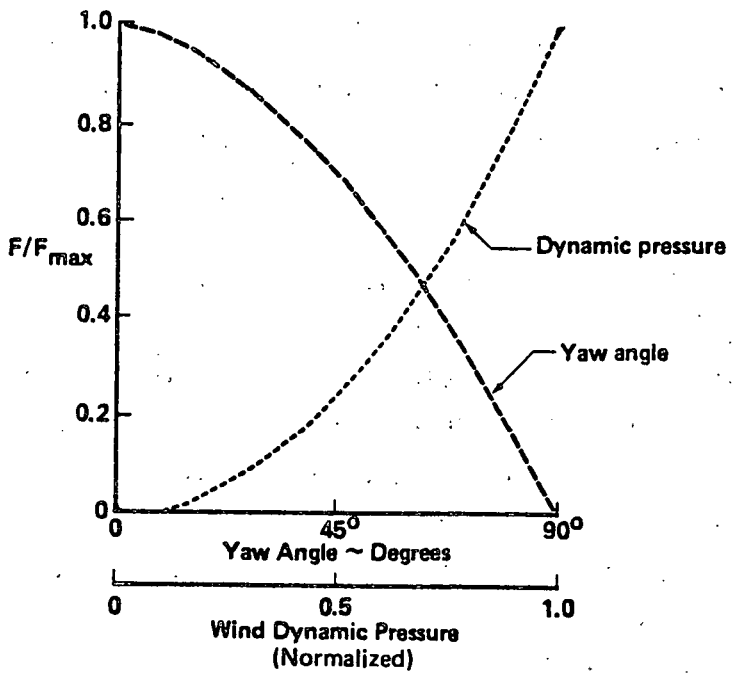

Figure 6-5. Key Wind Loads Parameters and Their Sensitivity in Separated Flow Analyses

Of these parameters shown in Figure 6-5, the largest aerodynamic force reduction can be obtained by minimizing the wind angle of attack to the array and the wind dynamic pressure (wind velocity). The sensitivity of the ground clearance and array spacing is not nearly as great as these other parameters.

6.4 Protective Wind Barriers and Resulting Array Loads

The use of wind barriers such as fences can effect some reduction in the steady state velocity of the wind by interrupting the air flow. Figure 4-1 of Section 4.0 shows conceptually the flow disruption that a fence will cause.

Based on published results in the literature and specifically from the paper presented by Raine[23], reduction in the steady state velocity behind a fence and the resulting aerodynamic steady state loading on a structure behind the fence can be estimated. The velocity isotachs (lines of equal velocity) behind the fences of different porosity are shown in Figure 4-2. It should be noted that these isotachs are for the condition that no barrier exists downstream of the fences. Barriers downstream (such as photovoltaic arrays) will affect the upstream flow depending on their location and shape. Nevertheless, these isotachs do give a quantitative idea of the flow field and are useful in positioning the arrays behind a fence and in evaluating the height and type of porosity of a fence to realize the greatest reduction in aerodynamic loads on the arrays.

The isotachs in Figure 4-2 were used to translate the effect that the fence has on the wind velocity behind a fence using a 1/7 power law for the free-stream velocity profile. The wind velocity profiles are presented in Figure 6-7 for five locations downstream shown in Figure 6-6 of a 2.5 m (8.2 ft) fence of different fence porosity. It should be noted that because the isotachs do not show flow directions, the velocity profiles derived from the isotachs also cannot show flow direction. In fact, some of the velocities shown in Figure 6-7 may be reversed. From Figure 6-7, the position close to the fence yields the largest decrease in steady state flow velocity. This is partially offset because the turbulence level in the flow is increased closer to the fence especially at fence top elevations as indicated by Figure 4-3.

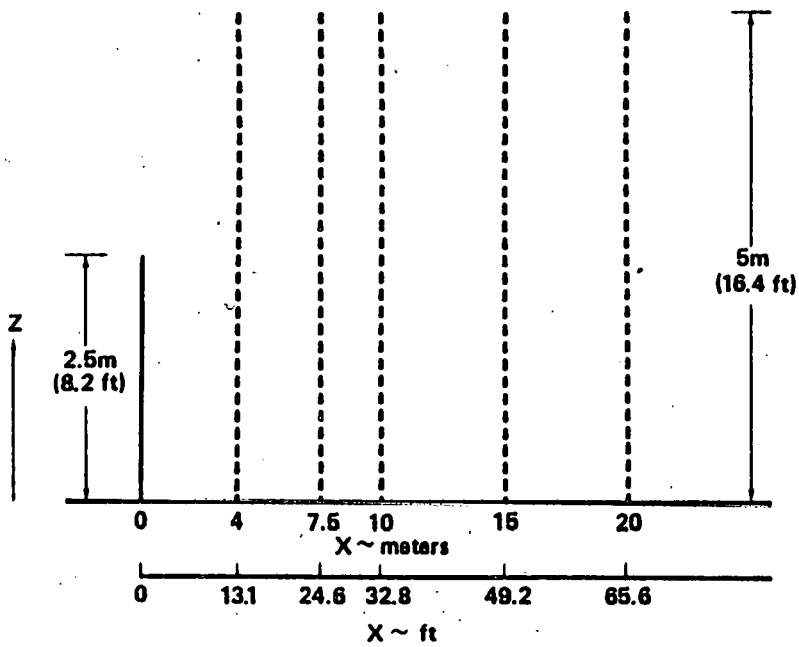

Figure 6-6. Location of Velocity Profile Determinations Relative to the Fence

CONDITIONS:

- Free stream velocity = 40 m/sec (90 mph) @ 10 m(32.8 ft) elevation
- Fence height = 2.5 m (8.2 ft)
- Steady state wind

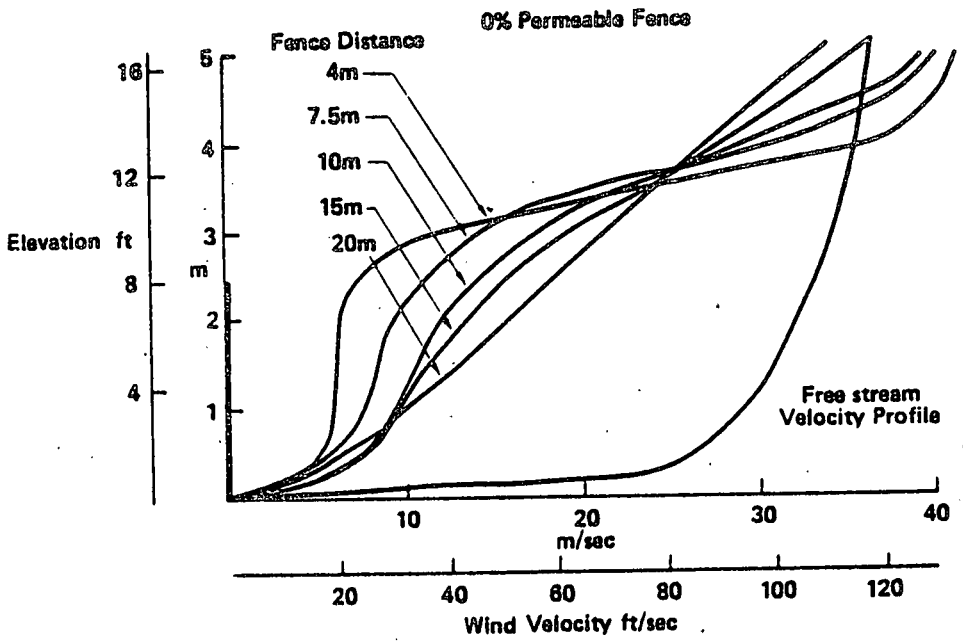

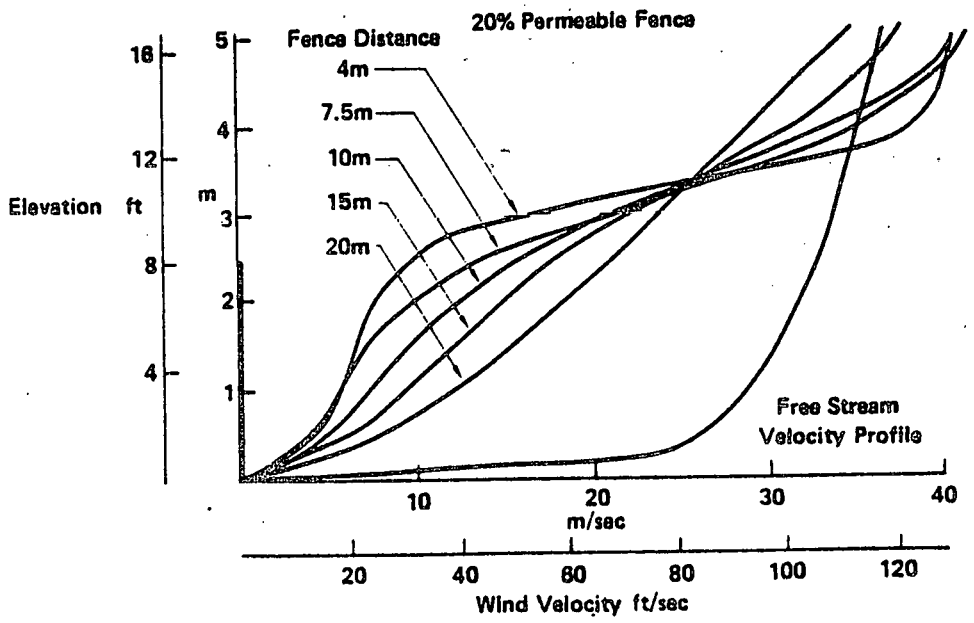

Figure 6-7. Fence Blockage Effect on Wind Velocity Profile

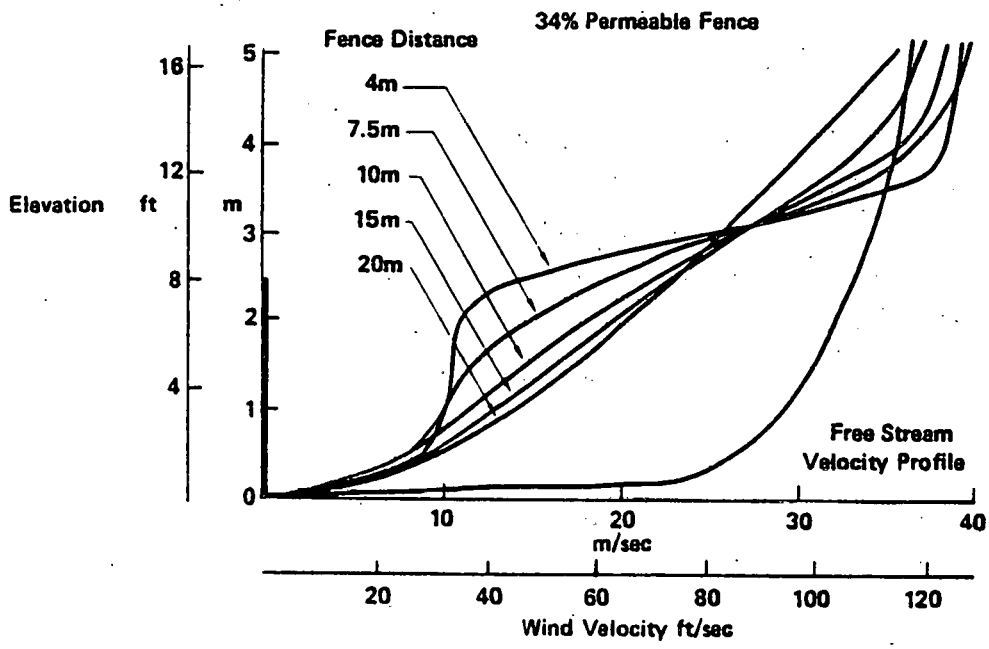

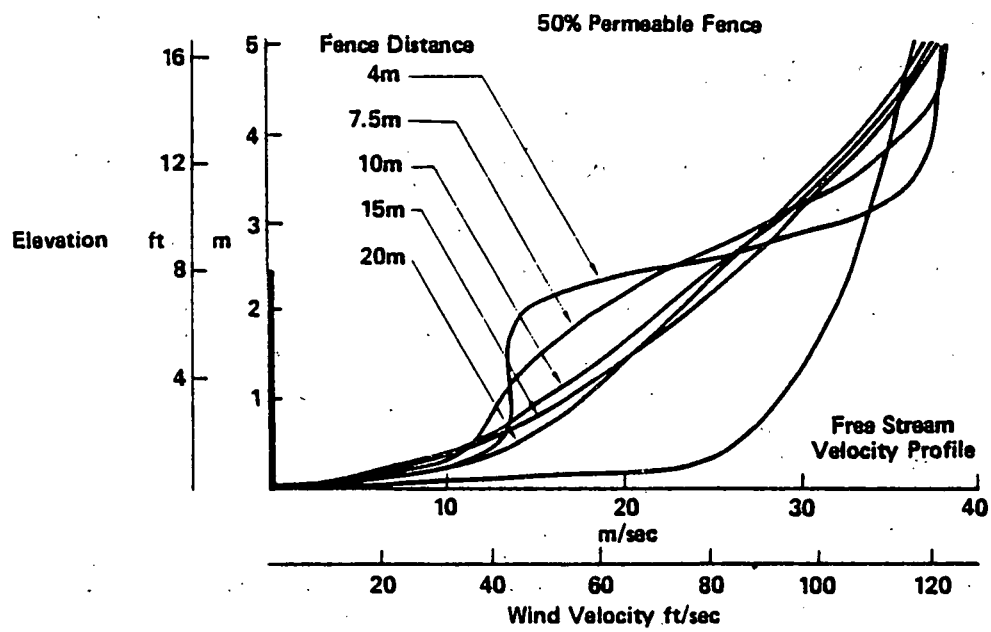

Figure 6-7. Fence Blockage Effect on Wind Velocity Profile – Concluded

Nevertheless, the reduction in steady state flow behind a fence causes significant reduction in wind dynamic pressures (as much as 90 percent) resulting in a net load reduction of as much as 60% because of the increased turbulence. This also indicates that if one array can be placed in the wake of another array, significant reduction of aerodynamic forces on downstream arrays could be achieved.

Performance and cost studies should be made if a wind barrier is considered as a device to reduce wind aerodynamic forces. Adjusting parameters of such things as height of fences relative to array heights, closeness of the fence to the array field and porosity of the fence may result in an overall cost reduction for an array field. Figure 6-8 is a cross plot of Figure 6-7 and details the velocity profiles as a function of fence permeability derived from the data presented from Raine[23]. This data shows that fences of 0% and 20% porosity give slightly better steady state wind protection than 35% and 50% porosity. However, from Figures 4-3 and 4-4 the root mean squared turbulence velocity (unsteady flow) is higher for the 0% porosity than the 50% porosity fence. The overall protection afforded by the fences appears to be best for the 20% porosity fence although this is also dependent on the location (distance and elevation) behind the fence.

Although the height of the fence used in Figures 6-7 and 6-8 is 2.5 m (8.2 ft) high, any fence higher than this can be evaluated from these figures by simply multiplying all scales of the figures by the ratio of new fence height in meters divided by 2.5 meters. The error involved using this procedure is minimal because the slope of the 1/7 power velocity profile curve at the fence height of 2.5 m (8.2 ft) and above is small. As an example, using this method for a 5 m (16.4 ft) high fence would result in an error less than 10% for the velocity profiles.

The results shown in Figures 6-7 and 6-8 can be used to estimate the reduction in the wind dynamic pressures and the resulting aerodynamic forces on arrays positioned behind a fence. This can be best shown by using an example of the effect that a fence located a specified distance from an array has on the forces in Table 6-1 for one ground clearance and array slant height. For this example, the conditions used are a 34% permeable 2.5 m (8.2 ft) fence with an array located 4 meters behind the fence. The array is assumed to have a 2.4 m (8 ft) slant height and a .6 m (2 ft) ground clearance.

CONDITIONS:

- Free stream velocity = 40m/sec (90 mph) @ 10m (32.8 ft) elevation
- Fence height = 2.5 m (8.2 ft)
- Steady state wind

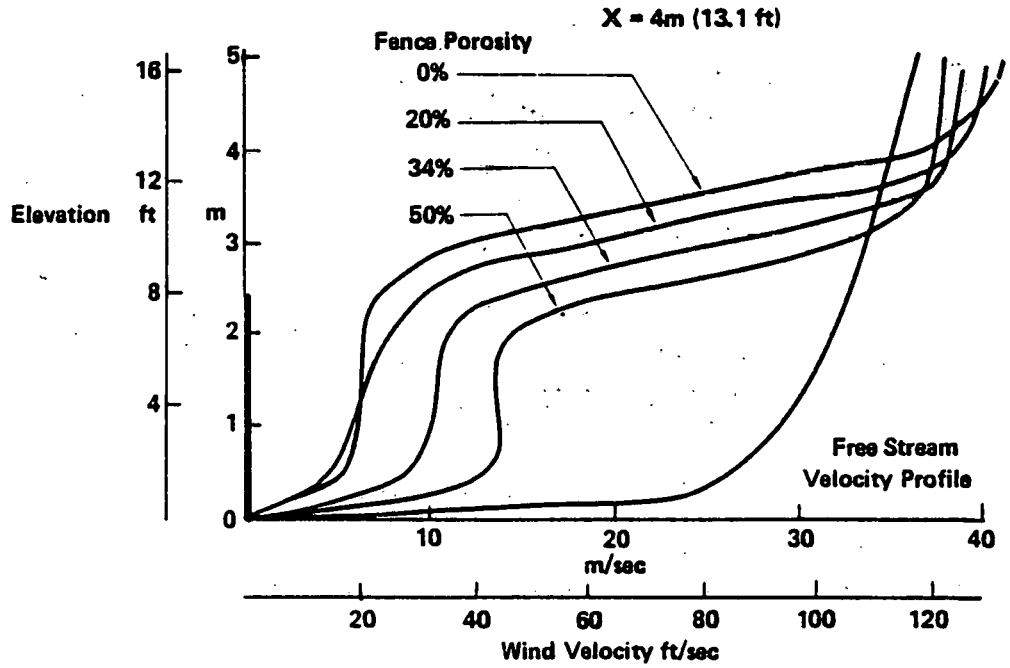

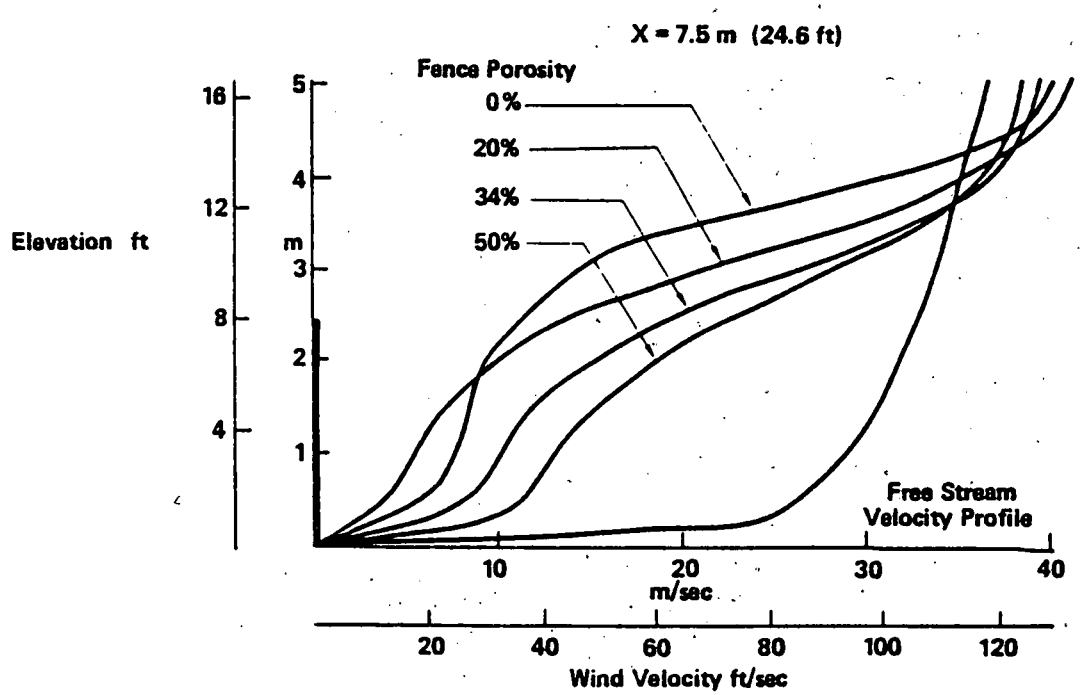

Figure 6-8. Effect of Fence Porosity on Wind Velocity Profile

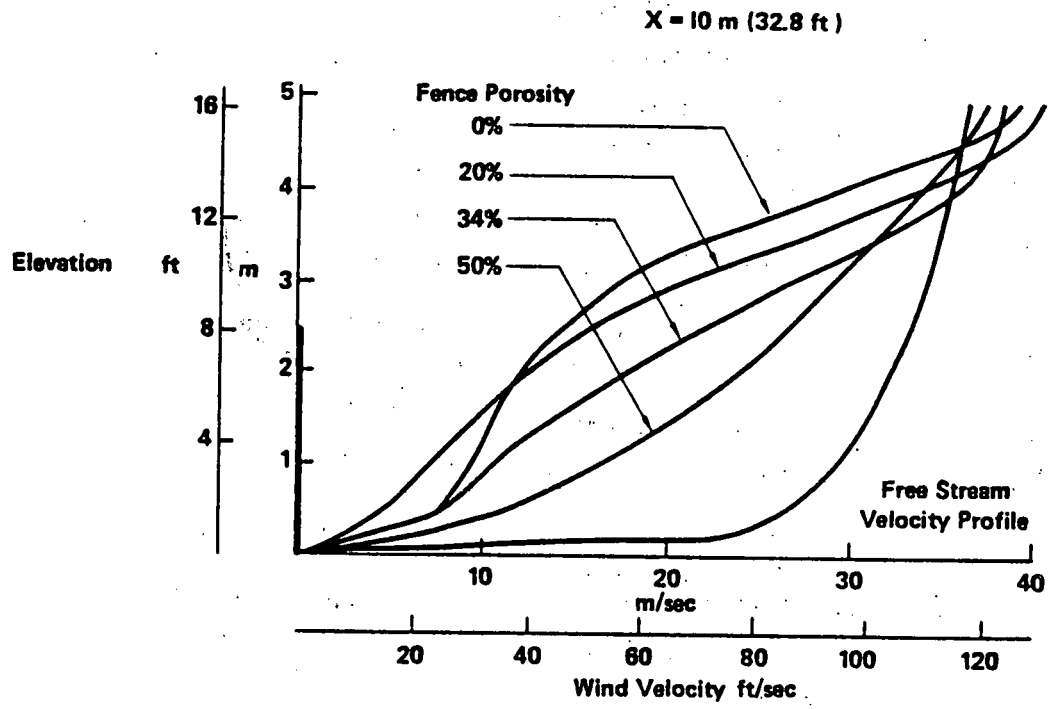

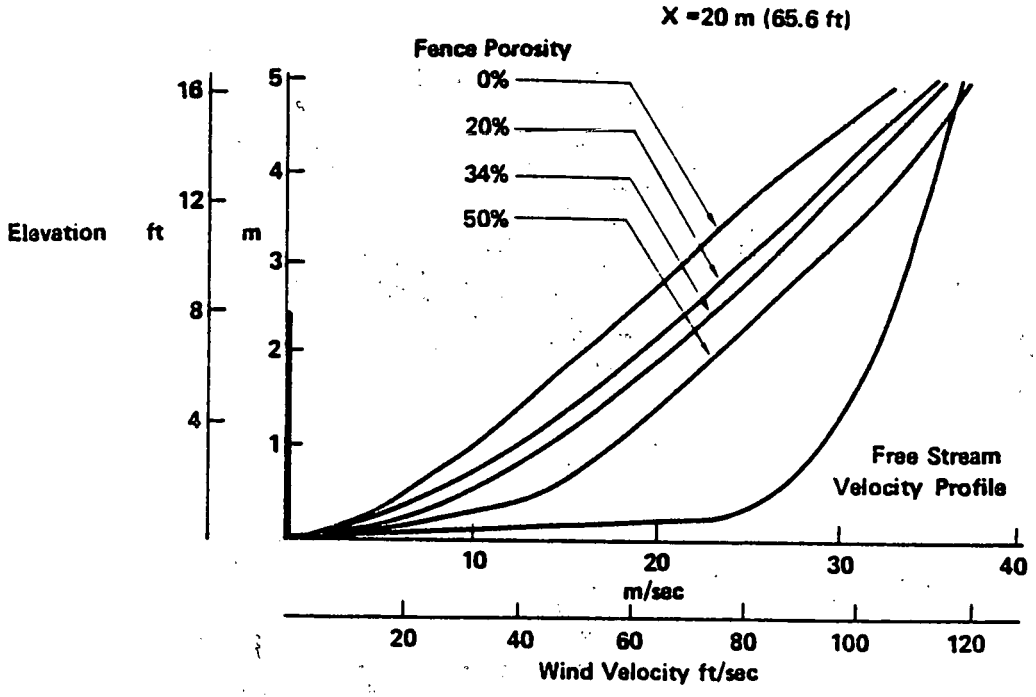

Figure 6-8. Effect of Fence Porosity on Wind Velocity Profile —Concluded

The top of an array with a tilt angle of 20°, ground clearance of .6 m (2 ft) and a slant height of 2.4 m (8 ft) would be located at:

$$Z = 8 \sin 20° + 2'$$
$$= 4.75 \text{ ft. above the ground}$$

Examining Figure 6-8 for a 34% permeable fence and a fence distance of 4 meters, the velocity at a height of 4.75 ft. is approximately 34 ft/sec. The dynamic pressure for a 34 ft/sec wind is calculated as:

$$q = 1/2 \rho V^2$$
$$= .5 (.002378)(34)^2$$
$$= 1.374 \text{ psf}$$

Raine[23] shows that the fence causes increased turbulence which as an estimate may increase the local velocity by 2 (local dynamic pressure by 4). If the local turbulence correlation function on the panel is one (1.0), that is, the velocity due to the turbulence affects all of the panel simultaneously (in phase and magnitude), the steady state wind loads would have to be increased by 400% to account for the unsteady wind loads due to turbulence. However, because turbulence is random, the local turbulence correlation function is much less than one, and the unsteady wind loads are only a fraction of the steady state loads varying from near zero to less than 50%[36]. It should be noted that although the unsteady wind loads are less than 50% of the steady state loads, the local unsteady pressures on any part of the panel may be several magnitudes larger than the steady state pressures. Using 50% in the example,which is conservative for the unsteady loads[36], the calculated steady state dynamic pressure is increased by 50% to account for the increased turbulence:

$$q = 1.5 \times 1.374$$
$$= 2.06 \text{ psf}$$

The dynamic pressure is calculated to be 11.7 psf without a fence. The normal force, drag force, and lift forces are calculated for a wind from the rear as:

$$F_N = q\, C_N$$
$$= 2.06 \times 1.18$$
$$= 2.44 \text{ psf}$$
$$F_D = .83 \text{ psf}$$
$$F_L = 2.29 \text{ psf}$$

Performing these calculations for all of the tilt angles presented in Table 6-1 and for an array of dimensions detailed in this example, the normal,drag,and lift forces are obtained and presented in Table 6-2. Comparing Table 6-2 to the applicable portion of Table 6-1 for the large tilt angle of 60°, the aerodynamic force on arrays behind the fence is 60% of those without a fence. The reduction in wind loads at this tilt angle would be much greater if the top of the array was lower compared to the fence. In this example, the top of the array is approximately three-quarter feet (3/4') above the top of the fence. For heights greater than the fence height, the wind velocity profile rapidly increases to the undisturbed wind velocity profile (see Figure 6.8) resulting in higher wind loads.

Table 6-2. Estimated Wind Loads Behind a Fence

Conditions
Array chord = 2.4 m (8 ft)
Array ground clearance = 0.6 m (2 ft)
Fence height = 2.5 m (8.2 ft)
Fence to array separation = 4m
Fence porosity = 34%

	Tilt angle degrees	Alpha degrees	Wind velocity fps*	Dynamic pressure psf**	C_N psf	F_N psf	F_D psf	F_L psf
Wind from rear	20	20	34	2.06	1.18	2.44	.83	2.29
	25	25	34	2.06	1.25	2.58	1.09	2.34
	30	30	34	2.06	1.34	2.77	1.39	2.40
	35	35	36	2.31	1.44	3.33	1.91	2.72
	40	40	42	3.14	1.55	4.87	3.13	3.73
	45	45	47	3.94	1.68	6.62	4.68	4.68
	50	50	53	5.01	1.79	8.97	6.87	5.77
	55	55	60	6.42	1.89	12.14	9.94	6.96
	60	60	69	8.49	1.98	16.81	14.56	8.41
Wind from front	60	120	69	8.49	1.70	14.43	12.50	−7.22
	55	125	60	6.42	1.58	10.14	8.30	−5.81
	50	130	53	5.01	1.44	7.22	5.53	−4.64
	45	135	47	3.94	1.31	5.16	3.65	−3.65
	40	140	42	3.14	1.18	3.71	2.39	−2.84
	35	145	36	2.31	1.06	2.45	1.40	−2.00
	30	150	35	2.06	.95	1.96	.98	−1.70
	25	155	34	2.06	.85	1.76	.74	−1.59
	20	160	34	2.06	.77	1.59	.55	−1.49

*Wind velocity 4 meter behind the fence and at the height corresponding to the top of the array.
**Includes a factor of 1.5 to account for turbulence generated by the fence.

For more accurate results, a wind tunnel or natural wind study is required since the air flow is influenced by the shape of the arrays and the position of the arrays relative to themselves and to the fence. The effect on array steady state aerodynamic forces for a number of fence and array parameters will be evaluated in a proposed wind tunnel test plan detailed in Appendix B if the test is implemented.

One condition that should be avoided or protected against when using fences as wind protective barriers, is to avoid changing fence direction with a sharp corner.[35] Sharp fence corners can generate a vortex from a wind yawed to one side and can actually increase the wind velocity in a narrow region. To avoid this, the fence should be built to go around the corner in a gentle radius or if a sharp corner is required, to build another fence in front of the corner and at an angle that is perpendicular to the bisect line of the corner.

6.5 Miscellaneous Potential Load Alleviation Techniques

There are several potential load alleviation techniques that may reduce the wind aerodynamic loading in a more cost effective manner than reducing the freestream velocity with protective barriers. These techniques will be discussed in this section but without regard to detailing any values of expected force reductions. Each of these techniques is dependent on the detailed geometry and actual force reduction values can only be obtained by test methods.

One of the most promising potential load alleviation techniques for high aspect ratio arrays is to have built-in air gaps within the array. Air gaps consisting of holes, slots, etc., will allow air to flow through the arrays and as such will cause decreased windward pressures as well as less negative pressures on the base pressure side. The air will move from the high pressure side through the air gaps to fill the air cavity on the base pressure side and result in a total force that is reduced from that of an array with no air gaps. Furthermore, this potential load alleviation tech-

nique may help to keep the arrays clean because of the turbulence that will be generated as the air passes through the array. Dust and dirt may be continually swirled and have a cleaning effect on the array when there is wind and/or rain. The shape of the air gaps may also affect the self-cleaning efficiency of the array. In practice, the photovoltaic arrays will probably be made up of a number of modules. Air gaps could be installed on the perimeter of these modules within the structure supporting the modules.

Another potential load alleviation technique when the arrays are at large angles of attack is to have one edge of the array positioned on the ground to block the flow of air under the array and thus reduce the suction effect on the base pressure side of the array. Unfortunately, this method of positioning the arrays on the ground will cause dirt to collect onto the lower part of the array during winds and rain because of an increased stagnation area on the windward side. As a result, an alternate technique would be to position the array off the ground but block the ground clearance gap around the perimeter of the array field. The advantage of this technique and of adding build-in air gaps within the arrays will be evaluated in a proposed wind tunnel test, the proposed plan of which is detailed in Appendix B .

A third technique to reduce the aerodynamic loads that does not have the potential of the preceding techniques but that might be incorporated into manufacturing techniques with little or no additional cost, is rounding the edges of the array as much as possible. The more gentle the curvature of the edges, the less drag that the plate generates. The drag on flat plates is reduced using this procedure by causing flow separation from the plate in a much smoother manner. Improving on this condition for the rear side of the array, further drag reductions could be achieved with the use of fairings that causes a slower transition of the flow from an attached to a separated flow. Caution must be exercised in designing such a fairing that an airfoil is not developed that reduces the drag but produces larger lift forces.

6.6 Unsteady Winds and Structural Dynamics Relationship

The previous discussions address only winds that are in a steady state condition. (The previous section, Section 6.4, uses a dynamic factor on the steady state condition which accounts for turbulence generated by other arrays or fences). If the winds are gusty and turbulent, the winds have an unsteady component that should also be considered in the design loads for solar arrays. To accurately predict wind loads on an array due to the unsteady wind component is costly, time consuming, and difficult to obtain. The reason for the difficulty in predicting these loads is that the unsteady wind will excite the structural modes of the array resulting in structural vibrations of the array. These vibrations may attenuate because of the internal damping in the structure or may build up and can even destroy the structure for conditions where phasing of the structural vibrations modes produce a flutter condition. To completely analyze the structure for unsteady wind loads, a dynamic structural analysis must be performed that considers both the wind properties (wind velocity magnitude and frequency content) and the array structural and aerodynamic properties (array aerodynamic shape and structural vibration mode shapes which is dependent on the structural mass, stiffness and shape).

In lieu of a detailed structural dynamic analysis, some indication of the unsteady wind loads can be obtained from basic structural dynamic considerations. The root mean square (rms) turbulence velocity level and frequency content of the wind should be obtained at the site where the solar arrays are to be located since both the wind rms turbulence level and the frequency content is affected by the local terrain. Once the determination of these wind unsteady parameters are obtained, the unsteady wind load magnitude can be approximated by scaling the steady state wind loads by the ratio of the rms turbulence velocity to steady state wind velocity. This unsteady wind load needs to be combined with the steady state wind loads for the total wind loads. In addition, the frequency of the array panels and support structure must be determined and the lowest frequency should be at least twice the frequency content of the wind turbulence to prevent excitation of the structural model vibrations. (This should also be considered for the turbulence generated be fences and other arrays).

7.0 PROPOSED WIND DESIGN PRESSURE DISTRIBUTIONS FOR HIGH ASPECT RATIO ARRAYS

The loads presented in Section 6.0 are useful in the design of the foundations and supporting structure. However, to structurally design the photovoltaic modules and panels for aerodynamic forces, it is necessary to know the aerodynamic pressure distribution across the modules and panels. The pressure coefficient distributions for the windward face and the base pressure face of the array is presented in Table 7-1 and 7-2, respectively, for various angles of attack (tilt angles) and array ground clearances. In addition, the total force coefficient and center of pressure as a function of the chord length and measured from the leading edge is also presented in the tables for both the windward and base pressure faces.

An example is presented to show the use of these tables. An array is assumed at 20°, a slant height (chord) of 2.4 m (8 ft), ground clearance of .25c and a wind from the rear of 40 meters/sec with a 1/7 law profile. From this data, the actual ground clearance of the array is:

$$Z = .25\ (8)$$
$$= 4 \text{ ft.}$$

The top of the array is at a height of:

$$H = 4 \text{ ft.} + 8 \sin 20°$$
$$= 6.74 \text{ ft.}$$

The dynamic pressure at a height of 6.74 ft. and a 40 m/sec wind velocity at 10 meters and with a 1/7 power law is calculated as:

$$q = .5\ (.002378)(99.5)^2$$
$$= 11.77 \text{ psf}$$

Note: the wind velocity at 6.74 ft. is 99.5 fps, assuming standard atmosphere density at sea level.

The pressures can be calculated along the chord from the table using the relationship that

$$p = q\ C_p$$

Using a location of .88c for the fraction of the chord in this example (C_p = -.0222), the pressure at this location is:

$$p = 11.77 \times -.0222$$

$$= -.261 \text{ psf}$$

which is a suction pressure or a pressure vector away from the windward face. This type of calculation can be performed for all locations on the length of the chord.

The location of the center of pressure on the windward side is:

$$\overline{X} = 8 \times .311$$

$$= 2.488 \text{ ft. from the leading edge}$$

It should be noted that these calculations are only for the windward side. The pressures on the base pressure side can be similarly calculated, and must be algebraically added to the front surface pressures to obtain the total pressure (assuming the module is a single plate with no cavity).

Table 7-1. Windward Face Pressure Coefficient Distribution

Angle of Attack (tilt angle) / Fraction of Chord From Leading Edge	Wind from rear											
	20° (20°)				40° (40°)				60° (60°)			
	Ground Clearance				Ground Clearance				Ground Clearance			
	∞	.5C	.25C	.125C	∞	.5C	.25C	.125C	∞	.5C	.25C	.125C
.99500	-.77641	-.73516	-.76542	-.79548	-1.15101	-.93897	-.89162	-.83976	-1.68130	-1.47593	-1.42422	-1.30360
.98450	-.53397	-.47442	-.47068	-.45716	-.71519	-.50145	-.40416	-.27735	-.93334	-.68821	-.56183	-.33613
.97400	-.44573	-.37761	-.35841	-.32051	-.54680	-.33119	-.21644	-.06411	-.65537	-.41094	-.26529	-.02619
.96350	-.38491	-.31049	-.27960	-.22258	-.43159	-.21544	-.08983	.07761	-.47140	-.23074	-.07630	.16375
.95300	-.33607	-.25653	-.21598	-.14271	-.34142	-.12562	.00738	.18437	-.33208	-.09656	.06167	.29729
.94300	-.30761	-.22318	-.17405	-.08636	-.28084	-.06407	.07509	.25940	-.23528	-.00320	.15731	.38823
.93250	-.27507	-.18664	-.12992	-.02935	-.21855	-.00256	.14072	.32918	-.14252	.08420	.24443	.46750
.92200	-.24389	-.15204	-.08840	.02371	-.16236	.05227	.19841	.38897	-.06151	.15949	.31807	.53236
.91150	-.24025	-.14328	-.07180	.05330	-.13434	.08300	.23415	.42931	-.01040	.20925	.36857	.57792
.90100	-.22439	-.12357	-.04526	.09074	-.09673	.12077	.27470	.47129	.04612	.26106	.41955	.62132
.89050	-.19586	-.09254	-.00890	.13548	-.05099	.16396	.31825	.51309	.10735	.31670	.47042	.66229
.88000	-.22613	-.11528	-.02220	.13728	-.05720	.16545	.32719	.52899	.12285	.33577	.49256	.68351
.86450	-.18355	-.06999	.02981	.19867	.00652	.22407	.38425	.58054	.20270	.40545	.55490	.73086
.84350	-.09477	.01805	.12223	.29529	.11235	.31613	.46813	.64982	.31742	.50107	.63605	.78832
.82300	-.05077	.06441	.17485	.35481	.17523	.37252	.52089	.69397	.39112	.56332	.68915	.82561
.80250	-.01309	.10427	.22028	.40554	.22997	.42127	.56577	.73034	.45420	.61593	.73318	.85559
.78150	.02067	.14013	.26116	.45046	.27927	.46480	.60520	.76128	.51006	.66191	.77091	.88048
.76050	.05099	.17233	.29770	.48979	.32351	.50364	.63962	.78741	.55916	.70177	.80296	.90098
.73950	.07923	.20226	.33142	.52512	.36446	.53929	.67059	.81022	.60349	.73725	.83096	.91843
.70850	.11770	.24276	.37641	.57075	.42026	.58703	.71132	.83923	.66198	.78519	.86641	.93961
.66700	.16543	.29243	.43027	.62274	.48759	.64349	.75815	.87110	.72949	.83486	.90493	.96190
.62500	.20995	.33823	.47841	.66659	.54903	.69383	.79853	.89730	.78746	.87777	.93553	.97625
.58350	.25169	.38031	.52111	.70328	.60485	.73853	.83334	.91907	.83641	.91261	.95906	.98955
.54200	.29210	.42025	.56019	.73501	.65689	.77929	.86420	.93767	.87868	.94131	.97709	.99673
.50000	.33238	.45933	.59707	.76340	.70675	.81748	.89234	.95410	.91535	.96471	.99013	.99888
.45850	.37221	.49736	.63173	.78882	.75385	.85275	.91762	.96831	.94590	.98237	.99784	.99863
.41700	.41289	.53535	.66530	.81249	.79905	.88570	.94060	.98056	.97054	.99438	.99991	.99228
.37500	.45547	.57449	.69892	.83541	.84302	.91676	.96133	.99060	.98874	.99984	.99516	.97936
.33350	.49962	.61445	.73251	.85777	.88443	.94483	.97886	.99751	.99871	.99712	.98189	.95817
.29200	.54679	.65653	.76715	.88052	.92337	.96947	.99232	.99998	.99824	.98373	.95698	.92521
.26050	.58502	.69026	.79456	.89829	.95017	.98475	.99855	.99739	.98852	.96411	.92773	.88975
.23950	.61231	.71413	.81380	.91069	.96641	.99274	1.00000	.99248	.97581	.94450	.90087	.85845
.21850	.64119	.73922	.83387	.92353	.98056	.99814	.99838	.98399	.95663	.91831	.86665	.81959
.19800	.67119	.76508	.85438	.93651	.99155	.99999	.99275	.97101	.92981	.88446	.82395	.77200
.17750	.70338	.79260	.87598	.94992	.99852	.99707	.98149	.95148	.89221	.83959	.76885	.71159
.15650	.73904	.82276	.89927	.96390	.99940	.98679	.96144	.92165	.83824	.77794	.69478	.63154
.13550	.77892	.85579	.92403	.97776	.99042	.96542	.92875	.87748	.76302	.69520	.59722	.52765
.11450	.81972	.88947	.94873	.99018	.96435	.92439	.87283	.80598	.64744	.57061	.45159	.37341
.09365	.86641	.92635	.97348	.99884	.90850	.85079	.78012	.69294	.47542	.39005	.24350	.15556
.07290	.91937	.96482	.99426	.99695	.79527	.71601	.61929	.50398	.20528	.11285	-.07165	-.17128
.05210	.97692	.99753	.99503	.95602	.50808	.39417	.24799	.07741	-.33662	-.43014	-.68614	-.79863
.03125	.97763	.99764	.99531	.95893	.47461	.36081	.21468	.04538	-.63078	-.72859	1.01435	-1.14097
C_N	.316	.417	.514	.634	.529	.626	.686	.744	.561	.629	.643	.675
$\bar{X}$	.167	.258	.311	.366	.324	.392	.431	.470	.426	.471	.516	.555

Table 7-1. Windward Face Pressure Coefficient Distribution - Concluded

Angle of Attack (tilt angle) / Fraction of Chord From Leading Edge	Wind from front 120° (60°)			140° (40°)			160° (20°)		
	Ground Clearance			Ground Clearance			Ground Clearance		
	.5C	.25C	.125C	.5C	.25C	.125C	.5C	.25C	.125C
.99500	-2.73401	-3.44529	-4.75120	-1.85696	-2.28977	-2.74680	-1.14629	-1.41868	-1.71554
.98450	-1.70024	-2.19229	-3.03948	-1.28128	-1.59639	-1.91512	-.83553	-1.04177	-1.25363
.97400	-1.32682	-1.74668	-2.45165	-1.05675	-1.33203	-1.60538	-.72245	-.90583	-1.09002
.96350	-1.08049	-1.45504	-2.07333	-.90363	-1.15354	-1.39855	-.64497	-.81347	-.98010
.95300	-.89415	-1.23573	-1.79270	-.78412	-1.01533	-1.23990	-.58322	-.74060	-.89435
.94300	-.76563	-1.08534	-1.60202	-.70415	-.92309	-1.13435	-.54672	-.69692	-.84230
.93250	-.64177	-.94089	-1.42078	-.62211	-.82919	-1.02796	-.50586	-.64911	-.78668
.92200	-.53335	-.81482	-1.26377	-.54827	-.74508	-.93320	-.46707	-.60422	-.73502
.91150	-.46719	-.73887	-1.17024	-.51209	-.70383	-.88650	-.46111	-.59561	-.72316
.90100	-.39252	-.65294	-1.06499	-.46325	-.64857	-.82467	-.44401	-.57189	-.69539
.89050	-.31002	-.55757	-.94816	-.40349	-.58118	-.74967	-.40625	-.53252	-.65112
.88000	-.29435	-.54179	-.93141	-.41326	-.59234	-.76190	-.44075	-.56879	-.68857
.86450	-.18612	-.41691	-.77973	-.33030	-.49936	-.65921	-.38953	-.51141	-.62492
.84350	-.02683	-.23191	-.55351	-.19157	-.34395	-.48793	-.28414	-.39521	-.49811
.82300	.07358	-.11658	-.41481	-.11018	-.25339	-.38877	-.23177	-.33724	-.43457
.80250	.15952	-.01815	-.29728	-.03967	-.17527	-.30361	-.18715	-.28605	-.38089
.78150	.23567	.06888	-.19391	.02357	-.10546	-.22781	-.14736	-.24437	-.33345
.76050	.30275	.14544	-.10346	.08012	-.04326	-.16057	-.11181	-.20552	-.29148
.73950	.36343	.21454	-.02217	.13229	.01393	-.09909	-.07886	-.16964	-.25291
.70850	.44382	.30600	.08484	.20309	.09125	-.01625	-.03433	-.12158	-.20155
.66700	.53744	.41255	.20885	.28828	.18389	.08248	.02050	-.06275	-.13911
.62500	.61897	.50554	.31674	.36584	.26790	.17149	-.07116	-.00884	-.08247
.58350	.68917	.58597	.40988	.43622	.34376	.25163	.11826	.04091	-.03060
.54200	.75144	.65790	.49327	.50194	.41448	.32601	.16351	.08824	.01827
.50000	.80759	.72351	.56981	.56512	.48244	.39731	-.20832	-.13483	-.06598
.45850	.85705	.78240	.63928	.62526	.54718	.46505	.25236	.18041	.11236
.41700	.90080	.83603	.70384	.68357	.61031	.53115	.29716	.22644	.15878
.37500	.93884	.88485	.76468	.74122	.67304	.59703	.34393	-.27428	-.20667
.33350	.96932	.92728	.82076	.79697	.73441	.66194	.39236	.32370	.25587
.29200	.99093	.96284	.87301	.85138	.79530	.72713	.44408	.37632	.30796
.26050	.99914	.98344	.90923	.89095	.84082	.77697	-.48613	-.41910	-.35020
.23950	.99955	.99342	.93198	.91648	.87091	.81055	.51623	.44971	.38039
.21850	.99434	.99914	.95290	.94058	.90036	.84426	.54820	.48228	.41248
.19800	.98224	.99931	.97101	.96209	.92799	.87701	-.58157	-.51638	-.44605
.17750	.96072	.99219	.98602	.98057	.95377	.90929	.61757	.55329	.48250
.15650	.92499	.97411	.99666	.99449	.97684	.94101	.65778	.59472	.52356
.13550	.86977	.94016	.99985	1.00000	.99389	.96975	-.70344	-.64237	-.57141
.11450	.77942	.87849	.99046	.99073	.99985	.99182	.75019	.69090	.61949
.09365	.63644	.77280	.95837	.95397	.98392	.99975	.80525	.74941	.67896
.07290	.39930	.58621	.88117	.86169	.92149	.97450	-.87061	-.82147	-.75506
.05210	-.09147	.18112	.67683	.59894	.71314	.83999	.94824	.91235	.85646
.03125	-.37008	-.04628	.57610	.57302	.69857	.83833	.94738	.90770	.84433
C_N	.433	.357	.209	.374	.290	.204	.197	.102	.012
$\bar{X}$	.264	.098	-.474	.144	-.031	-.352	-.086	-.764	-10.32

Table 7-2. Flat Plate Aerodynamic Base Pressure Coefficients in Close Ground Proximity

Wind from rear												
Tilt angle		20°				40°				60°			
Angle of attack		20°				40°				60°			
Ground clearance		∞	.5C	.25C	.125C	∞	.5C	.25C	.125C	∞	.5C	.25C	.125C
Base pressure face	C_N	−.65	−.62	−.67	−.71	−1.0	−.85	−.86	−.89	−1.42	−1.30	−1.34	−1.37
	$\bar{X}_{cp}$	.5	←									→	.5

Wind from the front										
Tilt angle		60°			40°			20°		
Angle of attack		120°			140°			160°		
Ground clearance		.5C	.25C	.125C	.5C	.25C	.125C	.5C	.25C	.125C
Base pressure face	C_N	−1.30	−1.34	−1.37	−.85	−.86	−.89	−.62	−.67	−.71
	X_{cp}	.5	←						→	.5

THIS PAGE

WAS INTENTIONALLY

LEFT BLANK

8.0 WIND TUNNEL TEST PLAN

Theoretical analysis techniques of boundary layer air flow over bluff bodies can at best analyze only very simple bodies and limited boundary conditions and must usually be supplemented with wind tunnel test results. The potential flow region ($\alpha = 10^0 - 15^0$ for $AR = \infty$) where the flow remains attached to the airfoil is fairly well studied and the theoretical results in this region match test results fairly well. Once the flow becomes separated, matching of the analytical results of simple airfoils and boundary conditions to test results is difficult. The matching of the results in this study for single flat plates at large angles of attack to the wind tunnel results are considered excellent for this type of flow even though the theoretically calculated base pressures appear to be overpredicted by approximately 30%. However, a theoretical analysis of the flow with arrays in the wake of other arrays is presently unattainable.

As a result of this theoretical study, a wind tunnel test plan was developed (the detailed test specifications are presented in Appendix B). This test plan is arranged to validate the theoretical results and obtain results for conditions not suitable for theoretical analysis. The test plan is intended to confirm that for large aspect ratio arrays, the aerodynamic force coefficients on arrays from studies with constant velocity profiles and 1/7 power law velocity profiles are essentially identical for arrays with chords of 2.4 m (8 ft) or greater. If this is confirmed, tests could be performed at most wind tunnel facilities rather than at those few facilities that have environmental wind tunnels. The test plan is also intended to confirm that aerodynamic loads are only affected in a secondary way from the ground clearance gap for gaps not approaching zero. Other parameters varied in the test plan for conditions not suitable for theoretical analysis are corner effects from yawed wind, array spacing, fence to array spacings and fence height to array height. Other potential load alleviation devices will be tested to determine their effectiveness in reducing the aerodynamic forces. These devices will consist of air gaps built into the arrays and the blockage of air flow beneath the arrays.

From the proposed wind tunnel test plan results and the analytical results from this study, a detailed set of design aerodynamic force and pressure loads will be presented for detailed module and panel structural design as well as array structural support design. The detailed set of design aerodynamic force and pressure loads will encompass most design conditions for an array field.

9.0 CONCLUSIONS AND RECOMMENDATIONS

A number of conclusions can be derived by examining the analytical results in Sections 5.0 through 7.0 and from the results reviewed in the literature and discussed in Section 4.0. Important conclusions regarding the wind aerodynamic loads on photovoltaic arrays are:

- Winds perpendicular to the array's long horizontal axis produce the largest aerodynamic loads on the structure;
- Winds from the sideways directions to the arrays produce insignificant aerodynamic loads resulting only from the skin friction;
- Aerodynamic loads increase as array tilt angles increase and are a maximum at a tilt angle of 90°;
- Aerodynamic loads increase with decreasing ground clearance;
- Arrays positioned in the wake of other arrays or behind fences will experience a reduction in aerodynamic loads.

Wind aerodynamic loads peak at two tilt angles for high aspect ratio arrays (10°-15° and 90°). The wind loads can be the highest depending on configuration at tilt angles of 10°-15° for the wind from the front or the rear. Below 10°-15°, the arrays act as an efficient airfoil and can generate significant lift forces. Above 20°, the arrays are bluff bodies resulting in separated flow and high drag forces with the aerodynamic force being a maximum at array tilt angles of 90°. Fortunately, in the continental U.S.A., fixed arrays will never be at tilt angles of 10°-15° or 90°. Consequently, the angles of attack of highest aerodynamic forces can be avoided. For the practical range of array tilt angles (20°-60°), the wind loads increase as tilt angle increases.

The effect of ground clearance greater than zero causes wind load coefficients to increase with decreasing clearance. This is offset by the wind dynamic pressure that decreases with decreasing elevation above the ground such that the effect of ground clearance on wind load increases only slightly for decreasing ground clearance. This trend is only true for tilt angles between 20° and 90°. Between 0-15°, wind loads increase significantly with decreasing ground clearance for ground clearances greater than zero. For a ground clearance of zero where the wind cannot flow under the array, the resulting wind loads are less than for arrays with ground clearances.

Array spacing has minimal effect on wind loads provided the arrays are not in the wake of another. For arrays in the wake of other arrays, the array spacing effect can only be estimated. The wind loads are estimated to decrease with decreasing array spacing to a minimum value of 40 percent of the array wind loads out of the wake effect.

Fences can significantly reduce the wind aerodynamic loads on arrays by as much as 60 percent. Fence heights greater than the array heights produce no significant benefits in increased load reductions than for a fence as high as the arrays. Based on Raine's results, a fence of 20% geometric porosity appears to produce the highest overall wind aerodynamic load reduction on the arrays when considering both steady and unsteady wind effects.

Because of unsteady wind loads, the array natural frequencies must be significantly higher than the frequency content of the turbulence. This is required to minimize wind loads and structural response that may occur from structural dynamics. If the frequencies of the array and turbulence are similar, large structure response may occur and needs to be calculated using structural dynamic techniques that are structural configuration dependent, both in shape and physical properties.

The theoretically derived design wind aerodynamic forces and pressures can be used for design purposes since they are conservative. A wind tunnel test plan is proposed that will augment the theoretically derived forces by developing design wind aerodynamic forces and pressures that currently cannot be analyzed theoretically. The test program will also investigate and appraise load alleviation devices such as building porosity into the array. It is recommended that the proposed test plan be implemented in order to remove some of the conservatism from the analytical design forces and also include forces from load alleviation devices for design purposes.

10.0 NEW TECHNOLOGY

No reportable items of new technology have been identified by Boeing during the contract of this work.

THIS PAGE

WAS INTENTIONALLY

LEFT BLANK

11.0 REFERENCES

1. National Photovoltaic Program, Program Plan, February 3, 1978, U.S. Department of Energy Division of Solar Technology.

2. "Feasibility Study of Solar Dome Encapsulation of Photovoltaic Arrays," DOE/JPL-No. 954833-78/1, Boeing Engineering and Construction Company, December, 1978.

3. "Module/Array Interface Study," DOE/JPL-No. 954698-78/1, Bechtel National, Inc., Research and Engineering Operation, August, 1978.

4. J. Van Eimern, R. Karschon, L. A. Razumova and G. W. Robertson, "Windbreaks and Shelterbelts," World Met. Organization Technical Note No. 59, 1964.

5. W. Frost, "Review of Data and Prediction Techniques for Wind Profiles Around Man-made Surface Obstructions," North Atlantic Treaty Organization, AGARD Conference Proceedings, No. 140, May 1973.

6. J. E. Cermak, "Applications of Fluid Mechanics to Wind Engineering - A. Freeman Scholar Lecture," Journal of Fluid Engineering, March 1975.

7. V. Sharan, "Dependence of Mean Flow Near-Wake Characteristics on Depth of Two-Dimensional Obstacles," Journal of Scientific and Industrial Research, Vol. 36, No. 3, 1977.

8. M. C. Good and P. N. Joubert, "The Form Drag of Two-Dimensional Bluff-Plates Immersed in Turbulent Boundary Layers," Journal of Fluid Mechanics, Vol. 31, Part 3, 1968.

9. M. Arie and H. Rouse, "Experiments on Two-Dimensional Flow Over a Normal Wall," Journal of Fluid Mechanics, Vol. 1, Part 2, 1956.

10. J. Bitte and W. Frost, "Atmospheric Flow Over Two-Dimensional Bluff Surface Obstructions," NASA CR-2750, October 1976.

11. M. Kiya, H. Sakamoto and M. Arie, "Theory of Inviscid Shear-Flow Over Bluff Bodies Attached to a Plane Wall, Part 1," Bulletin of the Japanese Society of Mechanical Engineers, Vol. 19, No. 131, May 1976.

12. M. Kiya and M. Arie, "A Free-Streamline Theory for Bluff Bodies Attached to a Plane Wall," Journal of Fluid Mechanics, Vol. 56, Part 2, 1972.

13. H. Sakamoto, M. Moriya and M. Arie, "A Study on the Flow Around Bluff Bodies Immersed in Turbulent Boundary Layers (Part 1, On the Form Drag of a Normal Plate)," Bulletin of the Japanese Society of Mechanical Engineers, Vol. 18, No. 124, October 1975.

14. H. Sakamoto, M. Moriya and M. Arie, "A Study on the Flow Around Bluff Bodies Immersed in Turbulent Boundary Layers (Part 2, The Pressure Forces Acting on Inclined Plates)," Bulletin of the Japanese Society of Mechanical Engineers, Vol. 20, No. 139, January 1977.

15. O. B. Taulbee and J. M. Robertson, "Turbulent Separation Analysis Ahead of a Step," Journal of Basic Engineering, Transactions of the ASME, September 1972.

16. I. Seginer and R. Sagi, "Drag on a Windbreak in Two-Dimensional Flow," Agricultural Meteorology, Vol. 9, 1972-73.

17. G. V. Parkinson and T. Jandali, "A Wake Source Model for Bluff Body Potential Flow," Journal of Fluid Mechanics, Vol. 40, Part 3, 1970.

18. J. Counihan, J. C. R. Hunt and P. S. Jackson, "Wakes Behind Two-Dimensional Surface Obstacles in Turbulent Boundary Layers," Journal of Fluid Mechanics, Vol. 64, Part 3, 1974.

19. I. P. Castro and J. E. Fackrell, "Note on Two-Dimensional Fence Flows with Emphasis on Wall Constraint," Journal of Industrial Aerodynamics, Vol. 3, No. 1, 1978.

20. N. P. Woodruff and A. W. Zingg, "A Comparative Analysis of Wind Tunnel and Atmospheric Air Flow Patterns About Single and Successive Barriers," E.O.S., Transaction of the American Geophysical Union, Vol. 36, No. 2, 1955.

21. M. Jensen, "Shelter Effects," The Danish Technical Press, Copenhagen, 1954.

22. R. Baltaxe, "Air Flow Patterns in the Lee of Model Windbreaks," Archiv for Meteorologie, Geophysik und Bioklimatologie, Klimatologie Bioklimatologie, Strahlungsforschung Band 15, Neft 3, 1967.

23. J. K. Raine and D. C. Stevenson, "Wind Protection by Model Fences in a Simulated Atmospheric Boundary Layer," Journal of Industrial Aerodynamics, 2 (1977).

24. K. G. R. Raju and R. J. Garde, "Resistance of an Inclined Plate Placed on a Plane Boundary in Two-Dimensional Flow," Transactions of the ASME, March 1970.

25. V. J. Modi and S. El-Sherbiny, "Wall Confinement Effects on Bluff Bodies in Turbulent Flows," Proceeding of the Fourth International Conference on Wind Effects on Buildings and Structures, 1975.

26. L. Prandtl, "The Mechanics of Viscous Fluids," Aerodynamic Theory, Vol. III, W. F. Durand, 1935.

27. T. Von Karman, "Mdw, Ges, Wisc.," Gotlingen, 1930.

28. H. B. Squire, "Phil. Mag." January, 1948.

29. A. G. Davenport, "Rationale for Determining Design Wind Velocities," Proceedings of the American Society of Civil Engineers, Vol. 86, No. ST5, May 1960.

30. J. W. Sturrock, "Aerodynamic Studies of Shelterbelts in New Zealand," New Zealand Journal of Science, Vol. 12, No. 4, 1969.

31. J. P. Giesing, T. P. Kalman, and W. P. Rodden, "Subsonic Unsteady Aerodynamics for General Configurations; Part I, Direct Application of the Nonplanar Doublet Lattice Method," AFFDL-TR-71-5, 1971.

32. M. L. Henderson, "Two-Dimensional Separated Wake Modeling and its Use to Predict Maximum Section Lift Coefficient," Proceedings of 16th, AIAA Conference, Huntville, Alabama, Jan., 1978.

33. P. Sachs, "Wind Forces in Engineering," Pergamon Press, 1972.

34. B. D. Giles, "Fluidics, the Coanda Effect, and Some Orographic Winds," Archiv Fur Meteorologie, Geophysik und Bioklematologie, Series A, Meteorologie und Geophysik, Vol. 25, No. 3, 1977, p. 273-279.

35. "Heliostat Field Wind-Effects Test," SAN/20422-2, Martin Marietta Corp., February, 1979.

36. "American National Standard Building Code Requirements for Minimum Design Loads in Buildings and Other Structures," ANSI A58.1-1972.

THIS PAGE

WAS INTENTIONALLY

LEFT BLANK

APPENDIX A

THEORETICAL AERODYNAMIC ANALYSIS OF FLAT PLATE ARRAYS IN THE SEPARATED AND POTENTIAL FLOW REGIME

Section 5.0 presents a brief description and discussion of the theoretical results. For completeness, this section presents in detail the theoretical aerodynamic results calculated by both potential flow and separated flow analysis theories.

A.1. Small Angles of Attack - Attached Flow

When flat plates are positioned at small angles of attack (angles less than 10°) to the freestream velocity, potential flow theory aerodynamic methods are valid. One such method extensively used in the aircraft industry is the Doublet Lattice Aerodynamic Program (a three dimensional finite element concept method that evaluates the integral equations relating pressure and normal wash on lifting surfaces) described in reference 31. Briefly, the lifting surface (plate) is paneled into a large number of quadilateral boxes of which two sides are parallel to the freestream direction. Doublets are located along the quarter chord of each box and used to calculate the aerodynamic pressures over the total plate surface. The aerodynamic pressures are assumed constant over each box and acting at the geometric center of the box.

Potential flow theories use a linear relationship between pressures and normal wash. Consequently, the Doublet Lattice Program can be exercised using a unit angle of attack and a unit dynamic pressure so that the pressures calculated over the surface are, in fact, pressure coefficients per unit angle of attack.

From these pressure coefficients per unit angle, pressures can be readily calculated for any condition using the relationship that:

$$p = q\, C_{p_\alpha} \alpha$$

where:

p = pressure

q = dynamic pressure

C_{p_α} = pressure coefficient

α = angle of attack (radians)

In addition, because the program calculates pressure coefficients on boxes that are located on chordwise strips with the box boundaries parallel to the freestream velocity, normal force curve slope coefficients can be obtained for each chordwise strip or for the total surface by the equations:

$$C_{n_\alpha} = \frac{1}{C} \int_C C_{p_\alpha}$$

and $$C_{n_\alpha} = \frac{1}{S} \int_S C_{p_\alpha}$$

respectively,

where:

C_{n_α} = normal force curve slope coefficient

C = chord length

S = surface area

Using this relationship with the actual environmental conditions for dynamic pressure and the angle of attack. The normal force coefficient and total normal force on the plate surface can be calculated by:

$$F_n = q\, S\, C_{n_\alpha} \alpha$$
$$= q\, S\, C_n$$

where:

C_n = normal force coefficient for the total surface

F_n = total normal force on the surface

It should be noted that using the preceding equations the pressures and the normal force can be calculated for any angle of attack because the theory is a linear idealization. However, since flow separation begins to occur between 10° and 15° angle of attack on large aspect ratio flat plates, the pressures and normal force calculations using these equations are only valid up to an angle of attack where separation begins. Above these angles the pres-

sures and normal forces are non-linear with respect to angle of attack and potential flow theory analyses are not valid.

Figure A-1 shows the paneling scheme modeled in the Doublet Lattice Program and the spanwise locations where results are displayed for the 2.4 m (8 ft) and 4.8 m (16 ft) chord flat plate arrays. Because each box is a constant pressure box in this technique, the density of the boxes should be more dense near the leading edge where the pressures vary rapidly if the pressure distribution in this region needs to be defined reasonably accurately.

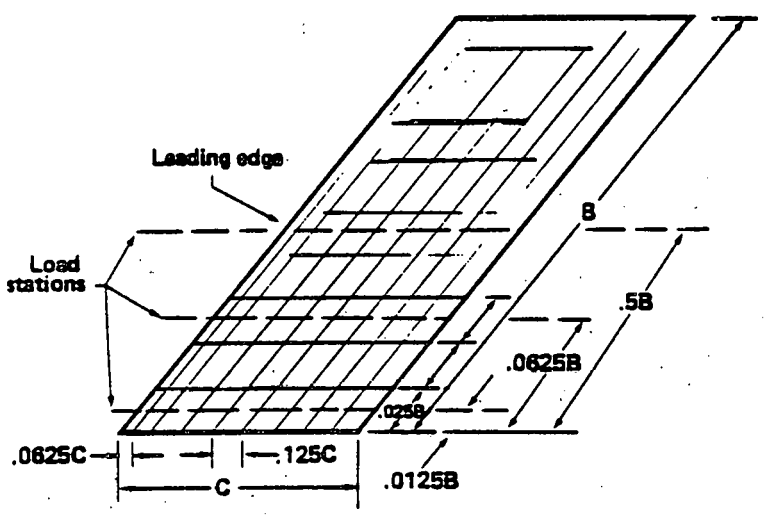

C = 2.4m (8 ft) and 4.8m (16 ft)
B = span*

*For program convenience, B = 36m (120 ft)

Figure A-1. Flat Plate Paneling Used in Doublet Lattice Program

A .1.1 Single Array, Head-On Wind

Figures A -2 to A -7 presents the results for a single array at various heights above the ground and for a head-on wind (a wind at 180° will produce identical results). Figures A -2 and A -3 shows the pressure coefficients along the chord at three spanwise stations: one station at the mid span location and two stations near the tip for chord lengths of 2.5 m (8 ft) and 4.8 m (16 ft) respectively. From these figures, the pressure coefficients are seen to vary from a large pressure on the leading edge to lower pressures towards the trailing edge. The center of pressure is located at the quarter chord location. The shape of the pressures at all three stations are similar with only the magnitude of the pressures decreasing towards the tip load stations compared to the mid span load station. These pressure coefficient distributions are typical for any high aspect ratio lifting surface before the onset of separated flow. Figures A -4 and A -5 depict the normal force slope coefficient at the three spanwise stations as it varies with ground clearance. Figures A -6 and A -7 are crossplots of Figures A -4 and A -5 and show the normal force slope coefficient along the span for ground clearances of .6 m (2 ft) and 1.2 m (4 ft) for the 2.4 m (8 ft) chord plate and 1.2 m (4 ft) for the 4.8 m (16 ft) chord plate. The theory will produce results for ground clearance very close to the ground but the results begin to become questionable. This is because the theory is based on inviscid (frictionless) flow and the viscous flow effects become more important when the ground clearance becomes small. The level where the confidence in the results deteriorates is below the non-dimensional value of ground clearance/chord length (Z/C) = .25 that corresponds to the plate ground clearance of .6 m (2 ft) and 1.2 m (4 ft) for the 2.4 m (8 ft) and 4.8 m (16 ft) chords, respectively.

A .1.2 Single Array, Wind at Oblique Angles

When the wind comes at an oblique angle different than head-on to the array (effectively, the array is yawed to the wind), the aerodynamic pressures will decrease. Figures A -8 and A -9 present the results for a

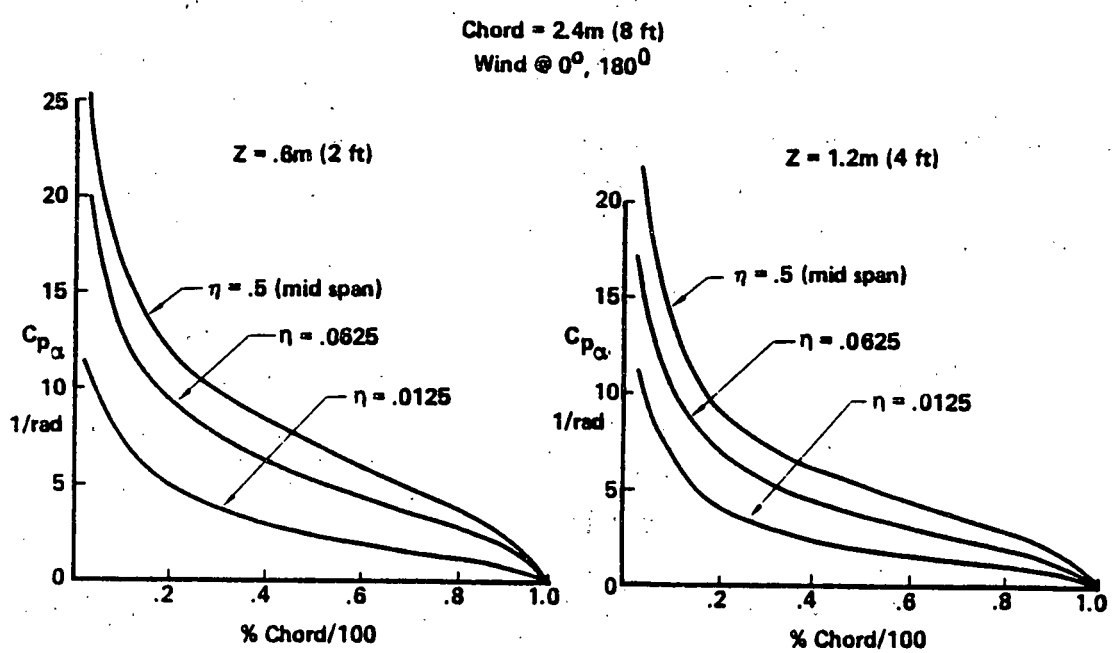

Figure A-2. Chordwise Pressure Coefficient Distribution at Small Angles of Attack

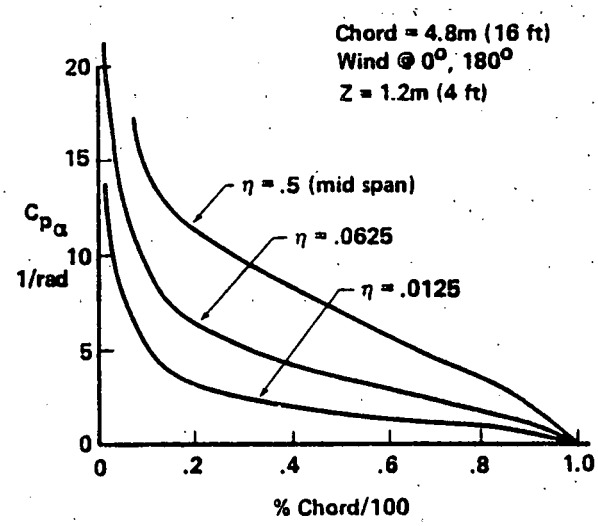

Figure A-3. Chordwise Pressure Coefficient Distribution at Small Angles of Attack

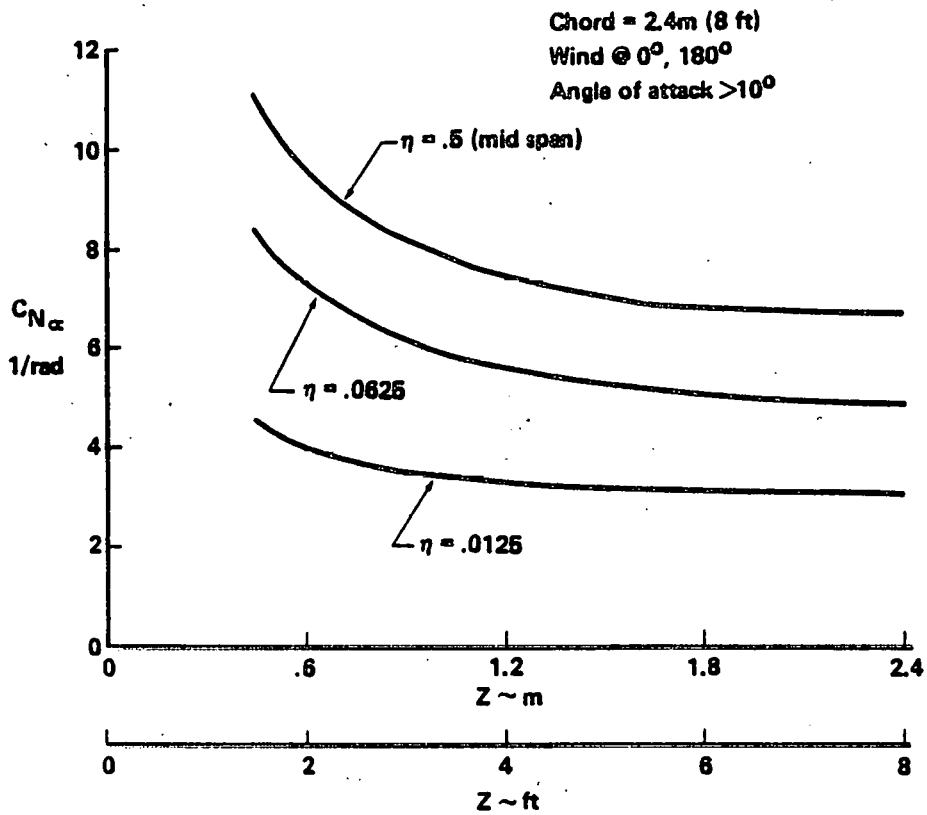

Figure A-4. Effect of Ground Clearance on Normal Force Slope Coefficient

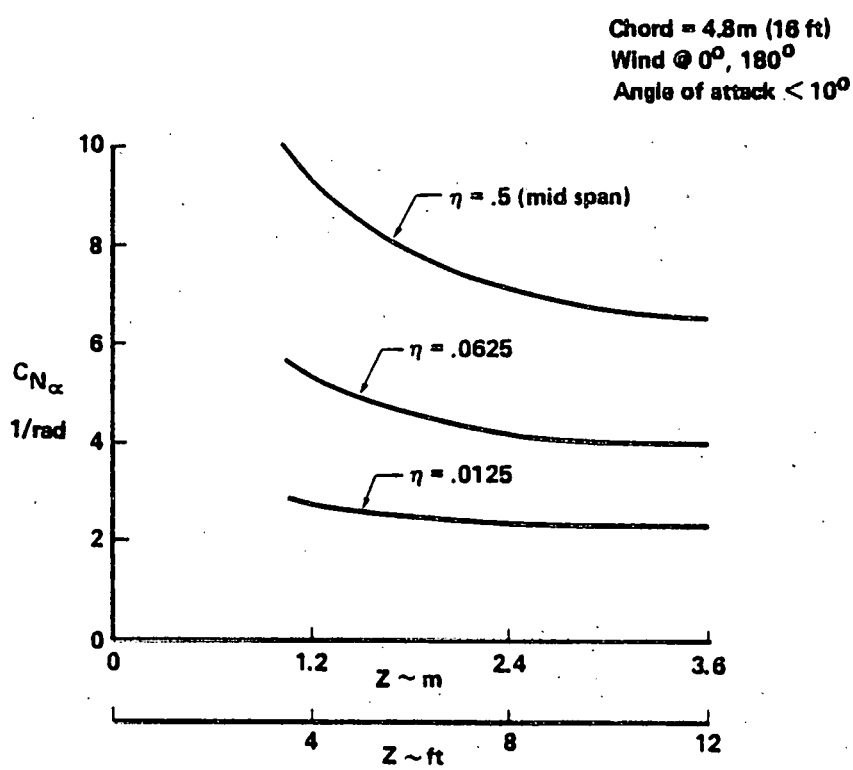

Figure A-5. Effect of Ground Clearance on Normal Force Slope Coefficient

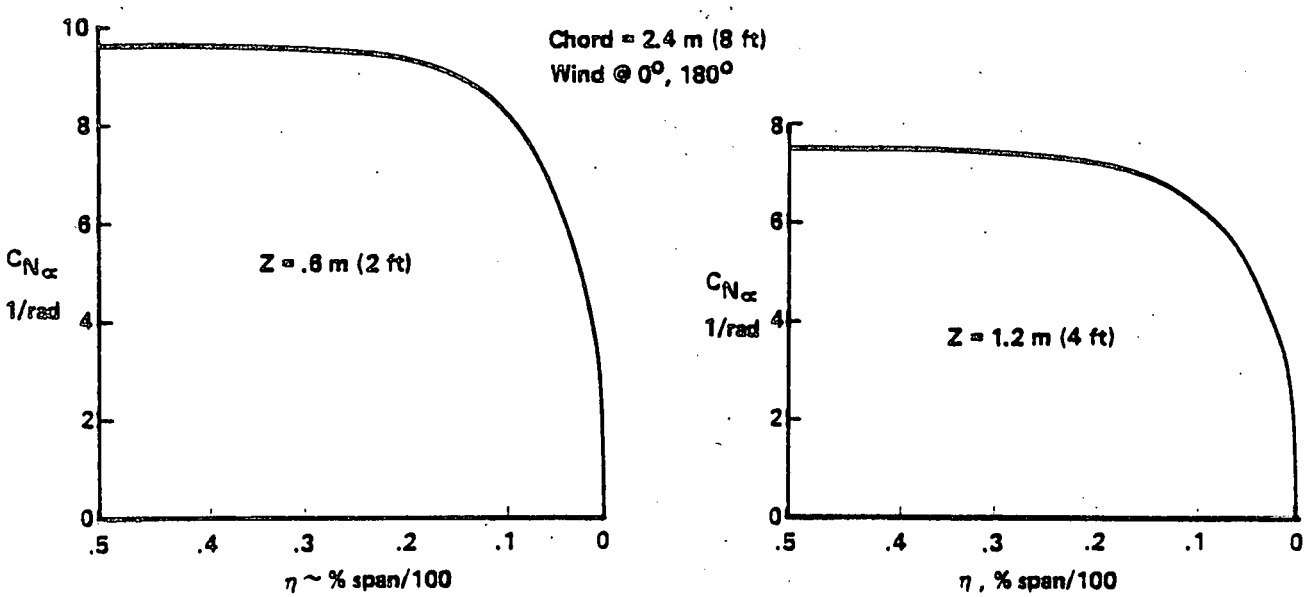

Figure A-6. Spanwise Force Slope Coefficient Distribution for a Flat Plate at Small Angles of Attack

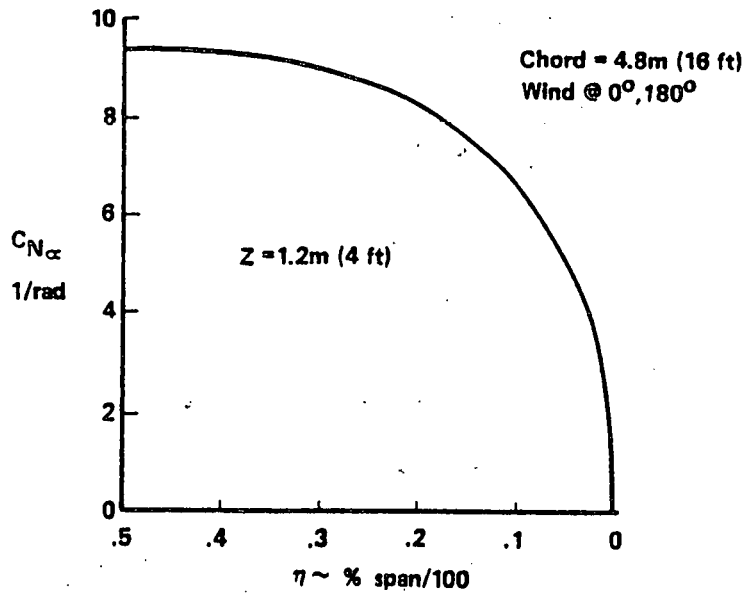

Figure A-7. Spanwise Force Slope Coefficient Distribution for a Flat Plate at Small Angles of Attack

single array with the array yawed at 45° to the wind (135° wind angle will produce identical results). Figure A-8 is a plot of the normal force slope coefficient along the span with the array yawed at 45° to the wind compared to the results for a head-on wind. The magnitude of the results for the yawed array are significantly lower. However, the shape of the force slope coefficient with the wind at 45 degrees is similar but slightly displaced compared to the head-on results. The peak loading and pressures occur slightly downwind of the mid span location. Figure A-9 shows the pressure coefficient along the chord for three spanwise stations, one station near each tip and one station at the span location of maximum pressure. The shape of the pressure distribution is typical of flat plates at small angles of attack: large leading edge pressures decreasing towards the trailing edge and the center of pressure at the quarter chord location.

The condition of an array yawed 90° to the wind was not analyzed because no aerodynamic forces result from this condition except for the forces resulting from skin drag. Skin drag is of many orders smaller than the lift forces generated by a plate even at very small angles of attack for a head-on wind.

A.1.3 Array Fields

When two arrays are placed in close proximity to each other, the downwash from the forward array will cause the pressure on the downstream array to decrease. Also, the downstream array will cause an induced pressure rise on the upstream array. Figures A-10 to A-17 presents the results for two arrays positioned in close proximity to each other and with the wind direction as head-on. Figures A-10 to A-13 are for 2.4 m (8 ft) chord arrays and Figures A-14 to A-17 are for 4.8 m (16 ft) chord arrays. Figure A-10 shows the effect that ground clearance has on the array aerodynamics. The results are very similar to the results for a single array with the aerodynamics forces increasing with decreasing ground clearance. The effect of varying the distances between the arrays is shown in Figure A-11. If the arrays are spaced at intervals greater than three times the chord (3C), the effect of one array on the other is minimal and varies very little. With

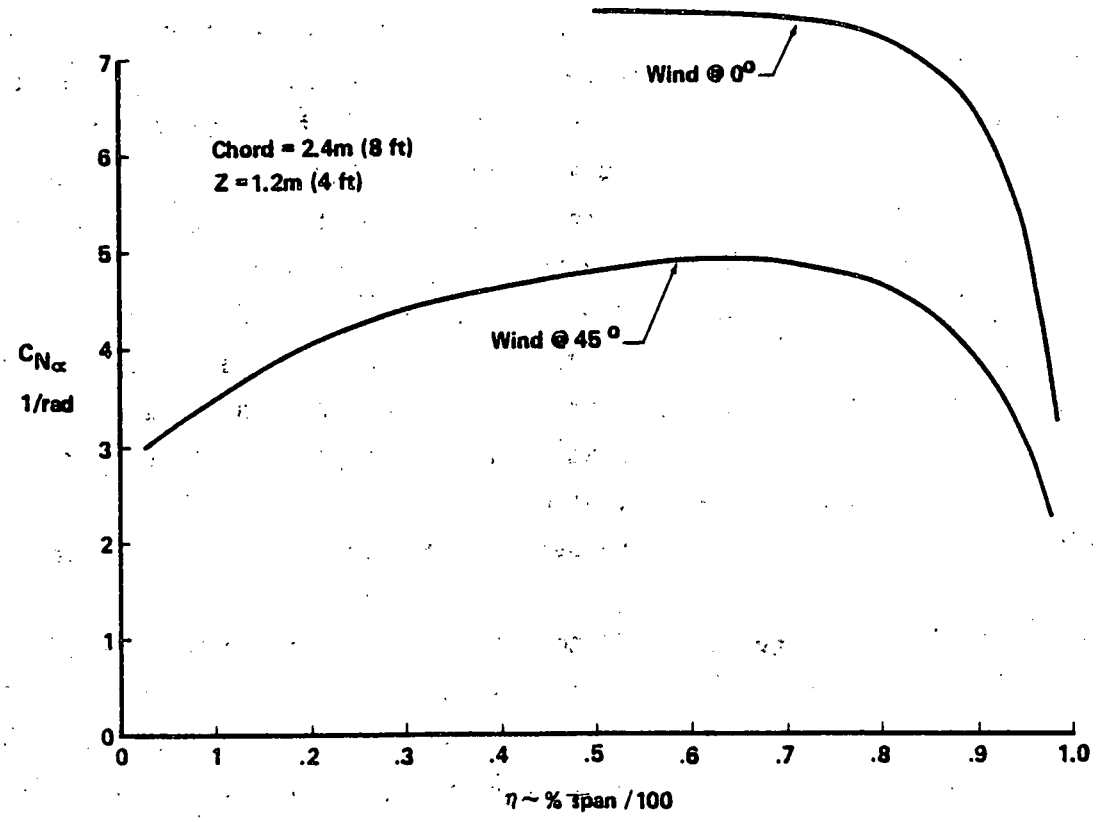

Figure A-8. Effect of Yawed Wind on Spanwise Force Slope Coefficient Distribution for a Flat Plate

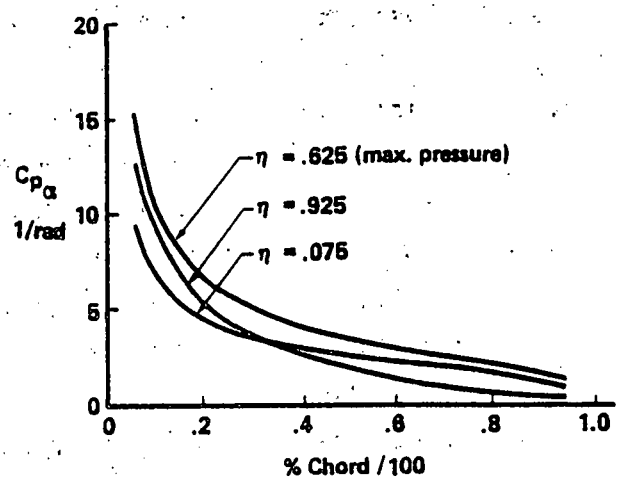

Figure A-9. Flat Plate Chordwise Pressure Distribution for Yawed Wind

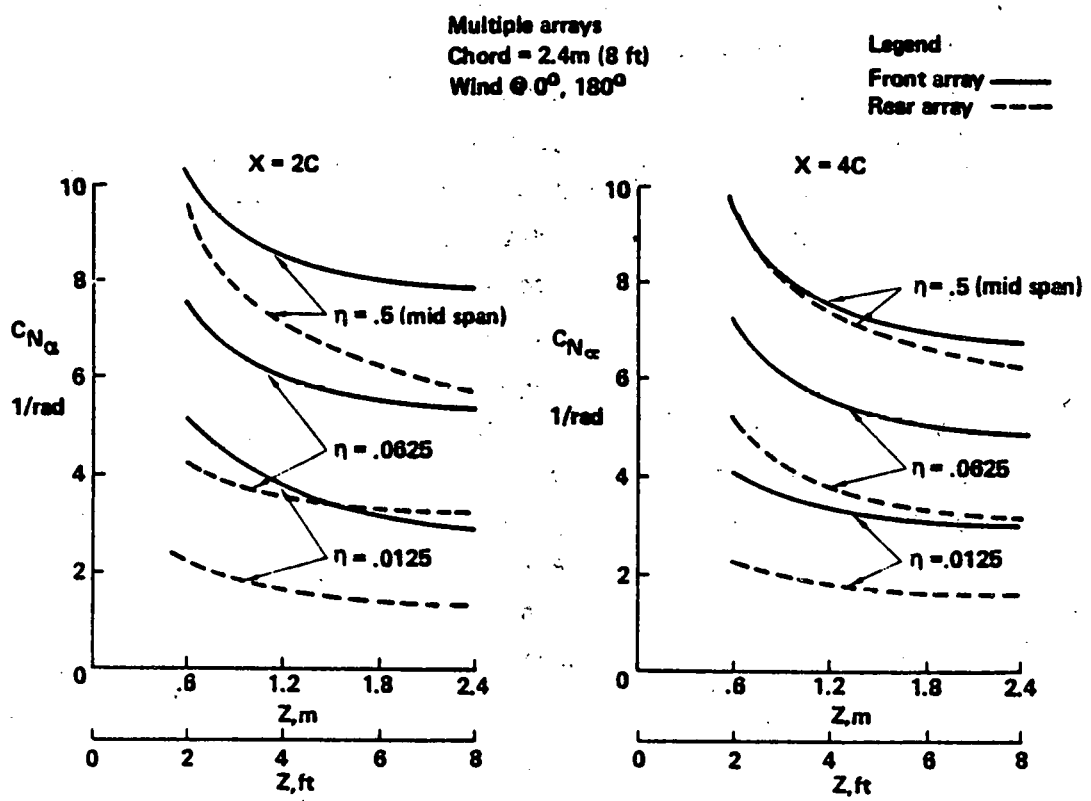

Figure A-10. Effect of Ground Clearance on Normal Force Curve Slope Coefficients

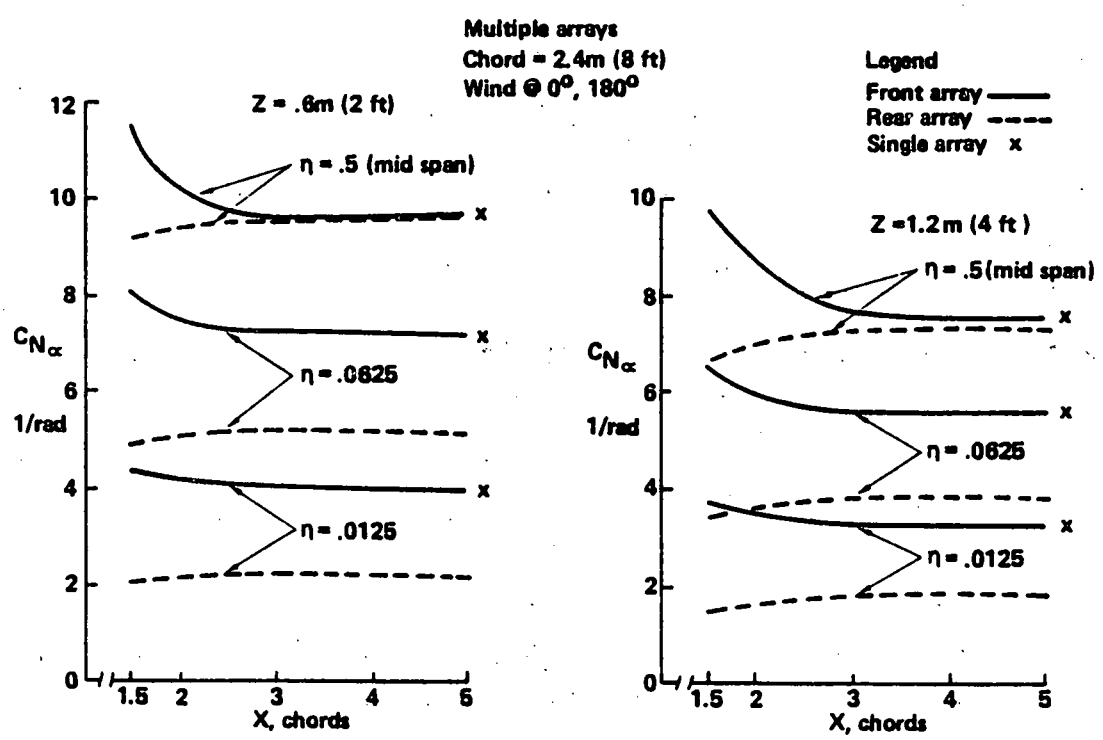

Figure A-11. Effect of Array Separation on Normal Force Curve Slope Coefficients

arrays spaced at closer intervals than three chords, the effect of one array on the other becomes more pronounced. The upstream array aerodynamic forces increase while the downstream array forces decrease with decreasing array spacings. As the spacing between arrays become very close (less than .5C) the flow affected by the gap causes potential flow theory to be questionable to its validity for solar array configurations. The theory is valid when the leading edge of the downstream array and the trailing edge of the upstream array are at the same height. In the theory, when the plates become close the trailing edge vortex of the upwind plate significantly affects the pressures on the downwind plate and vice versa. This effect would be significantly reduced for solar arrays because the leading edge of the arrays are at different heights than the trailing edges with the difference depending on the tilt angle of the arrays and the chord length. Consequently, no results are shown for arrays spaced at intervals closer than 1.5C (.5C separation distance between arrays).

The normal force slope distribution along the array span and the pressure coefficient distribution along the chord are presented in Figures A-12 and A-13, respectively. These results are as expected and typical of flat plates at small angles of attack and are very similar to the results for a single array. The center of pressure for Figure A-13 is located at the quarter chord (C/4) measured from the plate leading edge which is also typical of flat plates in potential flow. The discussion for Figures A-10 to A-13 on the 2.4 m (8 ft) arrays is also valid for the corresponding Figures A-14 to A-17 on the 4.8 m (16 ft) chord arrays.

Because the results for two arrays are similar to the results for a single array, no analysis was performed for the effect on the aerodynamic forces of array fields yawed to the wind. The results for the yawed arrays would produce pressures and forces of lesser magnitude than a head-on wind condition and as such would not be a design condition.

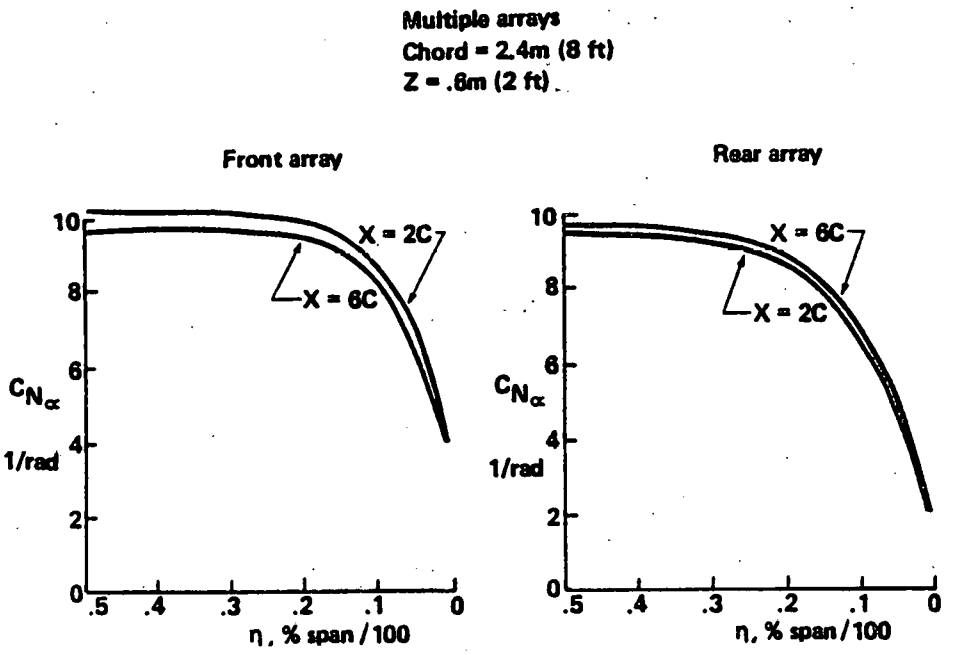

Figure A-12. Effect of Array Separation on Spanwise Normal Force Curve Slope Coefficients

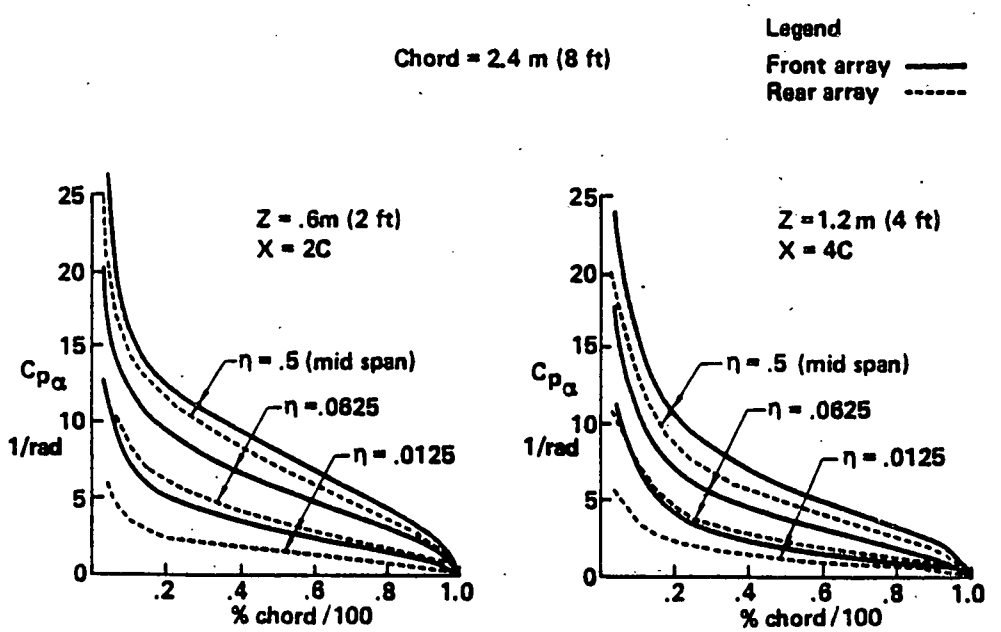

Figure A-13. Chordwise Pressure Distribution for Multiple Flat Plate Arrays

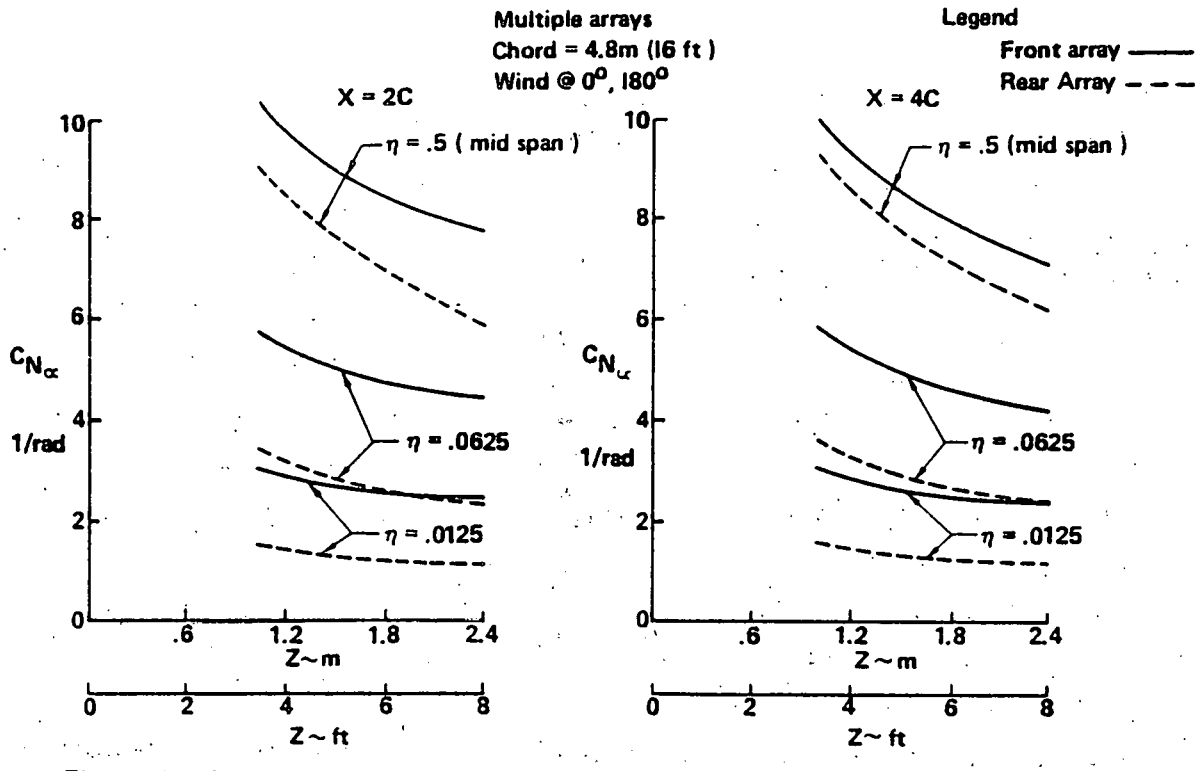

Figure A-14. Effect of Ground Clearance on Normal Force Curve Slope Coefficients

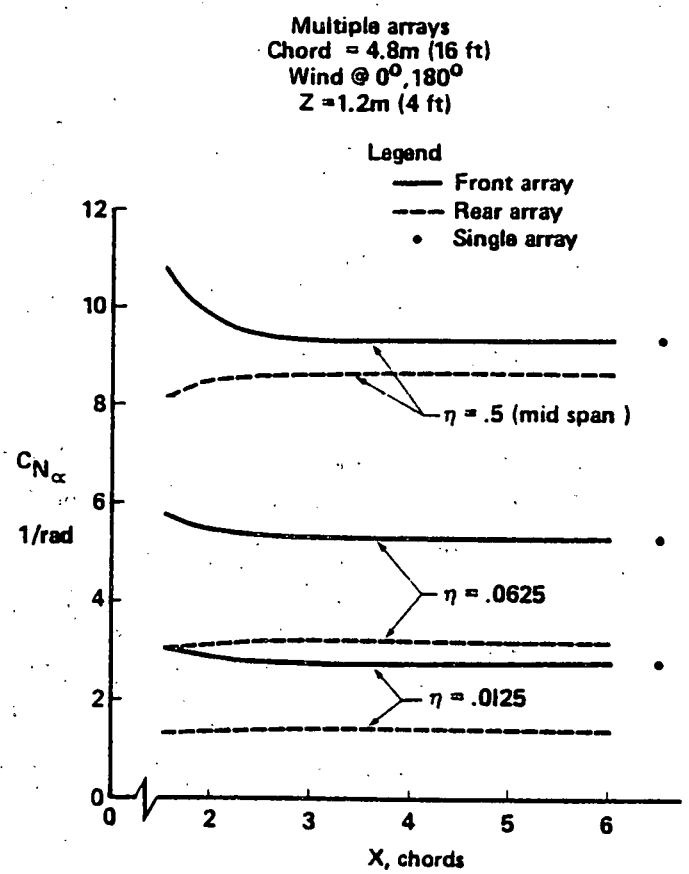

Figure A-15. Effect of Array Separation on Normal Force Curve Slope Coefficients

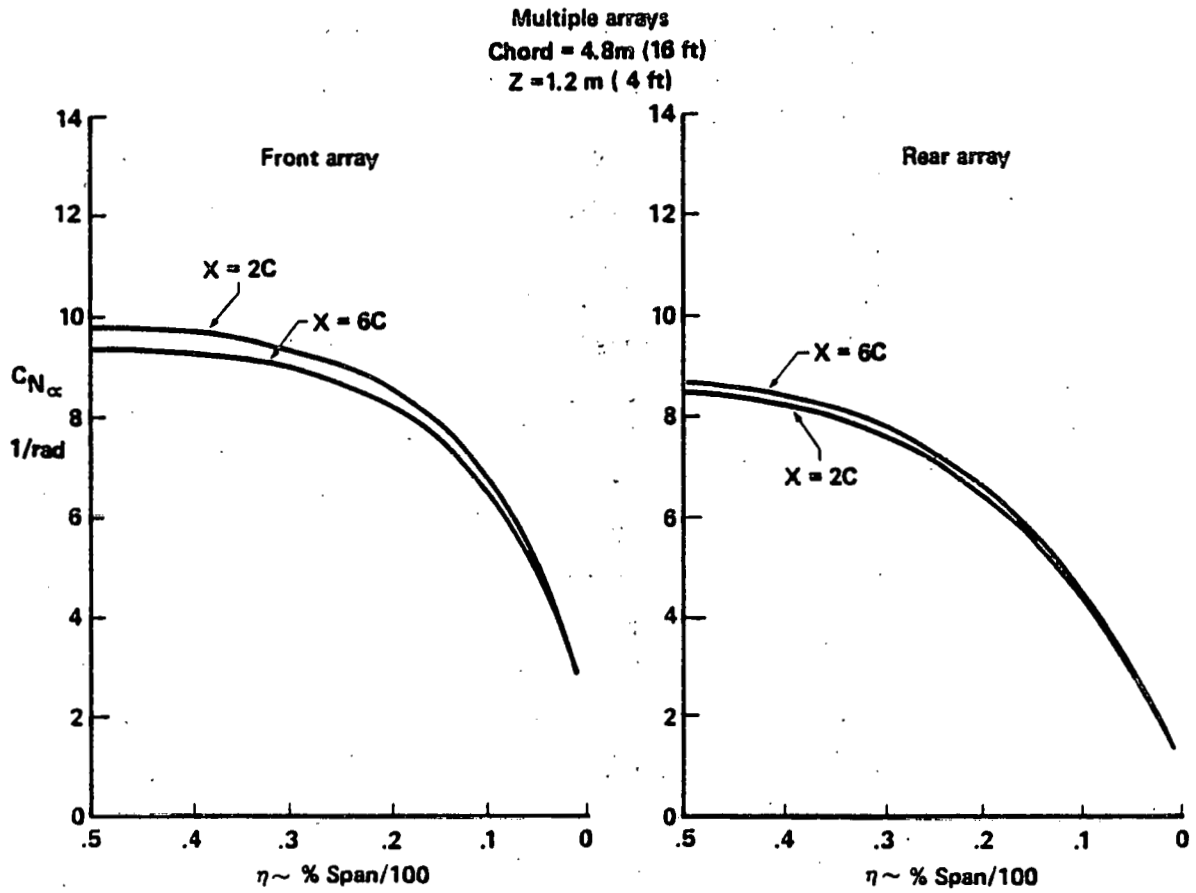

Figure A-16. Effect of Array Separation on Spanwise Normal Force Curve Slope Coeeficients

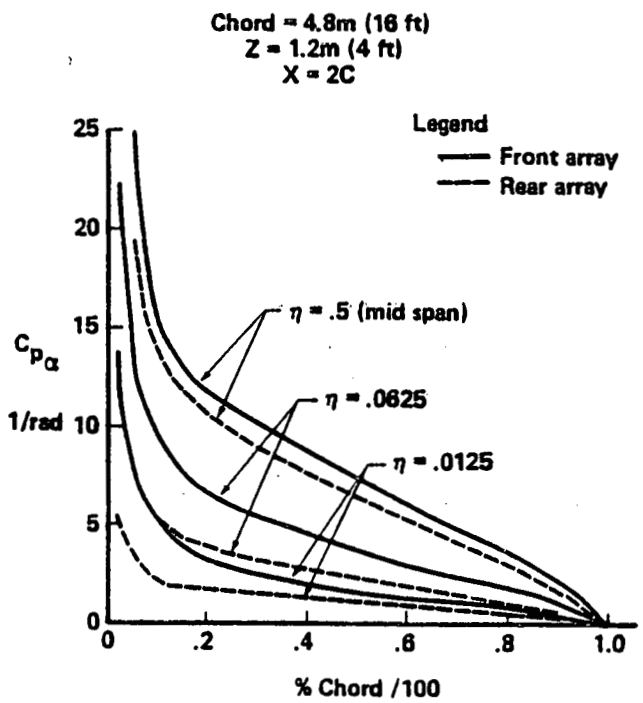

Figure A-17. Chordwise Pressure Distribution for Multiple Flat Plate Arrays

A .2 Large Angles of Attack - Separated Flow

Beyond angles of attack of 15° linear attached flow theory analysis must be replaced with separated flow theory techniques to predict the wind aerodynamic forces. A prototype program has been developed by the Boeing Commercial Airplane Company for use in computing the lift of two-dimensional multi-element airfoils in incompressible flow[32]. The procedure employs repeated application of a panel method to solve for the separated wake displacement surface using entirely inviscid boundary conditions. This procedure allows for the calculation of lift on an airfoil (flat plate) for any angle of attack. Ground effects can be included in the analysis by applying appropriate boundary conditions; the ground plane is modeled by a string of doublets that allow no flow through the string. Conditions that this analysis presently cannot solve is for lifting surfaces in contact with the ground or when one lifting surface is immersed in the wake of other surfaces. This precludes the analysis of an array field with arrays spaced sufficiently close such that downstream arrays are in the wake of the upstream arrays. Because this analysis technique is time consuming and costly to exercise, the angles of attack selected for analysis were limited to 20°, 40°, 60°, 120°, 140°, and 160° and with only a head-on wind direction.

The procedure employed in using this analysis technique to obtain aerodynamic forces on flat plates at large angles of attack was to:

- analyze the flow outside of the ground plane.
- compare the results with existing published experimental results in the literature for identical conditions.
- obtain a correction factor for the theoretical results by comparing them to the published experimental results.
- analyze theoretically the plate aerodynamic forces at large angles and in close proximity to the ground and apply correction factors if deemed necessary.

A .2.1 Single Array in Free Air

Figure A-18 depicts a flat plate positioned at three different angles of attack to the freestream wind velocity and outside of any ground effects. The separated flow program calculated the boundary of the wake and the velocity on the wake boundary relative to the freestream velocity. The pressures on the front (windward) and rear (base pressure) surfaces for the corresponding angles of attack are shown in Figure A-19. The pressures are integrated over the chord to produce normal force coefficients for the front and rear surfaces and the location of the center of pressure measured from the leading edte. This data is tabulated and presented in Table A-1. Using the geometric relationship between lift, drag and normal force as:

$$C_L = C_N \cos \alpha$$

$$C_D = C_N \sin \alpha$$

where

C_L = lift coefficient

C_D = drag coefficient

the lift and drag coefficients were calculated including the potential flow results from 0° to 10° and compared to the results published by Modi[25] and shown in Figure A-20. The theoretical results calculated using the separated flow program were approximately 30% higher than those published by Modi. Examining the pressure distributions in Figure A-19, the windward pressures appeared reasonable with a stagnation point (C_p = 1.0) lying between the mid chord and leading edge position. These pressures also compare favorably with those presented by Sachs in a text on wind forces[33]. By examination and comparison to the results presented by Sachs, the base pressures were suspected as being overpredicted. Consequently, the base pressure was adjusted at the angle of attack of 60° to match the base pressures published by Modi[25]. This adjustment ratio of .73 was then used to adjust the calculated base pressures for the other angles of attack. With the base pressures modified, the lift and drag forces match those published by Modi quite

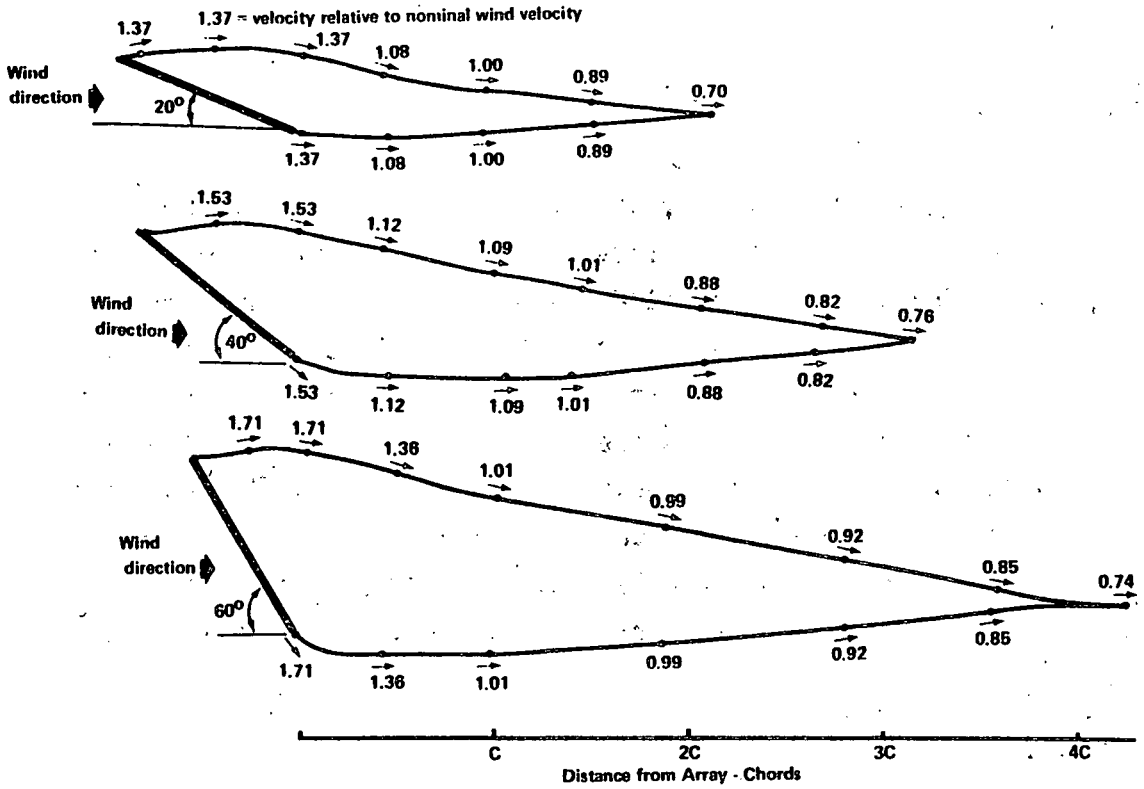

Figure A-18. Wake Definition and Velocity on Wake Boundaries for Flat Plates at Large Angles of Attack in Free Air

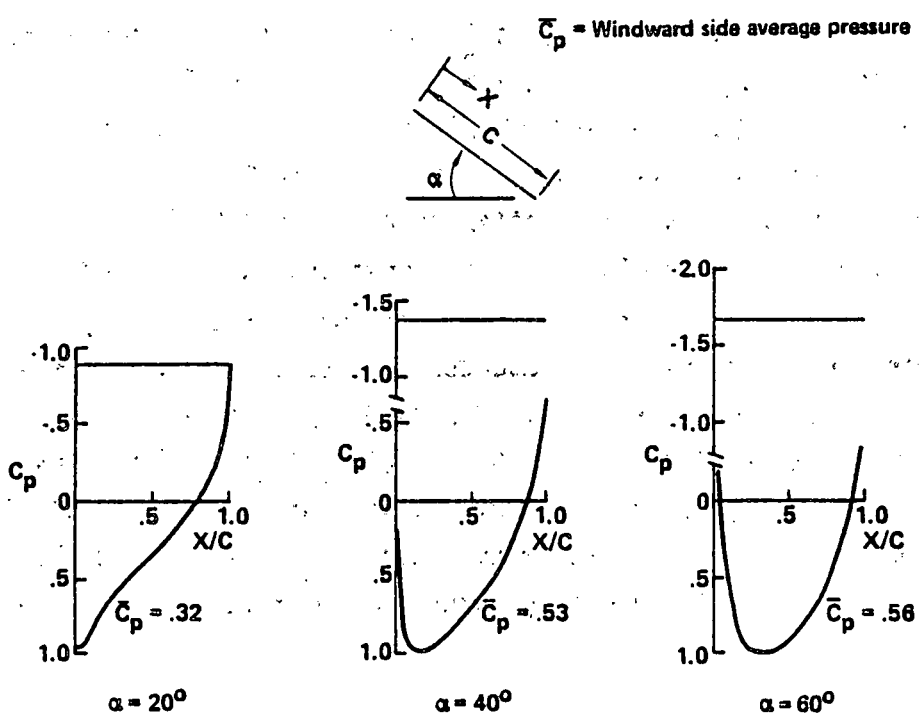

Figure A-19. Theoretical Separated Flow Analysis Pressure Distribution on Two-Dimensional Flat Plates in Free Air

Table A-1. Flat Plate Aerodynamic Coefficients in Free Air

Angle of attack	α	20°	40°	60°
Windward	C_N	.32	.53	.56
Face	Xcp*	.17	.32	.43
Base pressure	C_N	-.89	-1.37	-1.94
Face	Xcp	.5	.5	.5
Total	C_N	1.21	1.90	2.50
	Xcp	.41	.45	.48
Corrected base pressure **	C_N	-. 65	-1.0	-1.42
Total corrected	C_N	. 97	1.53	1.98
Coefficients	Xcp	.39	.44	.48
Lift coefficient	C_L	.91	1.17	.99
Drag coefficient	C_D	.33	.98	1.71

*Center of pressure measured as faction of chord measured from plate leading edge

**Correction factor = .732 based on theoretical pressure coefficients compared to test results shown by Modi

well, being slightly higher; when extrapolated to 90°, the predicted drag coefficient is at the upper range of the drag coefficients published in the literature and also shown in Figure A-20. The comparison obtained between Modi's results, other results in the literature and the separated flow program results was considered excellent. Based on these results, the separated flow analysis program was used to predict aerodynamic forces for flat plates located at close proximity to the ground and at large angles of attack.

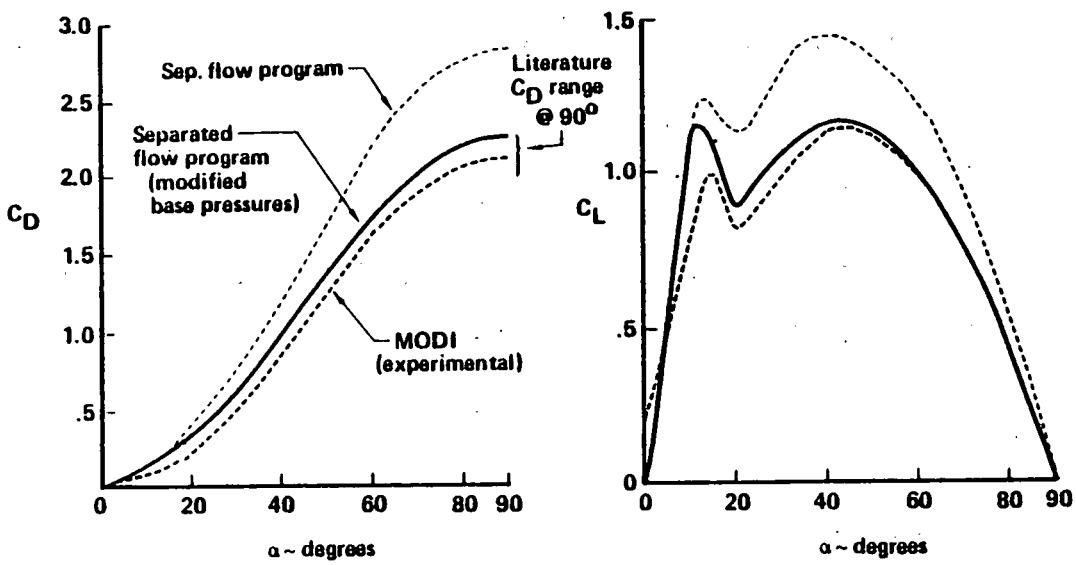

Figure A-20. Theoretical - Experimental Aerodynamic Force Comparison

A.2.2 Single Array in Ground Proximity

The ground clearance between the flat plate array and the ground was defined as a function of the plate chord. Figure A-21 pictures the wake boundary for the conditions of $\alpha = 20^0$ and 160^0 and a ground clearance of .125C. Of interest in Figure A-21 is that the wake for $\alpha = 160^0$ is sucked down towards the ground and flows parallel to the ground until it is past the plate. An analogous phenomenon happens in nature when wind flows through a gorge that opens up to a valley with hills on one side. The wind tends to be sucked to the hills and flow parallel to the hills. This phenomenon (the Coanda effect) is reported in papers in meteorology journals[34]. The pressure distribution for the conditions shown in Figure A-21 and also the other four angles calculated (40^0, 60^0, 120^0, and 140^0) are shown in Figure A-22. The normal force coefficients and the center of pressure locations for the six angles of attack (20^0, 40^0, 60^0, 120^0, 140^0 and 160^0) and the three ground clearances (.125C, .25C, and .50C) are tabulated in Table A-2. The wake boundaries and velocities on the wake for the three ground clearances and for three angles of attack (20°, 40° and 60°) are shown in Figure A-23.

The base pressures on the plate for the above conditions are overpredicted as they were for the free air condition. For angles of attack less than 90^0 it is reasonable to believe that the base pressures are overpredicted

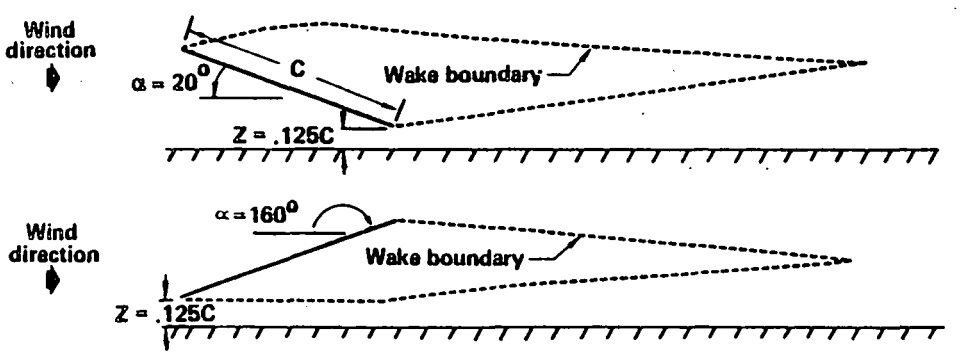

Figure A-21. Wake Boundary of Separated Flow Analysis

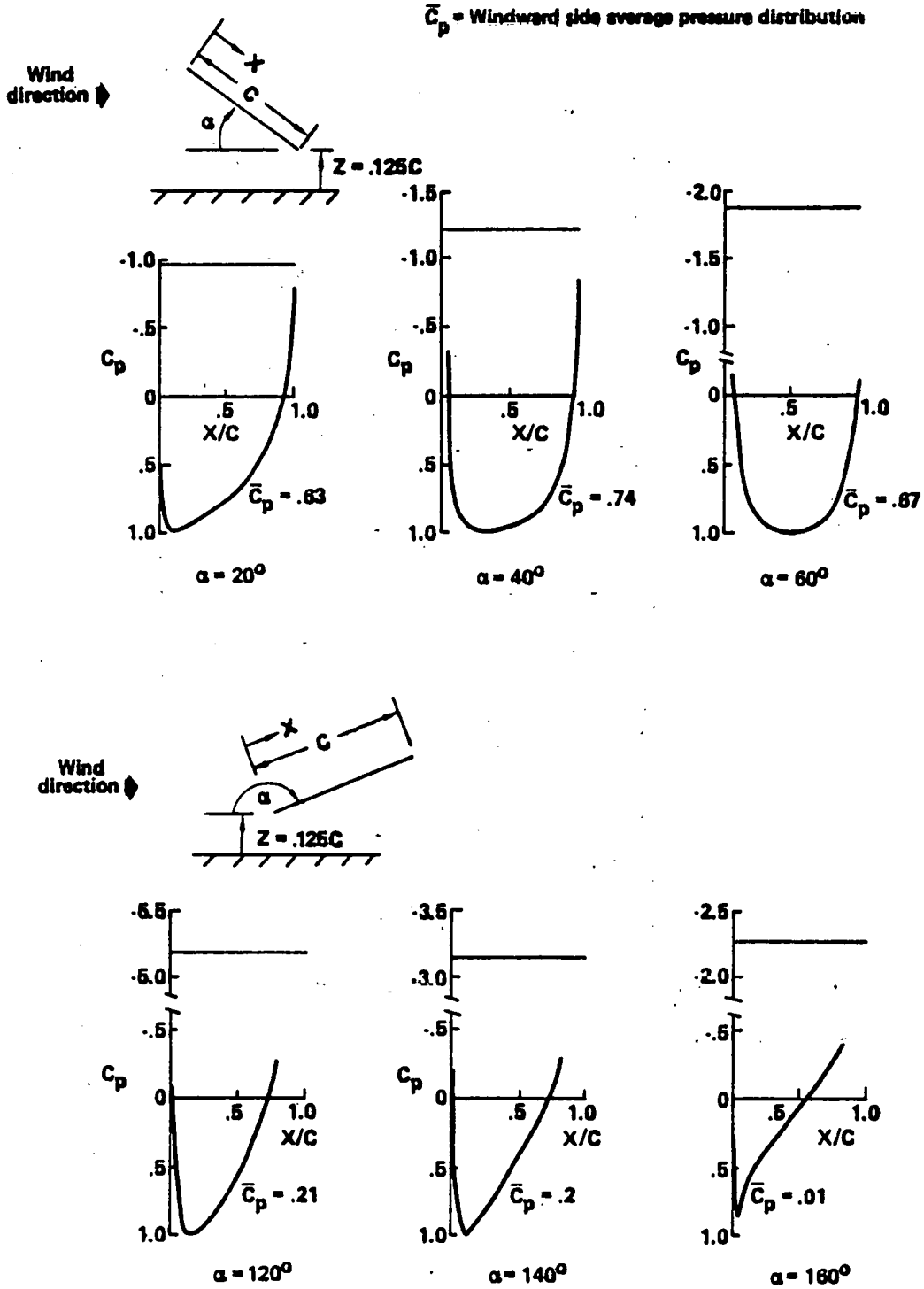

Figure A-22. Effect of Angle of Attack on Two-Dimensional Theoretical Plate Pressure Distribution in Close Ground Proximity

Table A-2. Flat Plate Aerodynamic Coefficients in Close Ground Proximity

Angle of attack		20°			40°			60°			120°			140°			160°		
Ground clearance		.125C	.25C	.5C	.125C	.25C	.5C	.125C	.25C	.5C	.125C	.25C	.5C	.125C	.25C	.5C	.125C	.25C	.5C
Windward face	C_N	.63	.51	.42	.74	.69	.63	.67	.64	.63	.21	.36	.44	.2	.29	.37	.01	.1	.2
	$\bar{X}_{CP}$*	.37	.31	.26	.47	.43	.39	.55	.52	.47	-.47	.10	.26	-.35	-.03	.14	-10.3	-.78	-.09
Base pressure face	C_N	-.97	-.91	-.85	-1.21	-1.17	-1.16	-1.87	-1.83	-1.77	-5.18	-3.8	-3.05	-3.12	-2.61	-2.11	-2.26	-1.62	-1.31
	$\bar{X}_{CP}$	.5 ←																	→ .5
Total	C_N	1.60	1.42	1.27	1.96	1.86	1.85	2.54	2.47	2.40	5.39	4.16	3.49	3.32	2.90	2.48	2.27	1.72	1.51
	$\bar{X}_{CP}$	.45	.43	.42	.49	.47	.45	.51	.50	.49	.46	.46	.47	.45	.45	.45	.45	.43	.42
Corrected base pressure C_N**		-.71	-.67	-.62	-.89	-.86	-.85	-1.37	-1.34	-1.30	-1.37	-1.34	-1.30	-.89	-.86	-.85	-.71	-.67	-.62
Total corrected Coefficients	C_N	1.34	1.18	1.04	1.63	1.55	1.48	2.04	1.98	1.93	1.58	1.70	1.74	1.09	1.18	1.22	.72	.77	.82
	$\bar{X}_{CP}$	.44	.42	.40	.49	.47	.45	.52	.51	.49	.37	.42	.44	.34	.36	.39	.35	.34	.36
Lift coefficient C_L		1.26	1.11	.98	1.25	1.19	1.13	1.02	.99	.97	-.79	-.85	-.87	-.83	-.9	-.93	-.68	-.72	-.77
Drag coefficient C_N		.46	.40	.36	1.05	1.0	.95	1.77	1.71	1.67	1.37	1.47	1.51	.7	.76	.78	.25	.26	.28

*Center of pressure measured as faction of chord measured from plate leading edge

**Correction factor = .732 based on theoretical pressure coefficients compared to test results shown by Modi

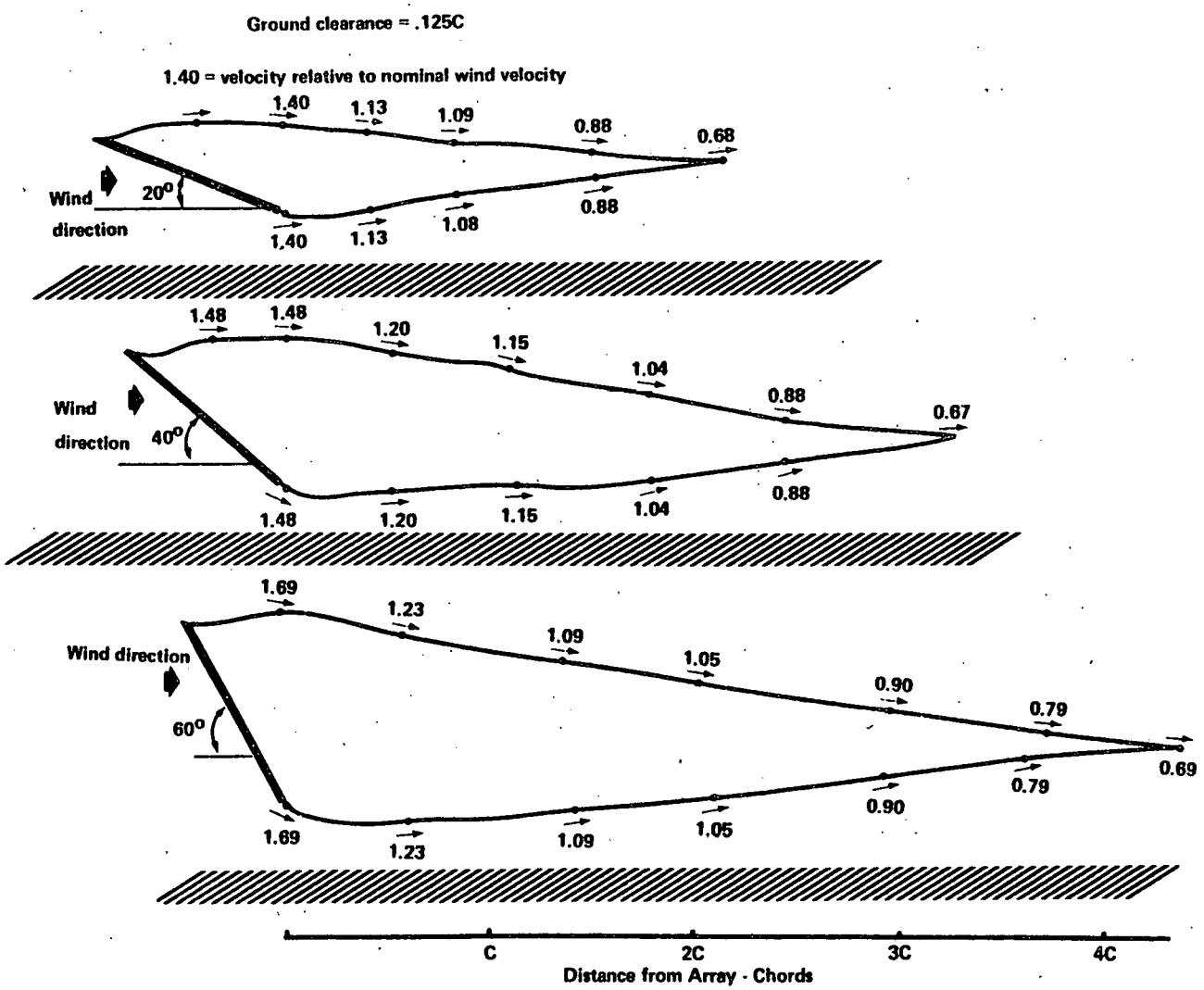

Figure A-23. Wake Definition and Velocity on Wake Boundaries for Flat Plates in Close Ground Proximity and at Large Angles of Attack

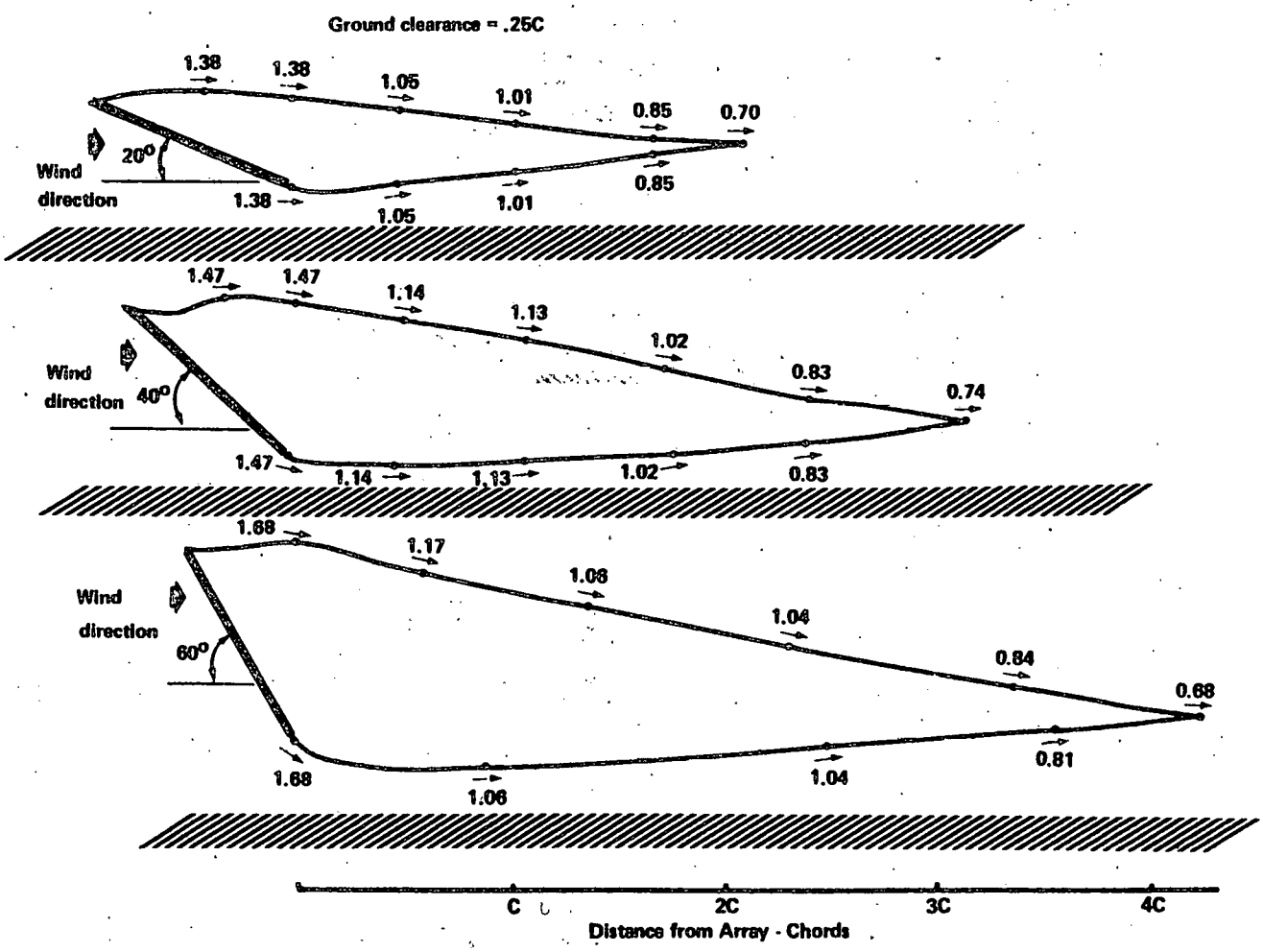

Figure A-23. Wake Definition and Velocity on Wake Boundaries for Flat Plates in Close Ground Proximity and at Large Angles of Attack – Continued

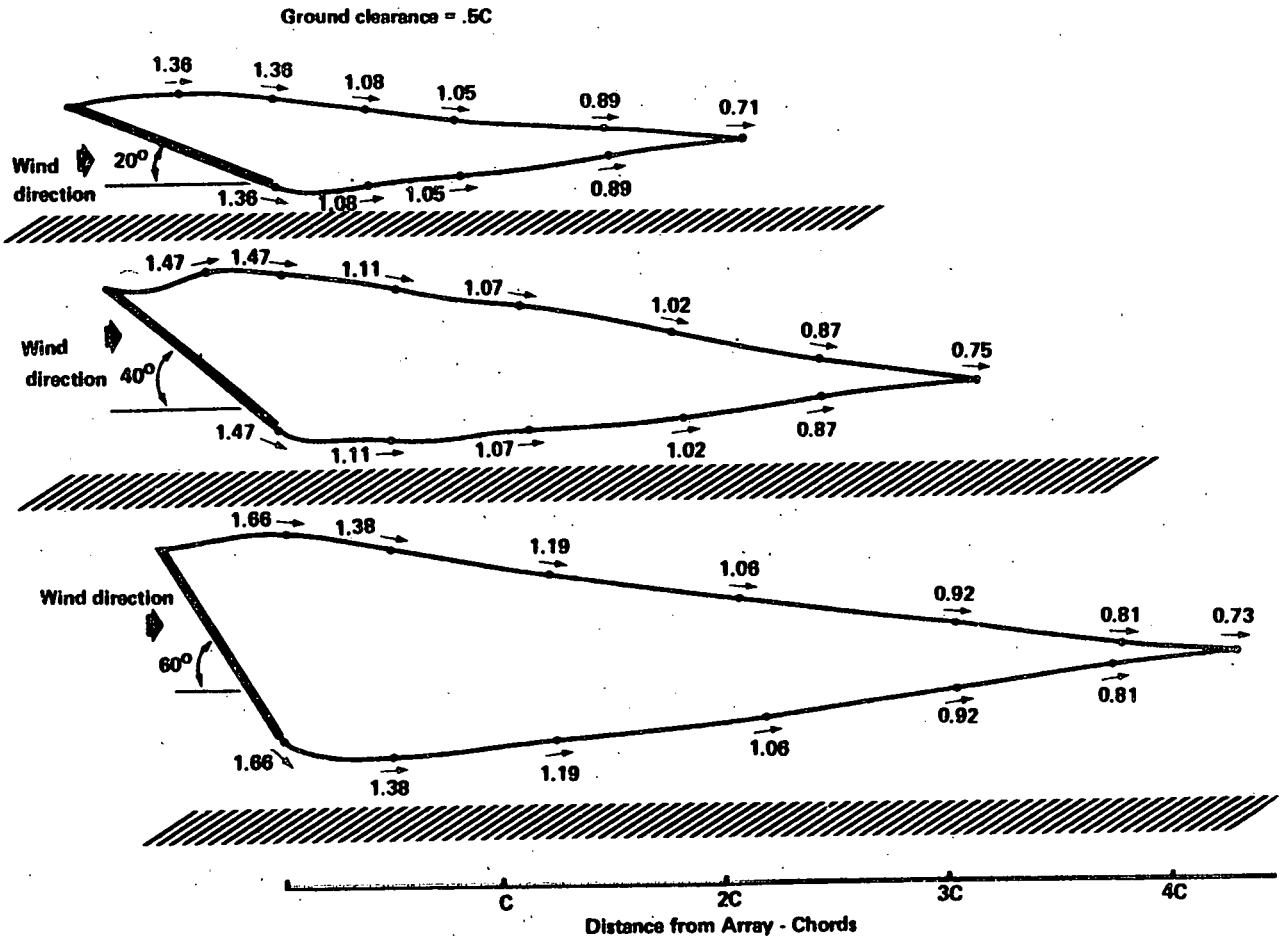

Figure A-23. Wake Definition and Velocity on Wake Boundaries for Flat Plates in Close Ground Proximity and at Large Angles of Attack — Concluded

by the same amount as those in free air. For angles of attack greater than 90°, the base pressures are greatly overpredicted and are considered invalid. These overprediction of the base pressures is believed to be caused by the use of inviscid flow techniques which result in larger flow velocities over the edges, and larger suction forces than for viscous flow, especially for angles greater than 90°. With angles greater than 90°, more volume of air splits in front of the plate and passes through the ground clearance gap than would occur if the flow was viscous. For this volume of air to pass through the ground clearance gap it must increase significantly in velocity. This increased velocity causes larger suction forces to be developed on the base pressure side than would occur if the flow was viscous. It is expected that the base pressures for α and $180^{o} - \alpha$ would be very similar in magnitude, based on the results presented by Sakamota[14] (Figure A-24). Sakamota performed a wind tunnel study of a flat plate in contact with the ground and for angles of attack of 30°, 60°, 90°, 120°, and 150°. Comparing his results shown in Figure A-24 for α and $180^{o} - \alpha$, the base pressures are equal or slightly higher in magnitude for α compared to $180^{o} - \alpha$. Thus, if the base pressures calculated by the separated flow analysis program for α are used in place of the results for $180^{o} - \alpha$, the results would be fairly accurate and conservative. Table A-2 shows the base pressures with this correction and with the correction factor determined from the free air analysis as well as the uncorrected results.

Another noteworthy result that can be seen from Table A-2 and Figure A-22 is that the plate windward side pressures and normal force coefficients increase as the angle of attack approaches 90°. In addition, the total normal force coefficient on the plate also increases as the ground clearance decreases. This will approach a maximum prior to a ground clearance of zero. As stated in a text book[33] on wind forces and also demonstrated by comparing Figures A-24 and A-22, the normal force coefficient for the condition where one edge of the plate is in contact with the ground is less than when off of the ground. This is because of the suction effect of the flow passing over each edge. If one edge is in contact with the ground, no flow and thus no suction is effected at this edge and so the base pressures are a minimum for these conditions. Again examining Figure A-22, the center of pressure for the base pressures are always at the mid chord

location while the center of pressure on the windward side moves in the direction from the leading edge to the mid chord as the angle of attacks approaches 90°. The center of pressure locations are also tabulated in Table A-2.

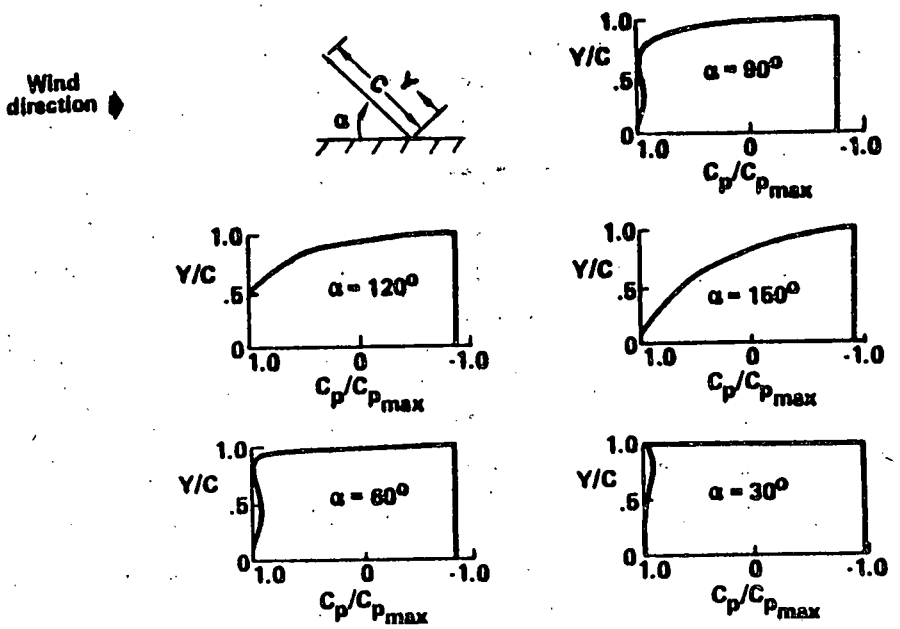

Figure A-24. Experimental Normalized Pressure Distribution for a Two-Dimensional Plate in Contact with the Ground

A.2.3 Array Fields

Only a few conditions were studied to evaluate the effect of one array on another because the analysis program was incapable of analyzing the flow when one array was in the wake of another. From the separated flow analysis, immersion in the wake of the upwind array occurs when spacing/chord ratios are less than 3C for $\alpha = 20^{\circ}$ and 5C for $\alpha = 60^{\circ}$. Table A-3 presents the normal force coefficient results for two arrays spaced at intervals of three chords and five chords compared to one array by itself for the two angles of attack (20° and 60°) respectively. From the results, the upwind array normal force coefficients increase slightly whereas the downwind array force coefficients decrease slightly. However, because of the program limitations, the benefit of the reduced loads from positioning arrays in the wake of another array cannot be evaluated analytically. One can only speculate on the load reduction afforded by immersing an array in the wake of another array from the wind velocity reduction behind fences. Using Raine's results[23] as a basis, a steady state dynamic pressure reduction factor of as much as 10 and an unsteady state dynamic pressure increase factor of at most 4 can be obtained assuming no dynamic response of the structure. This would produce a net aerodynamic load reduction factor of 2.5 compared to an array not in a wake. This aerodynamic load reduction of 60 percent appears to be a reasonable factor to expect for arrays positioned in the wake of other arrays.

A.3 Summary of Results

Using the results in Section A.1 and A.2 for one array and the geometric relationship between the normal force, lift, and drag coefficients and angle of attack, corrected normal force, lift and drag coefficients were calculated. The base pressure corrections as discussed in Section A.2 were applied. Briefly, for angles of attack between 20° and 160° the base pressures for $180^{\circ} - \alpha$ were replaced by the base pressures calculated at α and also the base pressures were modified by the factor .73 that was found to be required in matching wind tunnel test results. Figures A-25 to A-27 summarize the results in

Table A-3. Multi-Array Flat Plate Aerodynamic Coefficients

Angle of Attack = 60°, array spacing = 5C

		One Array	Two Arrays	
			Upwind	Downwind
Ground clearance = free air				
Windward face	C_N	.56	.57	.61
Base pressure face	C_N	-1.94	-1.93	-1.72
Total	C_N	2.50	2.50	2.33
Ground clearance = .125C				
Windward face	C_N	.67	.66	.71
Base pressure face	C_N	-1.87	-1.90	-1.54
Total	C_N	2.54	2.56	2.25
Ground clearance = .5C				
Windward face	C_N	.63	.59	.64
Base pressure face	C_N	-1.77	-2.0	-1.73
Total	C_N	2.40	2.59	2.37

Angle of Attack = 20°, array spacing = 3C

Ground clearance = .125C				
Windward face	C_N	.63	.63	.69
Base pressure face	C_N	-.97	-.99	-.81
Total	C_N	1.60	1.62	1.50

Sections A.1 and A.2. From the summary results shown in these figures, it can be seen that the arrays should not be positioned at angles of attack where the flow remains attached (10^0 to 15^0). At these small angles, the arrays act as an efficient airfoil. The lowest aerodynamic loads on the structure occur at angles slightly greater than 10^0 - 15^0 where the flow has separated but the aerodynamic force from the separated flow is at a minimum. This occurs near $\alpha = 20^0$.

At angles greater than 15^0 to 20^0, the difference between the force coefficients for ground clearances of .125C to .5C is minimal. The results for array fields are not presented because with the limitations of the theoretical analysis, the results for the windward array for all practical purposes is identical to the single array results. The results for the downstream array (not immersed in upstream array wake) are slightly reduced from the single array and thus using single array results would be slightly conservative. Experimental results are required for more closely spaced array fields. The yawed wind condition to the arrays was also not presented since it produces lower loads than the head-on condition and, as a result, is not a critical design condition.

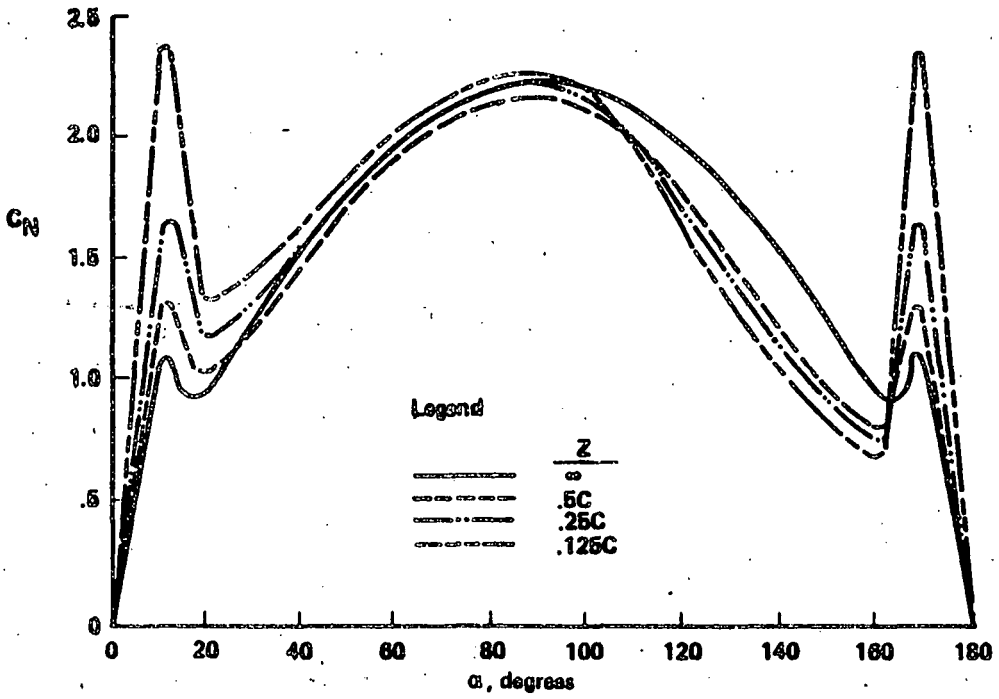

Figure A.-25. Two-Dimensional Plate Theoretical Normal Force Coefficient in Free Air and in Close Ground Proximity

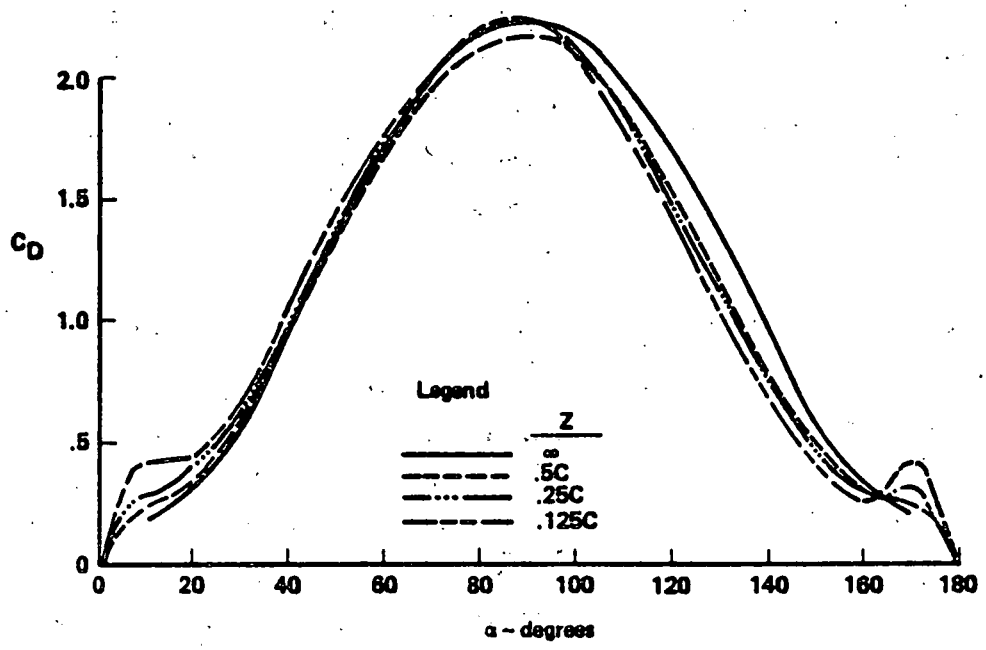

Figure A -26. Two-Dimensional Plate Theoretical Drag Coefficient in Free Air and in Close Ground Proximity

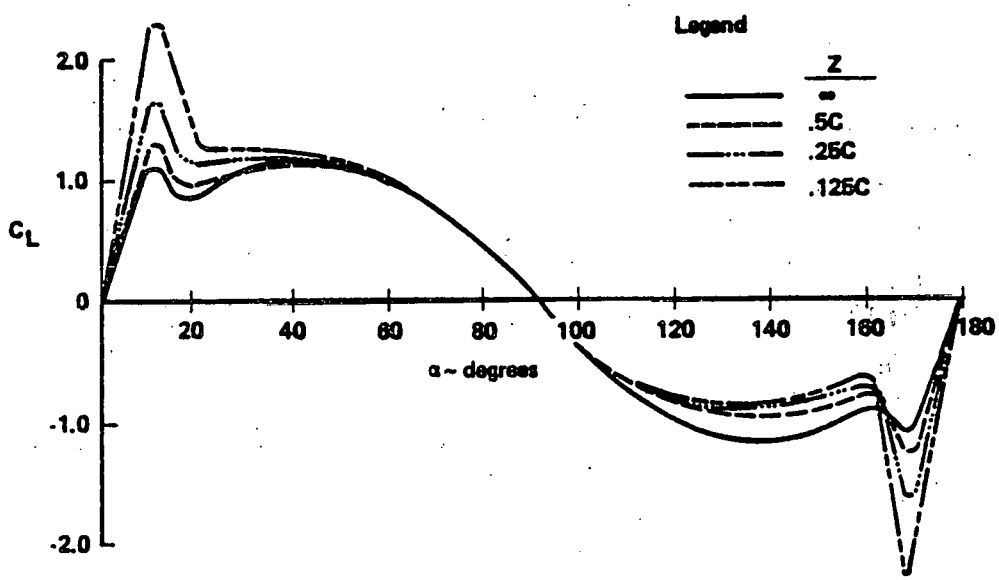

Figure A -27. Two-Dimensional Plate Theoretical Lift Coefficient in Free Air and in Close Ground Proximity

THIS PAGE

WAS INTENTIONALLY

LEFT BLANK

APPENDIX B

PHOTOVOLTAIC ARRAY WIND TUNNEL TEST PLAN

The specifications for a wind tunnel test of photovoltaic arrays to determine detailed aerodynamic pressures and loads for various key array parameters and load reducing techniques follows:

I. Photovoltaic Array Model Requirements:

1) 10 flat plate models sized to span the tunnel when at 90° to airflow consisting of:

   a) 8 flat plate dummy models sized to 8 ft. and 16 ft. chords;
   b) 1 test flat plate model with pressure taps located at the mid-span location and 15% of chord from the end of the span and 2 test flat plate models with pressure taps located only at the midspan location. Pressure taps are required on both front and rear surfaces and spaced in the chordwise direction such as to adequately define the pressure distribution on both surfaces. The pressure taps at the mid-span station will be used and assumed to represent the pressures over all of the individual plates of the array when the flow is 90° to the array. The pressure taps at 15% of the chord from the span edge will be used to evaluate the pressure loading near the array edges caused by flow disturbance from forward plate edges when the plates are at small yaw angles to the airflow.

2) The array model is required to be raised from the ground plane to c/2 above the ground plane.

3) The array plates are required to be rotated about "y" from 20° to 60° and 120° to 160° with the test angles being 20°, 30°, 45°, 60°, 120°, 135°, 150°, and 160°.

4) The array plate spacing needs to be varied from dense to sparse spacing.

5) To study the edge effects, the array is required to rotate approximately 20° into the wind about the z axis and the array edge positioned near the center of the tunnel to prevent wall effects.

II. Load Alleviation Model Requirements

1) Fences of 20% and 35% porosity and sized for actual height of 6 ft., 8.2 ft. and 16.4 ft. high and length that spans the tunnel.

2) Plate porosity to be located at the boundary of each module.

3) Panels to be attached to the array plates to block the flow from flowing under the plates.

III. Wind Tunnel Test Requirements - Steady State Test

A. Constant wind profile - design wind velocity = 40 m/s

i) one plate

ground clearance (z)	Angles of Attack (α) 20°	30°	45°	60°	120°	135°	160°	170°
0	✓	✓	✓	✓				
.25c	✓	✓	✓	✓	✓	✓	✓	✓
.5 c	✓	✓	✓	✓				
∞	✓	✓	✓	✓				

ii) multiple plates - measure pressures on plates 1, 2 and 5.
ground clearance is .125c

separation distance (x)	Angles of Attack (α) 20°	30°	45°	60°	120°	135°	150°	160°
1.5 c	✓	✓	✓			x	x	x
1.75c	✓	✓	✓	✓	✓**	✓**	✓**	✓**
3.0 c	✓	✓	✓	✓	x	x	x	x

Repeat for ground clearance = .25c

**Only do x's if the normal force for these angles are greater than for the corresponding acute angle forces

B. 1/7 power wind profile - design wind velocity of 40 m/s at 10 m

Plate chord = 8 ft.

i) one plate

Ground Clearance (z)	Angles of Attack (α) 20°	30°	45°	60°	120°	135°	160°	170°
0 ft	✓	✓	✓	✓				
2 ft	✓	✓	✓	✓	✓	✓	✓	✓
4 ft	✓	✓	✓	✓				

ii) multiple plates - measure pressures on plates 1, 2 and 5

ground clearance is 2 ft.

Separation Distance (x)	Angles of Attack (α) 20°	30°	45°	60°	120°	135°	150°	160°
12 ft	✓	✓	✓			x	x	x
16 ft	✓	✓	✓	✓	✓**	✓**	✓**	✓**
24 ft	✓	✓	✓	✓	x	x	x	x

Repeat for ground clearance = 4 ft.

**Only do x's if the normal force for these angles are greater than for the corresponding acute angle forces.

iii) repeat (ii) for ground clearance of 2 ft. only and with fence 10 ft. in front of array for:

a) 6 ft. fence of porosity 20% and 35%

b) 8.2 ft. fence of porosity 20% and 35%

iv) repeat (ii) for ground clearance of 2 ft. only and with fence 20 ft. in front of array for:

a) 8.2 ft. fence of porosity 35%

v) repeat (iv) with fence 40 ft. in front of array.

Pressures on the plates need only be recorded for plates 1, 2 and 5.

C. 1/7 power wind profile - Optional

Plate chord = 16 ft.

i) multiple plates - measure pressures on plates 1, 2 and 5.

ground clearance is 2 ft.

Separation Distance (x)	Angles of Attack (α) 20°	30°	45°	60°	120°	135°	150°	160°
24 ft	✓	✓	✓			x	x	x
32 ft	✓	✓	✓	✓	✓**	✓**	✓**	✓**

Repeat for ground clearance = 4 ft.

**See note from B

ii) repeat (i) for ground clearance of 2 ft. and with fence 20 ft. in front of array and porosity producing min. loads in (B(iii).

a) 8.2 ft. high fence

b) 16.4 ft. high fence

D. Edge effects

Repeat B(ii) for ground clearance of 2 ft. and with array rotated into flow for:

a) 10°

b) 20°

c) 0°

The pressure need only to be recorded from the pressure taps located near the array side edge. The array should be repositioned such that the wall of the tunnel does not affect the edge pressures.

E. Other load alleviation devices

a) Repeat B(ii) with flow blocked from flowing under the array plates

b) Repeat B(ii) for ground clearance of 2 ft. only and with porosity built into the plates for the following combination of module sizes.

z \ y	2'	4'	8'
4'	✓	✓	no
8'	no	✓	✓
16'	no	no	✓

F. Movie

Smoke visualization should be performed for each test and motion pictures taken so that a movie can be made of the test.

III. Wind Tunnel Test Requirements - Unsteady Test

A. 1/7 power wind profile

i) multiple plates - measure unsteady pressures on plates for one condition of test III B(iii) that is multiple plates with a fence positioned in front of the array.

Note: Besides pressure measurements along the chord, force results are desired by integrating the pressures over the chord.

☆U.S. GOVERNMENT PRINTING OFFICE:1980 -640 -258/ 1819